Journal of
Marine Science and Engineering

MDPI

Article

Improvements for the Eastern North Pacific ADCIRC Tidal Database (ENPAC15)

Christine Szpilka [1,*], Kendra Dresback [1], Randall Kolar [1] and T. Christopher Massey [2]

[1] School of Civil Engineering and Environmental Science, University of Oklahoma, 202 W. Boyd Room 334, Norman, OK 73019, USA; dresback@ou.edu (K.D.); kolar@ou.edu (R.K.)
[2] US Army Corps of Engineers, Eng. Research & Development Center, Coastal & Hydraulics Lab, 3909 Halls Ferry Road, Vicksburg, MS 39180, USA; Chris.Massey@usace.army.mil
* Correspondence: cmszpilka@ou.edu; Tel.: +1-405-325-5911

Received: 3 October 2018; Accepted: 2 November 2018; Published: 7 November 2018

Abstract: This research details the development and validation of the updated Eastern North Pacific (ENPAC) constituent tidal database, referred to as ENPAC15. The database was last updated in 2003 and was developed using the two-dimensional, depth integrated form of the ADvanced CIRCulation coastal hydrodynamic model, ADCIRC. Regional databases, such as ENPAC15, are capable of providing higher resolution near the coast, allowing users to more accurately define tidal forcing for smaller sub-regions. This study follows the same methodology as the EC2015 updates for the eastern coast of the United States and six main areas of improvement in the modeling configurations are examined: (1) placement of the open ocean boundary; (2) higher coastal resolution; (3) updated global bathymetry; (4) updated boundary forcing using two global tidal databases; (5) updated bottom friction formulations; and (6) improved model physics by incorporating the advective terms in ADCIRC. The skill of the improved database is compared to that of its predecessor and is calculated using harmonic data from three sources. Overall, the ENPAC15 database significantly (52% globally) reduces errors in the ENPAC03 database and improves the quality of tidal constituents available for sub-regional models in the ENPAC region.

Keywords: tidal constituent database; ADvanced CIRCulation model (ADCIRC); Eastern North Pacific Ocean (ENPAC); coastal ocean modeling

1. Introduction

Accurate predictions of the ocean's tides are necessary for many coastal engineering applications. The propagation of tides into localized coastal areas is highly dependent upon the shape and bathymetric profile of the estuary itself and its inlets, as well as proper assignment of tidal boundary conditions outside the estuary. Thus, even with a highly resolved and accurate model domain, localized simulation results are only as good as the boundary conditions that are applied.

Coastal ocean models often utilize tidal databases in order to specify the tidal boundary conditions in small-scale regional studies, such as those undertaken for storm surge inundation [1–3]; sediment transport [4–6]; sea level rise [7–10]; real-time surge forecast systems [11–14]; passive transport of oil spills [15]; passive fish and larval transport, as well as coupled ecological behavior [16–18]; coupled hydrodynamic-marsh interactions with biological feedback [19] and combined hydrologic and hydrodynamic processes [13,20]. For reliable modeling of these complex physical processes, it is necessary to have accurate representation of the tidal boundary forcing. When no other source is available, this forcing must be taken from global databases, which are highly accurate in the deep ocean but often lack the resolution to resolve the more complex interactions over the shelf and in shallower coastal regions [21]. More recently, the Oregon State University Tidal Inversion Software (OTIS) has added smaller regional scale products for many coastal regions; however, these are still provided

on relatively coarse grids (1/30° to 1/60°) and until recently only included the primary diurnal and semi-diurnal constituents [22]. Therefore, it is necessary to create regional tidal databases with higher resolution that can better represent the near-shore environment. Often, these high-resolution products are created for specific marine environments, for example: east Florida [23], Western North Atlantic Ocean [24–26], Eastern North Pacific Ocean [27] and Western Europe [28].

This study is concerned with the tidal response for the Pacific Ocean along the western coast of North America. This region falls within what has been called either the Northeast Pacific Region or the Eastern North Pacific (ENPAC) region, which encompasses all marine and coastal waters from the Bering Strait to the north along the west coast of North America to the Baja Peninsula and along the west coast of Mexico to the border with Guatemala [29]. Historically, three tidal databases utilizing the ADvanced CIRCulation (ADCIRC) hydrodynamic model have been developed for this region [27]; each of these databases developed the tidal profile within the domain by forcing the open ocean with global tidal data. Figure 1 presents these historical database domains, as well as the current database, (only open ocean boundaries shown) within the geographical ENPAC region. Note that, although these databases do not encompass the entire geographic region, it is convenient to use the ENPAC abbreviation.

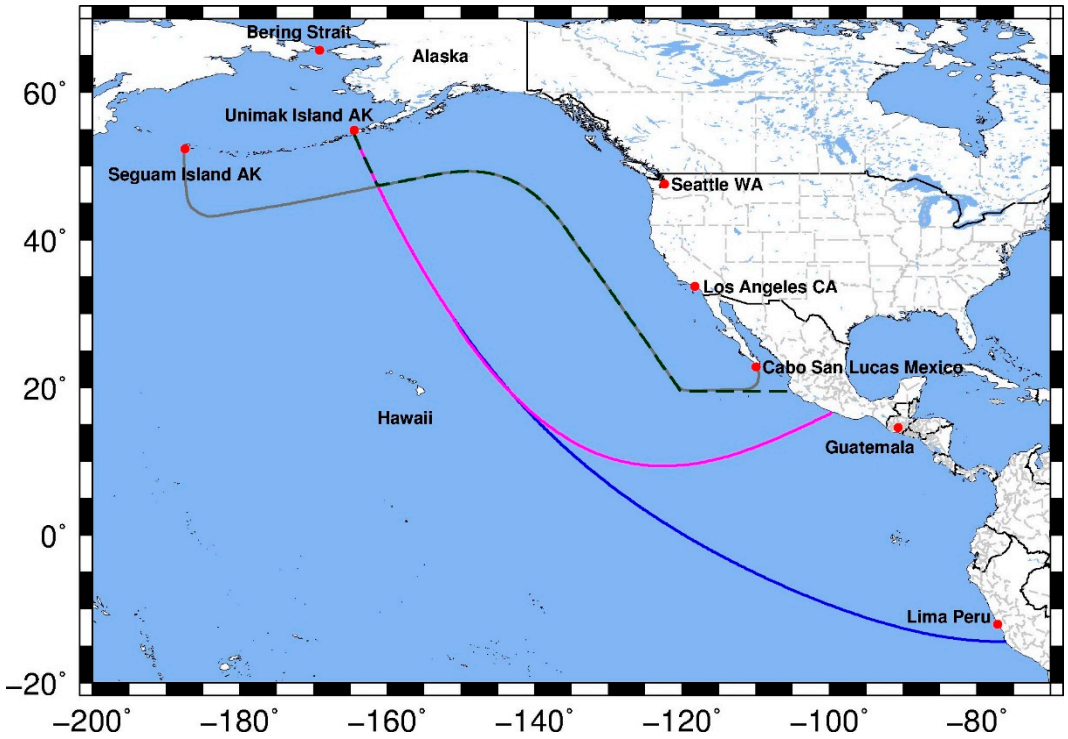

Figure 1. Location of current and historical tidal databases within the Eastern North Pacific region: ENPAC1994 (blue), ENPAC02 (magenta), ENPAC03 (dashed dark green) and ENPAC15 (gray).

The tidal database for the Eastern North PACific region was originally developed in 1994 (called ENPAC1994); it utilized an unstructured grid and resolution varied from about 15 km along the coast to 60 km in the open ocean. Bathymetric information was obtained from the 1988 version of the Earth Topography 5-arc-minute grid (ETOPO-5) [30]. However, the results from this tidal database did not provide good agreement with the field data, and, in some areas, did not provide any improvement over the global ocean tidal models [27].

The first update was not undertaken for nearly ten years; ENPAC02 included increased grid resolution, a reduction of the overall domain and updated bathymetric profiles. Bathymetry was defined from the available National Ocean Service (NOS) soundings database and the 1998 version of the ETOPO-2 product [31] where soundings were not available. The domain extent was reduced to

avoid the cluster of tidal amphidromes off the South American coast. The final ENPAC02 model had grid resolutions ranging from about 8 km along the coast to 60 km in the deep ocean. The combination of improved bathymetry, increased coastal resolution and reduction in the domain extent improved the results with the ENPAC02 database; however, major problems persisted with the amplitude and phase of the semi-diurnal constituents [27].

In 2003, further changes were made to the domain extent, primarily moving the boundary closer to shore; the area eliminated was a portion of the deep ocean waters where the amphidromes associated with the semi-diurnal constituents resided. Additionally, the entire coastline was resolved, even further resulting in an average coastal resolution of 1 km. These modifications to the model domain led to increased accuracy in the tidal results, particularly the semi-diurnal constituents, and the database was released as ENPAC03; it provided elevation harmonics for the eight major tidal constituents and three nonlinear constituents (K_1, O_1, P_1, Q_1, M_2, S_2, N_2, K_2, M_4, M_6, steady) at any location within the domain [27].

The latest version presented herein, ENPAC15, has significantly enhanced coastal resolution with a minimum element size of 20 m along small channels and man-made barriers and an average element size of 65 km at the open boundary. Typical resolution along the mainland United States coastline is 200–400 m; at this time, the Alaskan coastline has not been updated and resolutions in that area range from 2 to 5 km. The ENPAC15 database provides the amplitude and phase for the 37 standard NOS tidal constituents [32] for both elevation and velocity. The model domain features of the various ENPAC tidal databases are provided in Table 1.

Table 1. Summary of grid features for Eastern North Pacific domain ADCIRC tidal databases.

Database Name	Num. of Mesh Nodes	Num. of Mesh Elements	Avg. Coastal Resolution (km)	Min. Coastal Resolution (m)	Avg./Max Deep Ocean Resolution (km)
ENPAC1994	27,494	52,444	15–20	7900	58/90
ENPAC02	290,715	567,145	8 (15–20) [1]	3200	60/96
ENPAC03	272,913	531,680	1–2 (5) [2]	755	35/53
ENPAC15	553,802	1,038,443	0.2–0.4	28	65/85

[1] The coastline was only resolved from Vancouver Island to California, the remainder of mesh is same as ENPAC1994.
[2] The coastline was more finely resolved from Vancouver Island to Mexico, while the Alaskan coast remained coarser but was refined.

With each successive update, the ENPAC databases have gained accuracy in the internal tidal signals. However, the previous database (ENPAC03) still has significant errors (13% amplitude and 13° phase globally), particularly in the region near Vancouver Island where the interior passages have not been resolved (average errors of 22% amplitude and 25° phase). Furthermore, data availability and technological advancements in the past 10 years provide even greater levels of model sophistication and domain complexity. The overarching objective of this study is to reduce the global and regional errors of the ADCIRC tidal database in the ENPAC region. We realize this objective by incorporating six improvements into the latest generation tidal database: new open ocean boundary location, updated coastal resolution, updated bathymetry, boundary forcing using the latest global tidal databases, comparison of the bottom friction parameterization and inclusion of the advective terms within ADCIRC.

In the following sections, these improvements and the resulting error reductions are presented. The development of the ENPAC15 tidal constituent database and validation methods are summarized in Section 2; skill assessment for global, regional and site-specific locations are provided in Section 3 and a discussion of the results and limitations of the database are provided in Section 4. In the interest of brevity, the skill assessment only covers the eight primary constituents: M_2, S_2, N_2, K_2, O_1, K_1, P_1 and Q_1.

2. Materials and Methods

The methodology of this study closely follows that used for the development of the *EC2015* tidal database for the eastern coast of the United States [26]; therefore, the entire outline and much of the text provided in Section 2.1, Section 2.2, and Section 2.3 is similar to that of our previous study (in order that this paper is complete enough to stand alone for those readers who are not familiar with that study). While the methodology is similar, it is not the same, due to peculiarities of local regions, so readers are cautioned not to skip these sections entirely. In particular, the subsections within Section 2.2 are region specific to ENPAC and are important for thorough understanding of this current study, as are the discussion of the validation data and methods in Section 2.3.

2.1. ADCIRC Computational Model

2.1.1. General Model Details

The enhancements to this database employ the ADCIRC regional hydrodynamic model. ADCIRC utilizes the full nonlinear shallow water equations, using the traditional hydrostatic pressure and Boussinesq approximations. The depth-averaged generalized wave continuity equation (GWCE) is used to solve for the free surface elevations, while the non-conservative form of the momentum equation is used for the velocity components. There have been many papers written about the development and usage of the ADCIRC computational model, but basic details for the equations of ADCIRC can be found in [33–35].

One of the advances within ADCIRC since the West Coast database was last updated in 2003 is the addition of Manning's *n* to represent bottom friction. Users can now specify specific quadratic friction coefficients, Chezy friction coefficients or Manning's *n* values throughout the domain. For the Manning's implementation, the *n* values are converted to an equivalent quadratic friction coefficient within ADCIRC (for each node and at every time step) before the bottom stress is calculated [36]. Note that the computed quadratic friction coefficient can also be limited on the lower end by specifying the minimum *CF* value; otherwise, the values can become quite small as the depth becomes large.

2.1.2. Model Input Parameters

Unless otherwise noted in the appropriate methods and results' subsections, all the ADCIRC model runs used the parameters in the following descriptions. To capture the long-period nonlinear tides, the ENPAC15 tidal database was developed from a 410-day simulation. The model was run from a cold state (zero elevation potential and velocity) and a ramp was applied to both the boundary forcing and the tidal potential forcing functions for the first 25 days. Then, the model was run for another 20 days before the internal ADCIRC harmonic analysis was started for the final 365 days of the simulation (a one-minute interval is used for the internal harmonic decomposition). Tidal potential forcing was applied to the interior of the domain for the eight primary constituents (O_1, K_1, Q_1, P_1, M_2, N_2, S_2 and K_2). In addition to these, the open ocean boundary was also forced with two long-period constituents (Mm and Mf). Tidal boundary forcing was extracted from the OTIS TPXO8-atlas global tidal database [37].

A time-step of 1.0 sec and the default time weighting factors (0.35, 0.30 and 0.35) were used. The lateral eddy viscosity coefficient was set equal to 5.0 m^2/sec. With the exception of the various bottom-friction comparison runs, a nonlinear quadratic bottom-friction scheme with a constant value of 0.0025 was used. Specific friction settings for the Manning's *n* formulation and the variable *CF* runs are detailed in Section 2.2.5 below. The traditional spatially variable but temporally constant GWCE weighting parameter was used ($\tau_0 = -1$). Finally, variable Coriolis forces were enabled and the nonlinear finite amplitude option was utilized with wetting and drying enabled.

2.2. Improvements for the ADCIRC Tidal Database

Since the development of the ENPAC03 tidal database, many advances have occurred in global tidal databases, available coastal data, options within ADCIRC itself and general computing capability, thus allowing for the inclusion of additional coastal inland areas. For this current ENPAC tidal database, six areas of improvement were examined:

1. Assess the location of the open ocean boundary.
2. Improve the coastal resolution using the National Oceanic and Atmospheric Administration (NOAA) Vertical Datum Transformation (VDatum) product grids.
3. Update the deep-water bathymetry.
4. Use the latest global tidal database products for forcing on the open ocean boundary.
5. Compare three bottom friction schemes for improved accuracy.
6. Improve the model physics by enabling the advective terms within ADCIRC.

In the following subsections, the methods used for each of these areas are detailed. Actual improvements realized in the harmonic constituent accuracy will be presented in the results section.

2.2.1. Open Ocean Boundary Placement

While the removal of the amphidromic points from within the model domain significantly improved the results of the ENPAC03 database relative to the original 1994 database, the original intent of the ENPAC15 model was to include the Hawaiian Islands in the model domain. The operational mesh used by the Extratropical Surge and Tide Operational Forecast System for the Pacific Ocean (ESTOFS-Pacific), which was put into operation in June of 2014, was a good candidate for such an attempt [38]. Figure 2 shows the ESTOFS-Pacific model domain, along with the location of nearby amphidromic points and the various ENPAC domains.

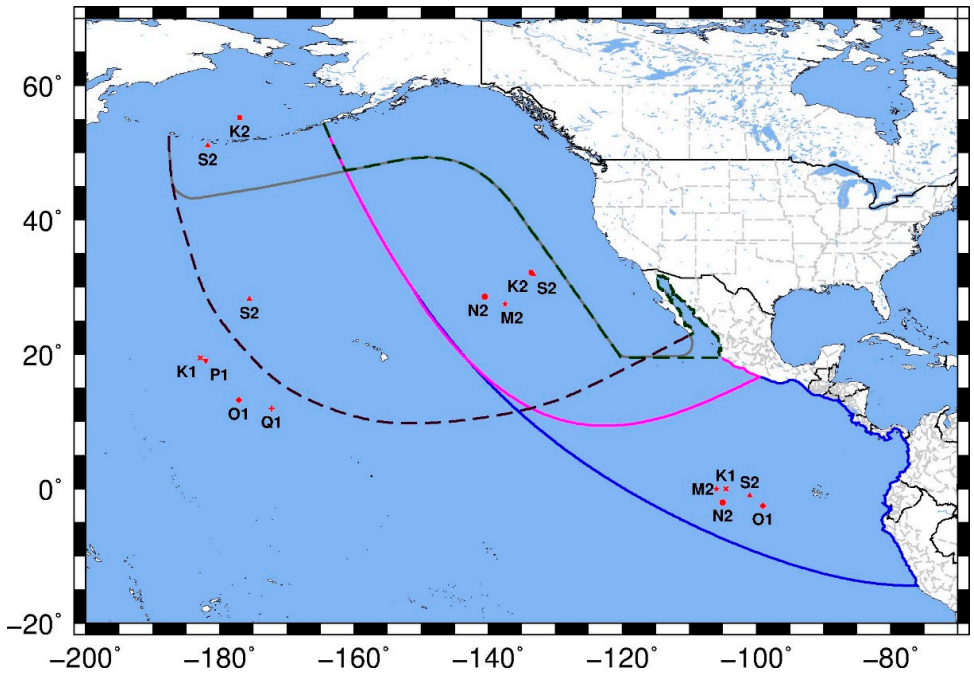

Figure 2. Location of amphidromic points relative to the ESTOFS-Pacific (dashed purple), ENPAC1994 (blue), ENPAC02 (magenta), ENPAC03 (dashed dark green) and ENPAC15 (gray) model domains.

During the development of the ESTOFS-Pacific model, it was determined that the semi-diurnal constituents were underestimated along the coast, particularly along Alaska. In order to mitigate that

this in the operational framework, a 20% increase of the semi-diurnal amplitudes along the open-ocean boundary had to be implemented [38]. While this fix was workable in the operational system (where the extended domain is necessary) and the amplitude errors at the Hawaiian Island stations were within acceptable bounds, it was determined that the over estimation at these island stations would not be acceptable in a tidal database. Furthermore, past experience with ENPAC1994 and ENPAC03 clearly indicate that the presence of the amphidromic points for the semidiurnal constituents within the domain degrades the harmonic results for the same constituents. Therefore, the coast-hugging paradigm of the earlier databases, which avoids these amphidromes, was continued for this version of the database, with the understanding that the Hawaiian Islands can be modeled with boundary conditions extracted from global tidal databases.

Further tests on the ENPAC03 model domain revealed that the presence of the shelf break across the open ocean boundary to the west prevented stable runs when ADCIRC's advective terms were enabled for use (this was confirmed upon examination of the ENPAC03 report as well [27]). Experience gained while updating the Western North Atlantic ADCIRC tidal constituent database revealed that the advective terms played an important role in reducing errors in the shallow near-shore regions [26]. In order to avoid the S2 amphidrome off the Aleutian Islands, an attempt was made to extend the ENPAC03 domain just west of the shelf near longitude -180°. Unfortunately, this was unsuccessful and the model was still unstable at the north-west extents of the open ocean boundary when the advective terms were utilized. Therefore, it was decided to extend the north-west boundary all the way out to the ESTOFS-Pacific extents, as that domain was stable when the advective terms were implemented. Although this incorporates one amphidrome within the domain, accuracy within that region of the model domain is already compromised by the treatment of the Aleutian Island chain as a closed mainland boundary—thus neglecting the interaction with the Bering Sea. Therefore, further inaccuracy in that immediate area was tolerable, with the caveat that the tidal database should not be used to extract boundary conditions for any points west of longitude -164.5° (Unimak Island, AK) where the previous ENPAC03 model domain ended.

Furthermore, the Baja Peninsula was also trimmed from the ENPAC03 model to remove any shelf issues on the south-east extents of the open boundary. The final open ocean boundary was chosen to curve smoothly from about Cabo San Lucas, Baja California Sur, Mexico to Seguam Island, Aleutians West, Alaska and hug the coast in a similar manner to the ENPAC03 model. Figure 2 above also shows the extents of the various ENPAC tidal database domains in relation to the ESTOFS-Pacific domain, as well as the approximate locations of nearby amphidromic points. Note that the ESTOFS-Pacific mesh was trimmed to the ENPAC15 ocean boundary for initial testing of the boundary location before the coastal resolution was increased; this mesh is referred to as ESTOFS-trim.

2.2.2. Increased Coastal Resolution

With each update to the ENPAC tidal database, as data and computational resources were more readily available, more resolution has been added to the coastline. As shown above in Table 1, the latest version has about twice the number of nodes when compared to the ENPAC03 mesh.

Over the past 20 years, NOAA has undertaken an ambitious study of the United States coastline to create a tool for transformation between different vertical datums. The VDatum (Vertical Datum Transformation) tool provides a single source for accurately and easily transforming geospatial data among different tidal, orthometric and ellipsoidal vertical datums along the Unites States coast. It allows the user to combine data from different horizontal and vertical reference systems into a common system in order to create integrated digital elevation models. The interested reader is referred to the VDatum website for more general information about the VDatum tool and for regional publications [39].

In order to create accurate tidal datum fields for the coastal regions, a series of highly resolved coastal grids were developed (or are being developed) for all United States waters. At the time of this study, the two most recent VDatum models available in the ENPAC15 model domain were the Pacific Northwest and Southern California domains, which together encompass the U.S. west coast

from Southern California to Washington. The domain for southeast Alaska was being developed concurrently with the ENPAC15 database and was not yet available to update the SE Alaskan coast. Individual reports [40,41] for each of the VDatum domains are available on the VDatum website.

It is important to note that the high-resolution meshes created for the VDatum project are in a Model Zero (MZ) vertical datum. The interested reader is referred to the VDatum Standard Operating Procedure manual [42], but the basic idea is that small corrections are added/subtracted from the original charted bathymetry in an iterative manner until the simulation converges to a solution. The converged solution is verified against harmonic constituent data available within the region. This was necessary because the original bathymetric sources were all in different tidal datums and no tool existed to transform them into a unified vertical datum. The resulting vertical datum of the high resolution coastline is MZ. Although, model zero is not necessarily the same as mean sea level (MSL) due to nonlinear dynamic effects, for our purposes, we have to assume that the VDatum coastline is approximately relative to MSL.

Additionally, it was desired to include the passages and channels north of Vancouver Island to better capture the hydrodynamics of the Salish Sea up through Johnstone Strait and Queen Charlotte Strait into Queen Charlotte Sound. This area has been extensively studied by the Institute of Ocean Sciences, Fisheries and Oceans Canada (IOS-FOC), who provided us with several unstructured mesh models, of which we decided to incorporate two: the Vancouver Island and Discovery Passage regions [43,44]. These meshes were used to guide our model development for that area, which could not be as detailed. Additionally, the unstructured meshes that had been modeled within a finite volume framework by IOS-FOC would not remain stable in the ADCIRC finite element framework.

As a first step, the Vancouver Island model was used as input to generate a localized truncation error analysis with complex derivatives (LTEA + CD) representation of the greater Vancouver Island region [45,46]. Then, bathymetric detail was updated where possible with the finer scale Discovery Passage model. Finally, extremely shallow regions were either removed by hand or artificially deepened. In general, the representation of that region was cut to the 3 m depth contour, unless that would eliminate important channels. If smaller channels that were important for hydraulic connectivity would be removed in this process, their minimum depth was set to 3.0 m and they were allowed to remain. As such, it is not expected that the results in the Canadian waters would be as accurate as those in the U.S. waters. However, as will be seen in the discussion of the ENPAC15 model results, the incorporation of these channels is important for accuracy in the Puget Sound region. The bathymetric profiles from the IOS-FOC models were in MSL.

Figure 3 shows the extents of the two VDatum and IOS-FOC nearshore domains superimposed on the ENPAC15 model domain, shown to clearly illustrate the regions where coastal resolution was updated. Note that the Discovery Passage region is only a very small part of the larger Vancouver Island domain so the details are not visible at this scale. Instead, a black box is shown around the region of the Vancouver Island model where the bathymetry was replaced with the highly resolved Discovery Passage model. Also note that, in the Kitimat region, the smaller inland channels, visible in the red boundary of Figure 3 near -127.5° longitude 52.5° latitude, were not included in the final ENPAC15 domain, as we are not interested in producing tidal data in that region of the Canadian waters and we had to minimize computational requirements.

Notice that there are several areas of overlap between these regional subdomains. For the overlap in the Pacific Northwest and Southern California VDatum domains, the individual grids were carefully pieced together in such a way as to preserve the source grid with the highest coastal resolution. For the offshore regions within these overlaps, a transitional mesh was created at an appropriate distance from the shoreline that smoothly blended the triangulations of the two VDatum meshes. Finally, the bathymetry from the highest resolution source was reapplied onto the new triangulation.

A slightly different approach was taken within the Salish Sea. A transect was chosen across the Strait of Juan de Fuca at about longitude -124.0°. This location was chosen because the resolution of the Pacific Northwest VDatum mesh and the LTEA + CD representation of the Vancouver Island

model from IOS-FOC was nearly the same at this location, providing a smooth transition from one model to the other. Additionally, a gentle curve just outside Queen Charlotte Strait to the southern coast of Vancouver Island was chosen as the extent at the other end of the northern Vancouver Island passages. This curve was chosen to encompass the shallow shelf off the northwestern tip of the island that was better represented within the IOS model and to ensure a smooth transition into the boundary of the Pacific NW model. Within the curved region and through the Salish Sea up to the transect across the Strait of Juan de Fuca, shown in Figure 3 by the thick blue lines, the model was taken from IOS-FOC sources. Everything outside of this region, including the triangulation for the southern coast of Vancouver Island, was taken from the Pacific Northwest VDatum mesh. However, the bathymetric representation for the southern coast of Vancouver Island was smoother in the IOS-FOC model, so the bathymetry for this immediate region was interpolated from the IOS-FOC model instead. The Puget Sound region was carefully compared to the VDatum model and it was determined that the resolution and bathymetry were essentially equivalent, with the exception of the occasional outliers in bathymetry that can sometimes occur during the model zero iterations of the VDatum process. Therefore, for ease of transition, the Puget Sound region was taken from the IOS-FOC model. Due to the ready availability of NOS data on the internet, the bathymetry sources was more than likely the same for both grids. The boundary was then smoothly transitioned into the Pacific Northwest VDatum model, in a similar manner to the process described earlier for the VDatum overlap region.

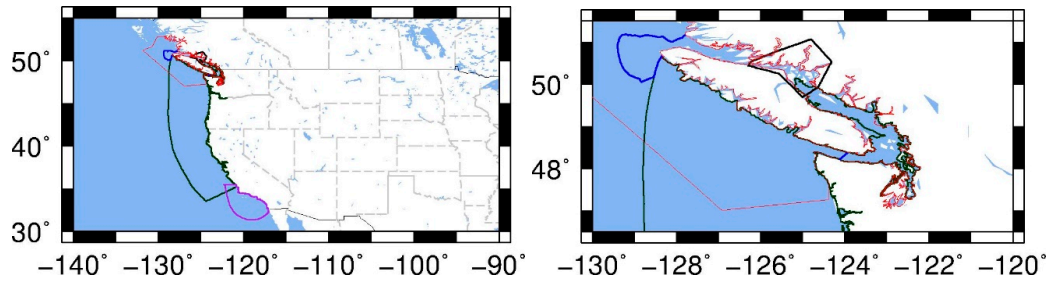

Figure 3. Location of available models for coastal refinement (extents only); global view (left panel) and zoom of Vancouver Island region (right panel): Southern California VDatum (purple), Pacific Northwest VDatum (dark green), Vancouver Island (red), Discovery Passage model (thick black), and location for merging Vancouver boundaries (thick blue).

A comparison of the Vancouver Island and Washington coast region in the ENPAC15 model and the previous ENPAC03 model is shown in Figure 4. Notice in particular that the passages north of the island have been added and in general that the newest model includes more inland channels, rivers and islands, as well as a more detailed shoreline in general. Also note that the region of larger elements south of Vancouver Island is a manifestation of the LTEA + CD process, which minimizes the number of elements in deeper regions.

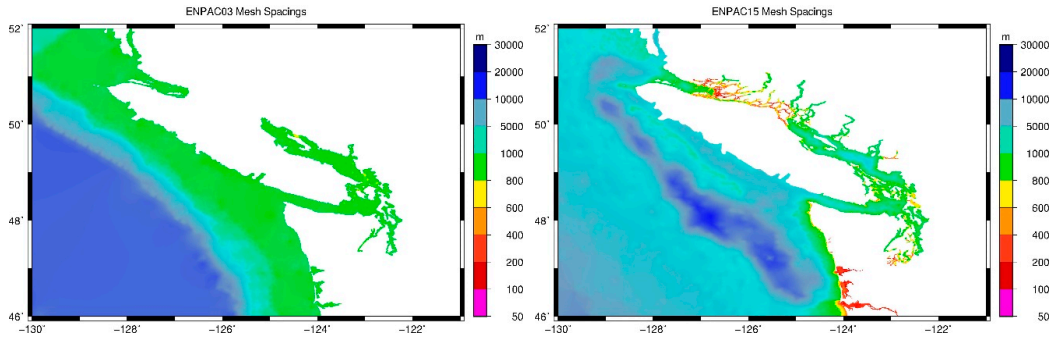

Figure 4. Comparison of coastal resolution in the ENPAC03 (left panel) and ENPAC15 (right panel) models for the Vancouver Island and Washington coast regions.

2.2.3. Updated Global Bathymetry

The final step of mesh development was to blend the highly resolved coastline into the global ocean described in Section 2.2.1 and update the deep-water bathymetry of the ENPAC03 model. The ESTOFS-Pacific model includes the most recent bathymetric profiles available from the National Ocean Service NOS/OCS hydrographic database maintained at the National Geophysical Data Center [47]. Additionally, the ESTOFS-Pacific model utilized the University of California-San Diego/Scripps' global 1-minute bathy/topo dataset [48] outside of the NOS survey areas. Therefore, it was decided that the most straightforward way to update the bathymetry in regions that were not included in VDatum grids or IOS-FOC grids was to trim the ESTOFS-Pacific mesh down to the ocean boundary selected for ENPAC15. This intermediate mesh was also used for some quick comparison tests because it was not as finely resolved along the coast; it will be referred to as ESTOFS-trim. Finally, the improved coastline from VDatum and IOS-FOC sources was merged into the ESTOFS-trim domain by removing all deep water from the merged coastal regions and creating a smooth mesh out to the boundary nodes; then, the ESTOFS-trim bathymetry was interpolated back onto the regions of the mesh that did not come from the high-resolution coastal domains. The resulting ENPAC15 model bathymetry, shown in Figure 5, is referenced to MSL.

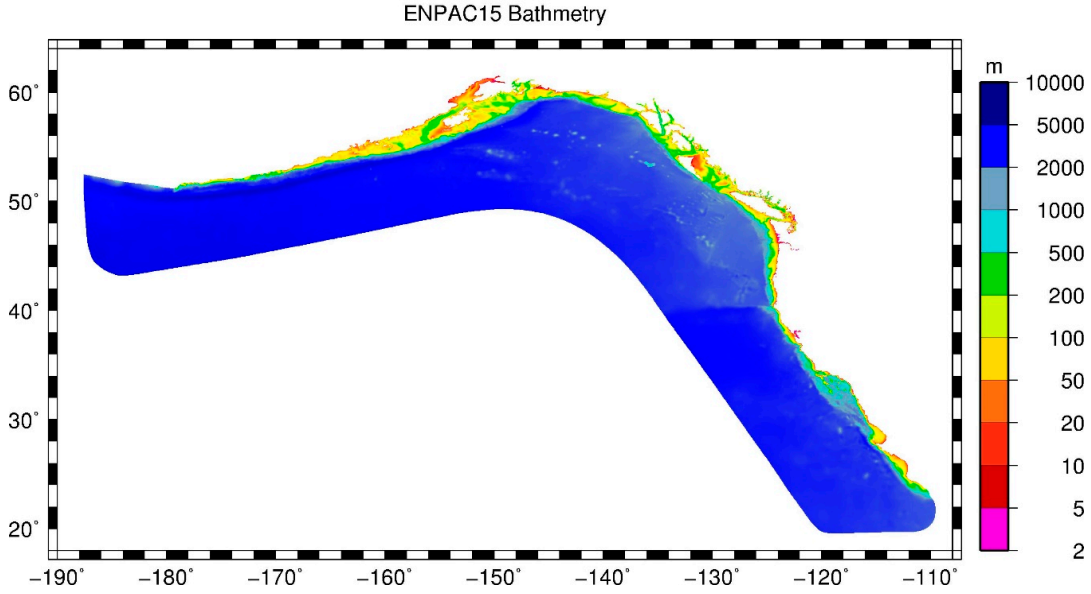

Figure 5. Bathymetry contours for ENPAC15 model.

2.2.4. Updated Open Ocean Forcing

Once an updated physical model had been developed for the entire ENPAC region, it was necessary to extract tidal forcing information from available global tidal models at the open-ocean boundary. Since the last version of the West Coast ADCIRC tidal database in 2003, significant improvements have been made in the global tidal modeling community as well. Herein, we compare two global models: the Oregon State University Tidal Inversion Prediction (sometimes called the OTIS or OSU TPXO system) and the French Tidal Group Finite Element Solution database (often simply called FES). Both of these use data assimilation methods for satellite altimeter data, such as Topex/Poseidon, in the development of their global database.

The FES model utilizes a global unstructured grid to model the tidal barotropic equations in a spectral configuration and then employs data assimilation from long-term satellite altimetry data to correct the tidal signals [49]. FES products are provided on a 1/16 degree resolution for 32 tidal constituents over the global ocean. The most recent version is FES2012, which is distributed by Aviso (Ramonville St. Agne, France) [50].

The OSU TPXO system follows the same general solution techniques with a least square best fit of the Laplace tidal equations and along track averaged data from Topex/Poseidon and Jason satellite altimetry [37,51,52]. The latest TPXO8-Atlas product provides 13 tidal constituents and utilizes a global structured grid with a resolution of 1/6 degree to model the global ocean with local patches of high resolution that use local refinement of 1/30 degree around many of the global coasts.

After extracting boundary information from the FES 2012 and TPXO8-Atlas databases, a visual comparison was made of the amplitude and phase information that would be used as input into the ADCIRC model; ten constituents are used to force the model (diurnal—O_1 K_1 P_1 Q_1; semi-diurnal—M_2 S_2 N_2 K_2; and long term—Mf Mm). In general, there were very few observable differences between these two models but those that did exist were typically concentrated near the coast, which may be due to the difference in near-shore resolution between the two global models. For the semi-diurnal constituents, the amplitude differences were focused near the southern boundary at Cabo San Lucas, Mexico (refer to Figure 1 or Figure 2 for geographic locations within the ENPAC domain); while the K_2 constituent also showed variation in phase along the northern boundary near Seguam Island, Alaska. Similarly, the P_1 and Q_1 constituents showed minor amplitude differences near both coastal boundaries and the other diurnal constituents were in good agreement for amplitude; while, for phase, the O_1 constituent was consistently 11–17 degrees higher along the entire ocean boundary for the TPXO8 database but was similar for the other three diurnal constituents. Finally, for the long-term constituents, both showed minor differences in amplitude and phase all along the boundary but were in fairly good agreement considering the small amplitudes (on the order of 10^{-3} to 10^{-2} m). A more quantitative comparison was made by calculating the maximum absolute difference in amplitude and phase over all 211 open ocean boundary nodes; these results are given in Table 2. Note that there was a single outlier in the S2 constituent phase for the forcing values extracted from the FES12 database; this outlier was removed before calculating the maximum absolute differences. These observations alone were not enough information to determine if one global model was better; actual ADCIRC harmonic differences due to the boundary forcing are examined in the results section.

Table 2. Maximum absolute differences in tidal harmonics for the ten forcing constituents used along the entire ENPAC15 boundary for the TPXO8-Atlas and FES2012 global tidal database products.

Harmonic	**O_1**	**K_1**	**P_1**	**Q_1**	**Mf**	**Mm**
Amplitude (cm)	0.77	1.04	1.58	1.30	0.09	0.09
Phase (degrees)	17.06	1.55	6.70	9.17	6.88	18.32
Harmonic	**M_2**	**N_2**	**S_2**	**K_2**	-	-
Amplitude (cm)	1.56	0.84	0.41	0.69	-	-
Phase (degrees)	2.05	9.21	2.82	22.39	-	-

2.2.5. Bottom Friction Assignment

In this study, three variations of the quadratic friction formulation were compared for the ENPAC15 database: a constant CF version and two variable friction formulations. For the first variable formulation, a combination of the CF values that had been developed for each of the VDatum regions was used, while the second scheme utilized the USGS Woods Hole Coastal and Marine Science Center's usSEABED [53] database of core samples to assign appropriate regional Manning's n friction values.

Of the two VDatum grids that fall within the ENPAC15 model domain, only the Pacific Northwest grid had a variable quadratic bottom friction scheme. Additionally, no bottom friction information was provided for the IOS-FOC domains in Canadian waters. Therefore, the values from the one available region were simply mapped onto the corresponding region of the ENPAC15 domain. Then, the default value from that domain (CF = 0.00375) was applied as the default for the entire ENPAC15 domain as well.

The usSEABED database contains three files for each region: "EXT—numeric data extracted from lab-based investigations, PRS—numeric data parsed from word-based data and CLC—numeric data

calculated from the application of models or empirical relationship files" [53]. Each of these datasets describes the data in different ways and has its own limitations; however, they can be combined to create a more extensive coverage of the seafloor characteristics. The database only covers the United States mainland coast and data was available only from about 117.00 W 32.24 N (north of the border with Mexico) to 122.57 W 48.78 N (near the SE end of the Strait of Georgia). Within this region, a multi-step process was utilized: (1) the three datasets were compared to make sure that they were in general agreement; (2) outliers from the comparison stage were removed; (3) duplicate points were preferentially taken from the EXT dataset; (4) the edited files were then combined into a single data source; (5) the combined file was then assessed and filtered one more time to remove large outliers that affected a wide region due to the sparsity of the data; and (6) finally any points that fell outside of the 1000 m bathymetry contour were removed. This final dataset was then interpolated onto the ENPAC15 model domain within the applicable region only.

The remainder of the domain was assigned shelf-wide values based on anecdotal evidence since no data was available and a depth-interpolation method similar to that used for the EC2015 database was used [26]. Namely, each larger coastal area was assigned a descriptive designation with an associated range of Manning's n values based upon typical values from literature. After a region was classified by bed type, depth-dependent interpolation was used to assign Manning's n values over each section of the coastal shelf. For water depths between 0 m and 5 m, the maximum value was assigned; for depths between 5 m and 200 m, values were linearly interpolated from the maximum at 5 m depth to the minimum value at 200 m depth; for depths between 200 m and 1000 m, the minimum manning value was assigned; finally, for depths greater than 1000 m the post-Ike "deep ocean" value of 0.012 was assigned. Table 3 provides the rough geographical regions that were used in this process, as well as the assigned min/max Manning's n values.

Table 3. Geographic regions used for Manning's n assignment.

Geographic Region	Bed Description	Minimum n Value	Maximum n Value
Baja California	Sandy/gravel	0.022	0.025
U.S. Mainland	assigned from usSEABED data		
S. Vancouver Island	Sandy/gravel	0.022	0.025
N. Vancouver Island	Gravel/rough rock	0.025	0.050
Alaska/ BC	Gravel/cobble	0.025	0.030

2.2.6. Inclusion of ADCIRC Nonlinear Advective Terms

The final effort to improve the physics was to include the nonlinear advective terms in the ADCIRC modeling setup; the interested reader is referred to [54] for details about the development of these terms and equations. In practice, these terms enter in by activating two flags in the ADCIRC input control file. In all previous versions of the ENPAC tidal database, the westernmost edge of the open ocean boundary over the shelf break near Unimak Island, Alaska caused instabilities when the advective terms were activated. Therefore, it was not possible to include advection and compare how the tidal response varied due to these terms. With the new extended open ocean boundary, it is possible for the model to remain stable with these terms activated.

2.2.7. Summary of Tidal Database Improvements

Six different areas of improvement have been presented for the ENPAC15 tidal database. When possible, each model improvement was isolated to determine the accuracy improvement due solely to that component of the project. However, the updated global bathymetry and open-ocean boundary location were combined in the intermediate ESTOFS-trim modeling domain and were not studied individually (recall that the ESTOFS-trim model is a reduction of the ESTOFS-Pacific operational model trimmed down to the ENPAC15 ocean boundary). A summary of the simulations

that were completed for this study, including the run designation, description, model domain, advection terms, bottom friction scheme and open ocean boundary forcing are provided in Table 4. For the boundary forcing, the textual label before the dash indicates which global tidal database was used while the number after the dash indicates how many constituents were used. In all subsequent sections, the results will be referred to by the run designation given in this table.

Table 4. Summary of ADCIRC model parameters for the model simulations completed in this study.

Run Designation	Description	Grid	Advection	Friction	Boundary Forcing [1]
ENPAC03	ENPAC03 extract	ENPAC03	Off	0.0025	TPXO6-8
ENPAC03R	ENPAC03 rerun	ENPAC03	Off	0.0025	TPXO8-10
ESTOFS-trim1	TPXO 8.0 forcing	ESTOFS-trim	Off	0.0025	TPXO8-10
ESTOFS-trim2	Advection on	ESTOFS-trim	On	0.0025	TPXO8-10
ESTOFS-trim6	FES 2012 forcing	ESTOFS-trim	Off	0.0025	FES12-10
ENPAC15-CF	Constant friction	ENPAC15	Off	0.0025	TPXO8-10
ENPAC15-Vdat	ENPAC15 release	ENPAC15	Off	VDatum	TPXO8-10
ENPAC15-Mann	Manning's n friction	ENPAC15	Off	Manning	TPXO8-10

[1] The label before the dash indicates which global tidal database was used, while the number after the dash indicates how many constituents were included.

To confirm that we could expect a fair comparison between all results, the ENPAC03 tidal database was rerun with the same version of ADCIRC (v51.06) used in this study. Error analysis verified that the new version of ADCIRC was recreating the harmonic constituents. In subsequent sections, all reference to ENPAC03 results indicate that constituents were directly extracted from the previous version of the database at the same locations as the recent improvements. Meanwhile, the ENPAC03 model domain was also rerun with the same input parameters as the ESTOFS-trim model, including tidal forcing extracted from the global TPXO8 database at the ENPAC03 boundary. Results from this run are denoted by ENPAC03R and are used to test the effects due solely to the boundary location. Note that these were two separate reruns: one with the same input as the original ENPAC03 tidal database to verify that nothing substantial has changed in the ADCIRC model itself (results are not shown herein), and another to mimic one of the ESTOFS-trim model results for boundary comparison (ENPAC03R).

A series of simulations using the ESTOFS-trim model were conducted to test the overall effect of the various database improvements in a faster computing environment. While many such runs were conducted, only three of these tests are discussed herein for comparison of the individual effects of boundary forcing, advective terms and coastal resolution. Recall that the ESTOFS-trim model includes more coastal features than the ENPAC03 model but is not as highly resolved as ENPAC15. Finally, three bottom friction schemes were explored using the full ENPAC15 model; these are denoted by ENPAC15-CF for constant friction, ENPAC15-Vdat for VDatum friction and ENPAC15-Mann for Manning's n friction.

2.3. Validation of the Improved ADCIRC Tidal Database

Three sources of harmonic constituent data were used to validate the new ENPAC15 tidal database; these sources are discussed in Section 2.3.1. Additionally, the various analysis techniques used to compute model errors are discussed in Section 2.3.2.

2.3.1. Validation Data

The National Oceanic and Atmospheric Administration's Center for Operational Oceanographic Products and Services (CO-OPS) keeps a record of tidal harmonic constituent data at stations throughout the coastal United States [55]. Tidal harmonic data was available at 139 such stations in the ENPAC domain. Further data was obtained for 39 stations within Canadian waters from the Institute of Ocean Sciences, Fisheries and Oceans Canada (IOS-FOC) [56]. Finally, historical data from the International Hydrographic Organization (IHO) was used to provide wider coverage, specifically in the deeper regions [57]. There is a certain degree of uncertainty in the IHO data, as information about the source of the constituents (e.g., length of analysis and data records) is not always available;

furthermore, the longitude and latitude coordinates used to locate the stations are only specified to three-decimal digits precision, which is sometimes insufficient to determine the physical location of the data collection. Of the about 4190 IHO stations available worldwide, 141 can be accurately located within the ENPAC15 domain; however, only 80 of those are unique locations not already provided in the other data sources (the 61 duplicates are used to assess the accuracy of the data itself). For skill assessment purposes, a total of 258 stations (139 from CO-OPS, 39 from IOS-FOC and 80 from IHO) were classified into three regional locations: California/Mexico, Oregon/Washington and British Columbia (Pacific Northwest) and Alaska. The global locations of the 258 available data stations are shown in Figure 6; while zoomed views with station numbers are provided in Appendix A.

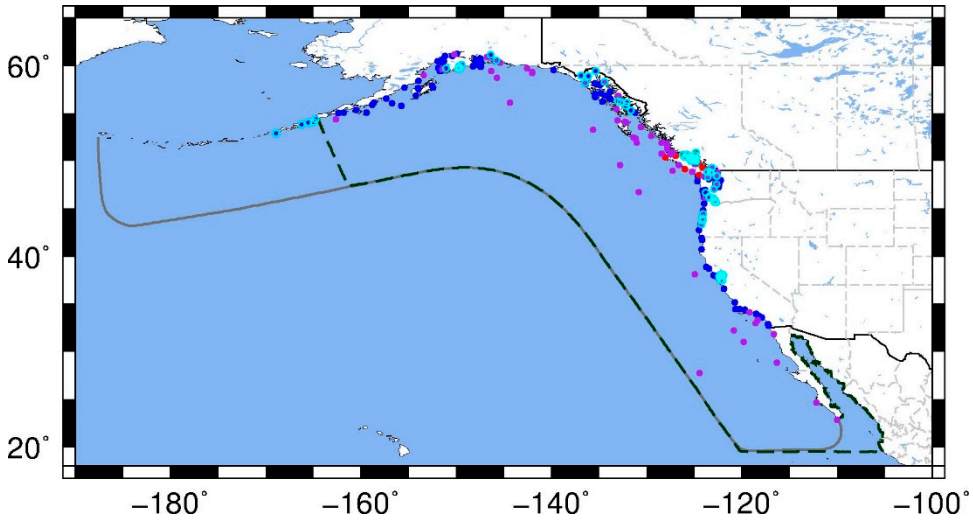

Figure 6. Locations of the 258 available validation stations shown with the ENPAC03 boundary (dashed dark green) and ENPAC15 boundary (gray); stations from three sources: CO-OPS (blue), IOS-FOC (red), and IHO (purple) with dry stations denoted with a cyan circle. Zoomed regional views provided in Appendix A.

Of these 258 stations, only 179 were considered "wet" in the ENPAC03 model—96 are truly within the bounds of the ENPAC03 model and the other 83 are close enough to the boundary to warrant including them (by using nearest element approximations). Stations that were far inland or within small channels that were not physically represented in the older database are not extracted from the ENPAC03 database. For Figure 6 and all the figures in Appendix A, data locations shown with a cyan circle around them are not wet in the ENPAC03 domain and are excluded from any error comparisons that specifically say that only wet stations were used. Appendix B provides a list of the station number, physical location (used for extraction from the ADCIRC databases), station name, assigned region, and the data source for all available stations.

2.3.2. Validation Methods

The same error measures as were used in the EC2015 study are used herein to determine which model best captured the tidal harmonics at the available data stations. For each station, scatter plots of measured and computed amplitude and phase were examined for the eight primary tidal constituents (M_2, S_2, N_2, K_2, O_1, K_1, P_1 and Q_1). Ideally, these plots would have a one-to-one correspondence. Scatter plots including all stations were also made for each of these eight constituents independently and a least-squares linear regression was computed. Additionally, scatter plots comparing the ENPAC03 and ENPAC15 databases for each of these eight constituents were created using 165 of the wet stations in the ENPAC03 database (fourteen of the wet British Columbia stations were neglected because they were located too close to the passages north of Vancouver Island, which were not resolved in the ENPAC03 model).

In addition to the above qualitative measures, three quantitative error measures were calculated to compare the skill of each model. For both the phase and amplitude, the mean absolute error (MAE) was computed as

$$\text{MAE} = \frac{1}{8\,np}\sum_{e=1}^{np}\sum_{k=1}^{8}\left|data_{e,k} - model_{e,k}\right|, \tag{1}$$

where the absolute errors are summed over both the number of constituents (k) and the number of data points for a region (e). To calculate the mean errors for an individual constituent, the second sum would only be computed for k = 1 and the 8 is removed from the denominator. In all of the error plots that follow, the first eight points on the left side are for the individual constituents summed for all data stations and the regional error means are shown on the right, separated by a vertical line.

Due to some constituents having very small amplitudes, the mean relative error (MRE) was computed for amplitudes only as

$$\text{MRE} = \frac{1}{8\,np}\sum_{e=1}^{np}\sum_{k=1}^{8}\frac{\left|data_{e,k} - model_{e,k}\right|}{data_{e,k}}, \tag{2}$$

where the same summation rules apply. Note that if the errors are on the same order of magnitude as the data, the relative errors will be close to 100%. Additionally, a composite error, combining the errors in phase and amplitude for each constituent into a single error metric, was computed for each station as

$$A_E = \sqrt{0.5(A_m^2 + A_o^2) - A_m A_o \cos(\pi(h_m - h_o)/180)}, \tag{3}$$

where A_m is the modeled amplitude in meters, A_o is the observed amplitude in meters, h_m is the modeled phase (degrees GMT) and h_o is the observed phase (degrees GMT). As before, the mean root-mean-square error (RMSE) was computed by summing over the number of data points for any region as well as the number of constituents,

$$\textit{Mean}\ \text{RMSE} = \frac{1}{8\,np}\sum_{e=1}^{np}\sum_{k=1}^{8}(A_E)_{e,k}. \tag{4}$$

To compare the skill of the new ENPAC15 database versus the previous ENPAC03 database, harmonic constituents were extracted from the 2003 database at the stations that were within (or close enough to) the bounds of the ENPAC03 model, the wet 2003 stations. Additionally, when comparing the two database versions, only the data stations that were not located within or too close to the inside passages north of Vancouver Island were used for global statistics, even if they were designated as wet (this is due to the fact that, without the passages in the domain, the results for ENPAC03 database at these stations are not valid). Of the 179 stations that were considered wet within the ENPAC03 model, only 165 were used for global statistics; mean errors were then computed for both databases at those 165 locations. However, mean errors were also calculated at all 258 stations for the new ENPAC15 database, as it was not limited by the missing passages. Table 5 provides the total number of stations in each region that were used for statistics for each model. For reference, parenthetical numbers include only the stations that were physically within the lower resolution domains, not the nearest neighbors. Note that station details are also provided for the ESTOFS-trim model; however, in order to be consistent when comparing errors, only the 165 wet (non-passage) ENPAC03 stations are used for computing errors on this model domain.

Table 5. Total number of validation stations available in each region for the most recent models in the ENPAC region.

Model	Global	Alaska	Pacific Northwest	California and Mexico	Deep
ENPAC03	179 (96) [1] /165 [2]	61 (35)	70 (34)	37 (16)	11
ENPAC15	258	84	116	47	11
ESTOFS-trim	180 (162)	83 (81)	54 (41)	32 (29)	11

[1] Numbers in parentheses indicate how many were within the model domain while the first number includes those stations approximated with nearest neighbors. [2] Fourteen of the wet stations in the Pacific Northwest region were located within the inside passages above Vancouver Island and were not included in the global statistics or the global constituent scatter plots; therefore, there are 165 stations that were used in global statistics/scatters—subsequently indicated by Global (no passage).

3. Results

3.1. Results for the Various Improvements

In this section, some of the model improvements are examined independently to determine how each improvement affects the RMS error. Full error analysis, as described in Section 2.3.2, will be provided in Section 3.2, where the ENPAC03 model is compared to the final release ENPAC15 model. Figure 7 presents the regional mean RMS errors for all eight simulations that were previously presented in Table 4. These mean errors were computed using the 165 wet stations that are common to all model domains (recall that global statistics do not include the 14 stations that are inside the passages around Vancouver Island). Recall also that the ENPAC03R results are from a substantially different simulation than the original extraction from the ENPAC03 database. Differences include: (1) length of simulation (410-day versus 60-day); (2) nodal factors (specific factors for analysis annum 2005 versus default nodal factors); and (3) application of boundary conditions (extracted from the newer TPXO8-Atlas database for 10 constituents versus only the eight primary constituents from the TPXO6 database), such that we would not expect the resulting composite errors to be the same.

While not shown herein, it is of note that the stations located in deeper water and along the Mexican coast do not realize any significant improvements for any of the various models since the modeling domain itself is largely unchanged in this area and the most significant change is related only to the global tidal boundary forcing. Four regions are used for regional error summation: Global (without the passages), Alaska, Pacific Northwest (includes British Columbia, Washington and Oregon) and California/Mexico.

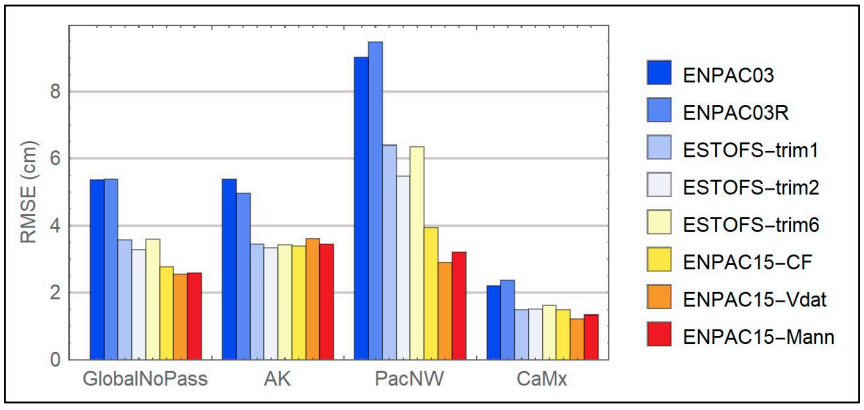

Figure 7. Comparison of regional mean root mean square errors using the 165 wet stations (neglect the stations near inside passages) for all eight study simulations summarized in Table 4.

3.1.1. Comparison of Boundary Placement

As described in Section 2.2.1, the open ocean boundary has been moved further west of the shelf near the Aleutian island chain and continues to hug the coastline to avoid amphidromic points. In order to test how much of an affect the new boundary placement has on the extracted harmonic constituents, the old ENPAC03 model was run with an identical input file as was used for the ESTOFS-trim model: all input parameters are as described in Section 2.1.2.

Concentrating only on the ENPAC03R and ESTOFS-trim1 bars in Figure 7, we note that significant gains in accuracy are realized for all regions, with percent reductions ranging from 30% in Alaska to 37% in California. Unfortunately, it is difficult to determine if this is related solely to the new open boundary location or the change in resolution along the boundary itself for the ESTOFS-trim model domain. Additionally, the deep-water bathymetry was also updated in the ESTOFS-trim model, making it difficult to separate the individual effects of boundary placement, boundary coarseness and deep water bathymetry.

3.1.2. Comparison of Open Ocean Boundary Forcing

As described in Section 2.2.4, two different global tidal databases have been examined as input to the ENPAC15 model: FES12 and TPXO8-Atlas. Looking at the ESTOFS-trim1 and ESTOFS-trim6 bars in Figure 7, we note that the composite errors are similar for all regions; however, the errors from the FES12 boundary conditions are slightly higher, more noticeably in the southern region. These differences are not significant, however, and given the historical application of TPXO products for boundary forcing in the ADCIRC tidal databases and its slightly better performance in this application, it was decided to use the TPXO8-Atlas global products for this latest database update. Meanwhile, examining the ENPAC03 and EPAC03R bars, the inclusion of the two long-term forcing terms (Mm and Mf) and the updated global forcing from TPXO6 to TPXO8 does not appear to significantly affect the results; there are minor changes in the regional mean RMS errors but not globally.

3.1.3. Comparison of Advection

As described in Section 2.2.6, it was desired to include the advective terms within ADCIRC for the latest update. When examining the ESTOFS-trim1 and ESTOFS-trim2 bars, we note that while there is no noticeable difference in the California and Alaska stations, there is a significant improvement (mean RMS error reduction of 0.9 cm or 14%) in the Pacific Northwest stations when the advective terms are utilized, which also improves the global performance. Examination of individual stations in this region indicates typical mean RMS error reductions of 1.5 to 2.0 cm in the inside passages north of Vancouver Island and a maximum reduction of 3.43 cm. This is to be expected since the region north of Vancouver Island has been documented to dissipate a great deal of turbulent and internal tidal energy [43,58], which are not explicitly accounted for in the ADCIRC model. The utilization of the advective terms would allow the model to account for some of this nonlinear dissipation. However, when we turned these terms on with the fully resolved ENPAC15 model domain, instabilities developed in the shallow and narrow passageways north of Vancouver Island. Efforts are ongoing to stabilize this region (through further grid and bathymetry refinement) and allow for incorporation of the advective terms in an updated release, but for now the ENPAC15 tidal database does not include these terms.

3.1.4. Comparison of Increased Coastal Resolution

As described in Section 2.2.3, several refinements were made to the coastal geometry and bathymetry along the North American west coast. Since the operational ESTOFS-Pacific mesh (from which the ESTOFS-trim mesh was cut away) has an even coarser resolution along the coastline than the ENPAC03 model domain, we can compare the ESTOFS-trim1 and ENPAC15-CF bars in Figure 7 to get an idea of what affect this additional resolution has. Recall that we would not expect any improvement in the Alaska region because the coastal resolution was not updated in that area.

Similarly, no improvement is noticed in the mean RMS errors in the California region. However, more significant improvements (38%) are realized in the Pacific Northwest stations, which reduces the global error by 22%. Much of this improvement is likely due to the inclusion of the passages north of Vancouver Island, which were previously absent from all of the ADCIRC tidal databases for the ENPAC region.

3.1.5. Comparison of Bottom Friction Schemes

In this study, three different bottom friction schemes are compared: constant CF = 0.0025, VDatum quadratic friction coefficients and Manning's n formulation with n values estimated using the USGS usSEABEDS data. Looking at the mean RMS errors for all of the ENPAC15 bars in Figure 7, we note that both of the variable friction options (VDatum and Manning's n) provide lower errors than the constant CF version. Furthermore, there is a slight improvement of the VDatum versus Manning's n friction schemes. When we recall that the VDatum scheme is essentially constant everywhere except the Columbia River, then it would appear that the slightly higher default value (CF = 0.00375) is responsible for this error reduction rather than the variability of the friction itself. Additionally, we note that the friction schemes tested in this study do not appear to affect the Alaska region much at all, which might be expected since the coastal bathymetry and resolution has not been updated and most of the water is deep enough to make the friction irrelevant.

3.2. Comparison of ENPAC15 and ENPAC03

For this latest ENPAC15 tidal database release, the VDatum friction formulation was used; all other model input parameters are as described in Section 2.1.2. For results and discussion, when we refer to ENPAC03, we have extracted tidal harmonics directly from the previously released database. Scatter plots of computed versus measured amplitudes and phases (and their linear best-fit) for the ENPAC03 and ENPAC15 databases are shown in Figure 8 for the dominant diurnal and semi-diurnal tidal signals: K_1 and M_2. Additionally, Table 6 provides the best fit statistics for all eight primary constituents at the 165 validation stations that are common to both databases (neglecting the inside passage stations). For a perfect fit of the validation data, both the slope and R^2 values would have a value of unity. Notice that the slope is improved for nearly all of the eight constituents, with the exception being O_1 amplitude, Q_1 amplitude and phase, and K_2 amplitude; meanwhile, the R^2 value is closer to unity for all amplitudes and phases, indicating a tighter distribution.

Table 6. Summary of best-fit linear statistics for the 165 common validation stations in the ENPAC03 and ENPAC15 tidal databases.

Tidal		**Harmonic Amplitudes**							
Database		O1	K1	P1	Q1	M2	S2	N2	K2
ENPAC03	Slope	0.982	0.943	0.937	0.967	0.953	0.883	0.931	1.008
	R^2	0.968	0.960	0.976	0.974	0.962	0.955	0.958	0.856
ENPAC15	Slope	1.033	1.027	0.981	0.962	0.968	0.949	0.951	0.975
	R^2	0.996	0.998	0.994	0.989	0.991	0.989	0.988	0.989
Tidal		**Harmonic Phases**							
Database		O1	K1	P1	Q1	M2	S2	N2	K2
ENPAC03	Slope	1.001	0.988	0.980	0.937	0.988	0.960	0.964	0.980
	R^2	0.988	0.994	0.996	0.936	0.982	0.966	0.986	0.970
ENPAC15	Slope	0.996	0.996	0.994	0.923	0.997	0.996	0.995	0.985
	R^2	1.000	1.000	1.000	0.941	0.999	0.999	0.999	0.998

Similarly, if we look at scatter plots of individual stations, we can compare how each of the databases performs for that point. Since there are 258 validation stations, only a few representative stations are provided herein. Figures A6–A14 in Appendix C provide plots for the eighteen stations

that were shown by a black X in Figures A1–A5 in Appendix A; plots are grouped together by sub region: Southern California, San Francisco Bay, Northern California, Washington/Oregon, Puget Sound, British Columbia, Southeast Alaska and Southern Alaska. In order to illustrate the station differences due to the friction formulation, results for both the VDatum and Manning's n friction formulations are shown in these plots, along with the extracted ENPAC03 results. Other than the bottom friction itself, all other ADCIRC parameters are the same for the two newer data sets.

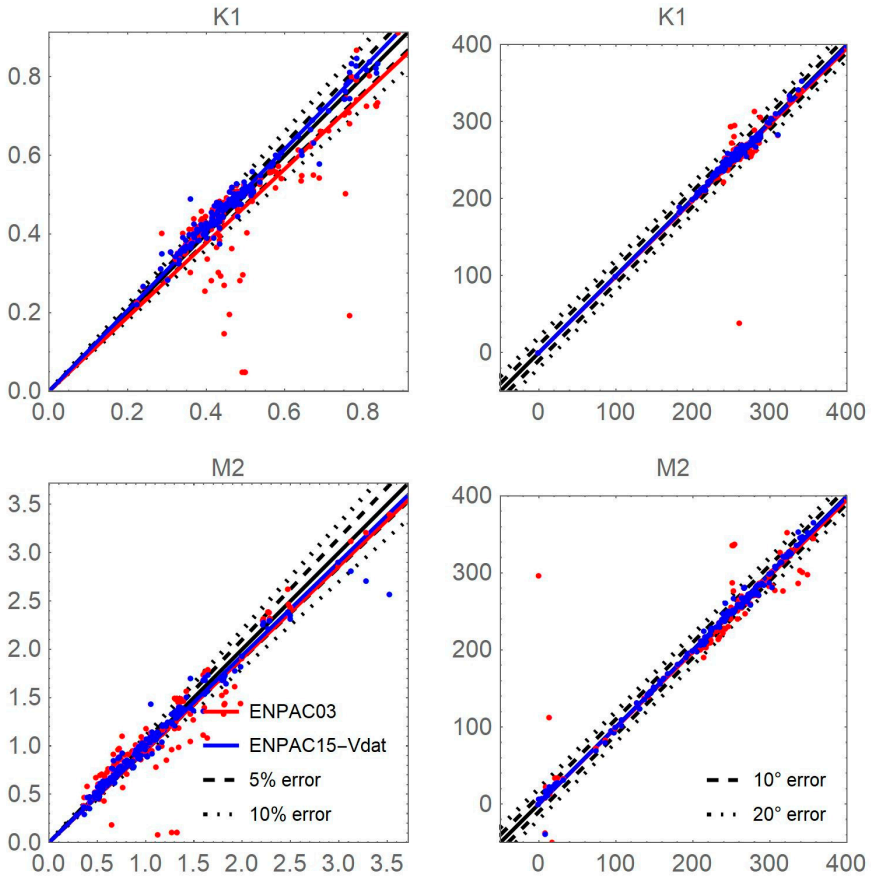

Figure 8. Comparison of scatter plots for the dominant constituents (K_1, M_2) for the ENPAC03 and ENPAC15 tidal databases using the 165 common validation data stations.

We note that very little improvement is seen in the Southern or Northern California stations (Figures A6 and A7), which is expected since the coastline and bathymetry did not change drastically. However, the San Francisco Bay region is more resolved in the newer database, resulting in better amplitude and phase correspondence; note also that the friction formulation makes a significant difference in this shallower water body. Similarly, along the Washington and Oregon coasts, there is marked improvement in the new database due to the inclusion of more coastal features and upper bay water bodies. In the Puget Sound region (Figure A10), we note that the friction formulation plays a more significant role at these shallower stations; and that the phase has been improved but there is still room for improvement in the dominant amplitudes. Notice that the inclusion of the passages north of Vancouver Island has significantly improved the amplitude and phase responses at the stations on either end of the passage (stations 146 and 176), despite them being far removed from the interior passages. Results are not shown within the passages themselves, since the region was not resolved in the ENPAC03 database and no comparison can be made; however, the new database has fairly good agreement throughout this region, although the dominant constituents are overestimated. Additionally, no real improvement is noticed on the southern extents of Vancouver Island since no additional coastal refinement was added. Despite the fact that very little coastal refinement was added

in the Southeast Alaska region, there are significant error reductions at these stations (Figure A12). Meanwhile, the Southern Alaska coast, which had few improvements in coastal resolution but several bathymetry corrections in this latest database, has minor amplitude improvement. Note that the results along the Alaskan coast are largely independent of the friction scheme, except for the shallower areas (station 117 in Figure A13).

A comparison of constituent RMS errors by region are shown in Figure 9, while mean absolute phase errors and mean relative amplitude errors are provided in Table 7. Looking primarily at the 165 validation stations that are common to both databases (blue diamonds for ENPAC03 and red circles for ENPAC15), we can draw several general conclusions.

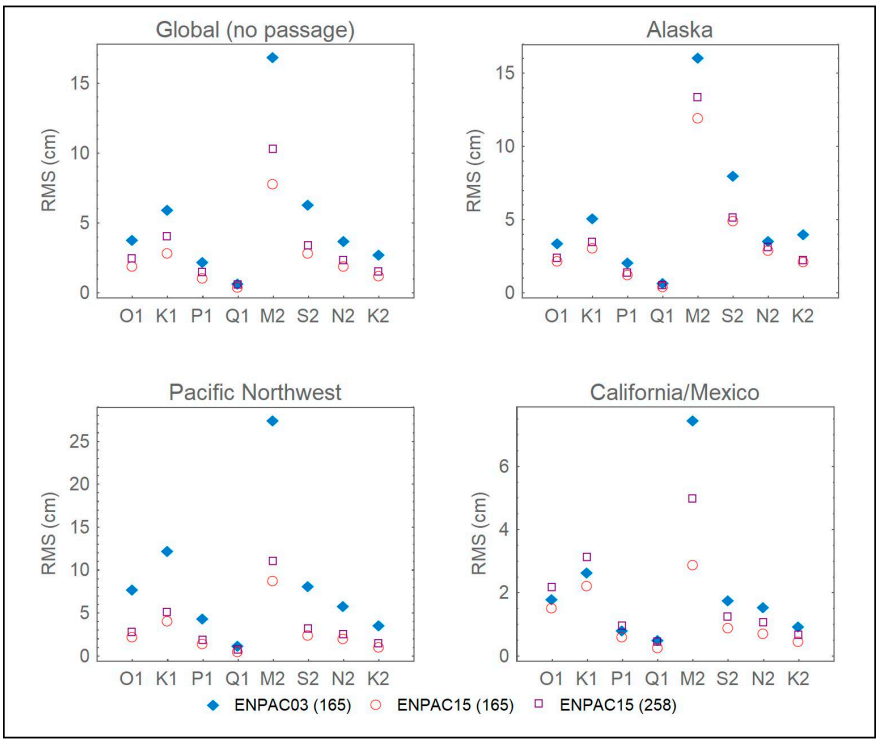

Figure 9. Mean root mean square errors (cm) in harmonic constituents for the ENPAC03 and ENPAC15 ADCIRC tidal databases for each region of the ENPAC model domain (note that the scale is not the same for each region).

- Globally, the greatest improvement in the RMS error is realized for the M_2 constituent (9 cm reduction) and the average reduction is 2.8 cm. Reductions in absolute phase errors range from 4° for the K_1 constituent to 13° for the S_2 constituent, with an average reduction of 8° over all of the constituents. Meanwhile, reductions in mean relative amplitude errors range from 3% for the O_1 constituent to 17% for the K_2 constituent, with an average reduction of 7%. For all error measures, the largest reductions were realized for the semi-diurnal constituents.
- For the Alaskan region, the reductions in RMS errors range from 0.2 cm for the Q_1 constituent to 3.7 cm for M_2, with an average reduction of 1.6 cm. Reduction in absolute phase errors ranged from 1.2° for the M_2 constituent to 6.7° for the K_2 constituent, with an average of 3.5° for all constituents, while the relative amplitude error reductions ranged from about 2% for Q_1 to 20% for K_2, with an average of 6%. In general, the largest amplitude reductions were realized for the semi-diurnal constituents, but the phase errors improved most for the diurnal constituents.
- The greatest improvement was realized in the Pacific Northwest region. Mean RMS error reductions ranged from 0.6 cm for Q_1 to 18.7 cm for M_2, with an average improvement of 6 cm. Meanwhile, the range of mean absolute phase error improvements varies from 8° for K_1 to 37° for K_2, with an average improvement of 21°; and the relative amplitude improvements range

from 7% for P_1 to 29% for K_2, with an average of 13% overall improvement. The semi-diurnal constituents realize the greatest overall improvement in amplitude and phase.

- In the California and Mexico region, moderate improvements are realized; the mean RMS errors improve by 0.2 cm for Q_1 to 4.6 cm for M_2, with an average of 1 cm. Similarly, improvements in the mean absolute phase errors range from 0° for K_1 to 6.2° for K_2, with an average improvement of 2.6°, while improvements in the relative amplitude errors range from 0.6% for O_1 to about 8% for Q_1, with an average improvement of 4% overall. Again, the semi-diurnal constituents realize the greatest overall improvement in amplitude and phase.

Table 7. Comparison of mean relative amplitude (%) and mean absolute phase errors (deg) by region for each of the eight primary harmonic constituents and summed over all 8 constituents for the ENPAC03 (2003) and ENPAC15 (2015) tidal databases: only the 179 wet validation stations are used in the summations.

Mean Relative Amplitude Errors (%)								
	Global (No Passage)		**Alaskan Coast**		**Pacific Northwest**		**California/Mexico**	
	2003	2015	2003	2015	2003	2015	2003	2015
O1	9.68	6.41	8.51	6.55	17.30	5.13	8.60	7.96
K1	10.84	4.93	9.32	4.65	17.10	4.20	9.27	6.94
P1	9.58	5.75	8.44	5.04	14.14	6.77	7.70	5.04
Q1	11.13	7.47	7.56	5.82	18.57	9.27	14.10	6.54
M2	12.49	5.85	10.71	4.73	20.67	10.66	11.07	5.07
S2	16.24	6.93	13.76	6.36	26.54	11.25	11.15	5.62
N2	12.94	6.68	11.37	6.61	21.26	10.45	9.24	5.22
K2	26.10	9.05	26.21	6.44	44.87	15.82	14.00	9.34
All 8	13.64	6.62	11.98	5.78	22.61	9.18	10.61	6.47
Mean Absolute Phase Errors (deg)								
	Global (no Passage)		**Alaskan Coast**		**Pacific Northwest**		**California/Mexico**	
	2003	2015	2003	2015	2003	2015	2003	2015
O1	10.45	3.32	7.91	3.71	21.44	3.85	3.87	2.62
K1	7.13	3.31	7.78	3.85	12.21	4.33	2.30	2.30
P1	9.06	4.05	8.76	5.03	16.77	4.38	3.45	2.78
Q1	13.79	9.36	20.77	16.73	16.22	4.50	4.74	3.46
M2	13.33	3.82	5.90	4.75	29.71	4.16	6.30	2.21
S2	17.00	4.24	8.14	5.46	35.57	4.04	5.69	2.64
N2	13.64	4.60	7.24	5.40	25.62	4.72	7.44	3.21
K2	20.94	8.11	17.97	11.27	44.86	7.95	11.16	4.96
All 8	13.15	5.05	10.54	7.01	25.46	4.74	5.63	3.02

Finally, it is also instructive to see if there are sub-regional patterns in the errors (at the individual water body scale), which can help to guide future efforts at improving the tidal database. Plots of relative amplitude and absolute phase errors for the dominant M_2 constituent at each of the 258 stations are provided for the global domain for the ENPAC15 model in Figure 10 in the text, while zoomed views of the smaller sub-regions are provided in Figures A15–A25 in Appendix D (the same zoom views given in Appendix A). For this study area, the M_2 constituent is dominant for all regions except the inside passages north of Vancouver Island and Puget Sound, where the K_1 constituent is of similar magnitude in some areas. Therefore, error plots for the K_1 constituent are also provided for the Puget Sound sub region (Figure A20) and the Vancouver Island sub region (Figure A22). Points shown in blue are underestimating the amplitudes (or exhibit a phase lag), while points shown in red are overestimating (exhibit a phase lead). The symbol shapes indicate to what degree the model is over/under estimating; we would like to see amplitude errors less than 10% and phase errors less than

20°. Unless specifically noted, all subsequent comments refer to the M_2 constituent. Several general trends can be gleaned from these plots.

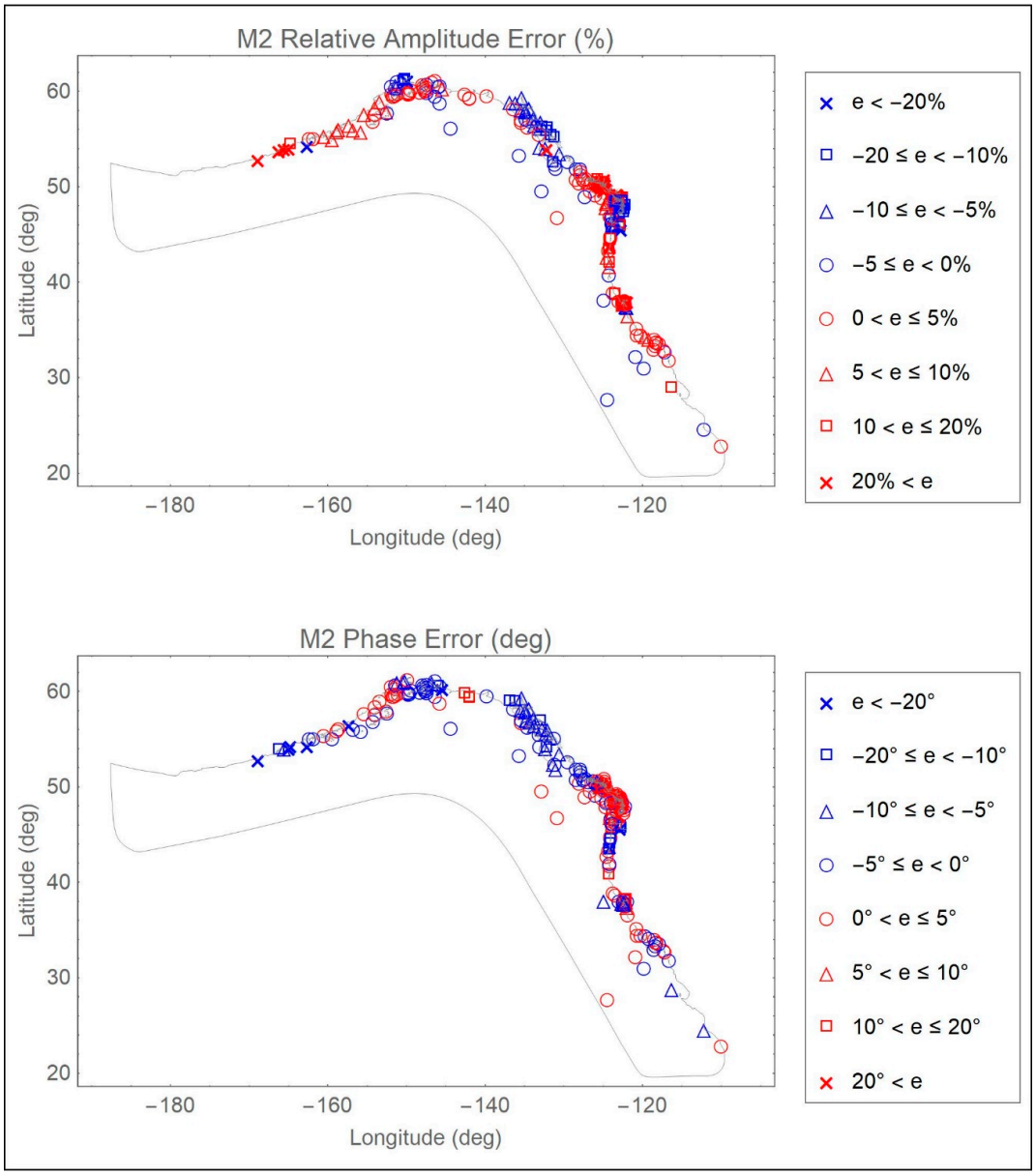

Figure 10. Relative amplitude (%) and absolute phase errors (deg) in the M_2 constituent at each of the 258 global validation stations for the ENPAC15 database. Zoomed views are provided in Appendix D.

- For Southern California, the ENPAC15 database is slightly overestimating the amplitude (generally within 5%) and phases are within ±5° from the data. Meanwhile, in San Francisco Bay, the database is more significantly overestimating the amplitudes, with the exception of the lower bay are where the data is underestimated; and the phases are generally within ±5° to 10°. This indicates the need to verify the bathymetry in this area and try a variable friction representation. Finally, along the Northern California coast, the amplitudes are overestimated by a more significant amount (over 20% for some stations), but the phases are generally within ±5°.
- Along the Oregon and Washington coast, generally, the amplitudes are underestimated and the phases are within ±5°. However, the further upriver stations in the Columbia River have higher errors, which may be indicative of the boundary being placed within the tidally influenced zone

that is not being captured with the boundary condition at the end of the river, as well as the lack of freshwater inflow at the boundary.

- In the Puget Sound region, it is interesting that the M_2 amplitudes are significantly overestimated (greater than 20%) in the channels heading east above Vancouver Island but are underestimated by 5–10% in the lower Puget Sound region; meanwhile, the phases exhibit a lead throughout much of this region (ranging from 5–20°). While the K_1 amplitudes exhibit the same over/under regional trend, they are generally within 5% of the data; however, the phases exhibit a more conservative lag (5–10°) instead of a lead as compared to M_2 constituent. Similarly in the Canadian waters above Vancouver Island, the M_2 constituent is significantly overestimated (greater than 20%) in the interior passages but is more conservatively overestimated (0–10%) as you enter Queen Charlotte Strait to the east, while the interior passages exhibit slight phase leads and the easternmost parts of the channels slight phase lags (±5°). Meanwhile, the K_1 constituent exhibits moderate amplitude overestimation of 0–10% and phase lags of 0–10°. For the region above Vancouver Island, it is important to note that the freshwater riverine flow can be significant in many of these channels, but it is neglected in our model. This neglegance has an impact on the accuracy of the tidal signal as you progress further up the channels.
- Along the southeast coast of Alaska, the amplitudes are underestimated by 5–20% in the interior passages and slightly overestimated (less than 5%) on the exterior coast, while the phases exhibit lags from 5 to 20°. Meanwhile, along the southern Alaskan coast, there is generally very good agreement for both amplitudes and phases (within ±5% or 5°), with the exception of the upper reaches of Cook Inlet, where amplitudes are underestimated up to 20%. Recall that the entire Alaskan coast received only minor bathymetric and coastline alignment updates, so we would not expect significant improvements. As you progress further west along the coast (past about 153° W), the amplitudes are more severely overestimated starting at 5% and going above 20% as you approach the boundary of the model, but the phase remains in good agreement until you pass 162° W. Recall that the coastline past Unimak Island is defined by a mainland boundary condition and does not include the interaction with the Bering Sea through the Aleutian Islands; therefore, we would not expect good agreement past 165° W.

4. Discussion

Table 8 provides a summary of the global RMS errors for the eight primary constituents, as well as the mean regional errors summed over these constituents (graphically presented in Figure 7), for each of the eight model simulations done as part of this study (statistics computed using only the 165 common validation data points). Returning to the six improvements (presented in Section 2.2) that were implemented to meet the objective of reducing the errors realized in the ENPAC03 database, we note the following:

- The placement of the open ocean boundary itself results in significant improvements for all regions (ENPAC03R vs. ESTOFS-trim1): global improvement of 33%. As was seen in previous databases for the ENPAC region, the location of the open ocean boundary can have significant impact on the accuracy of the interior model. However, as the ESTOFS-trim model incorporates newer bathymetry and has different resolution throughout, it is impossible to separate the effects of boundary placement, coarser mesh resolution at the boundary and updated deep water bathymetry when determining the source of these noted improvements.
- The improvements in coastal resolution (ESTOFS-trim1 vs. ENPAC15-CF) result in significant reductions in error for the Pacific Northwest region (38%), but no measurable change in the Alaska and California regions: global reduction of 22%. Recall that the coast of Alaska was not updated, as the VDatum project for that region is still ongoing. Furthermore, examination of individual station scatterplots for the California region indicate that some significant improvements are realized in the San Francisco Bay area but not in the open ocean coastal stations. The Pacific Northwest improvements are most likely attributable to the inclusion of the passages north of Vancouver Island.

- Meanwhile, the updated boundary forcing (ENPAC03 vs. ENPAC03R) slightly increases the mean RMS errors for some constituents (K_1, M_2) while decreasing others (S_2 and K_2). Comparison of the along boundary forcing values applied from the TPXO6 and TPXO8 products indicate only minor changes in amplitudes and no changes in applied phases near the westernmost ocean boundary (near Alaska) and no changes elsewhere. Therefore, the changes between the resulting harmonics are more than likely due to the addition of the long-term constituents in the forcing suite; recall that the ENPAC database was only forced with the diurnal and semi-diurnal constituents. However, there is very little change noted when results are compared for the TPXO8 (ESTOFS-trim1) and FES12 (ESTOFS-trim6) forcing.
- In general, the use of a variable bottom friction scheme (ENPAC15-Mann) results in lower error metrics than when a constant value is used (ENPAC15-CF), for all constituents and regions. However, the same effect can also be attained by using a slightly higher constant value (ENPAC15-Vdat). Therefore, more work needs to be done in determining appropriate variable values and comparing scatterplots by station instead of just regionally, in order to decide which scheme is best. Ideally, each sub region would be carefully calibrated taking into consideration actual bed formations and sea bed materials.
- The inclusion of the advective terms in the governing equations (ESTOFS-trim1 vs. ESTOFS-trim2), most notably, results in improvements in the Pacific Northwest region (14%) and particularly the M_2 and K_1 constituents. This is to be expected as the passages north of Vancouver Island are known to dissipate a great deal of internal energy. Further work must be done to stabilize these passages so that the advective terms can be utilized in the next tidal database release.
- The overall error reductions due to the combined effects of all five improvements (no advection) that were used in the latest database (ENPAC15-VDat vs. ENPAC03) are as follows: the global errors are reduced by 52%; while the regional errors are reduced by 33% in Alaska, 68% in the Pacific Northwest and 45% in California. Users of ENPAC15 can expect greater accuracy in any localized region where they apply boundary conditions, but particularly in the Pacific Northwest.

These results indicate that most of the reduction in harmonic constituent errors are due to the increased coastal resolution and updated bathymetry, as well as the actual placement of the boundary itself. Furthermore, the addition of the advective terms would improve the results in the Pacific Northwest region, if the model was to remain stable. On average, very little overall improvement was realized solely from the bottom friction representation; however, the friction contributes to localized effects on the harmonic accuracy and it is important to have an accurate representation of the bottom friction in the shallower regions. Finally, the updated ocean boundary forcing does not have a large effect on the overall accuracy.

To put these errors in context, the mean RMS error (summed over all eight primary constituents) between the three data sets (CO-OPS, IOS-FOC and IHO) was computed at the 61 stations that were duplicated in any two data sets. The mean error for all 61 stations was 1.1 cm, while the minimum and maximum error over all stations were 0.01 cm and 7.6 cm, respectively. Therefore, on average, one could expect the data itself to be in error by about 1 cm at a given station, which accounts for about 20% of the global RMS errors reported for the ENPAC03 model in Table 8, about 30% of the ESTOFS-trim models and 40% of the error for the ENPAC15 models. The error measures reported throughout the paper include these errors in the data; thus, a significant portion of the reported errors may stem from the uncertainty in the data itself.

Future improvements to the ENPAC tidal database should include updated resolution and bathymetry for the Alaskan coastal waters and could include better bottom friction representations in individual water bodies that have not been optimized (e.g., San Francisco Bay, Puget Sound, the inside passages north of Vancouver Island and in southeast Alaska and Cook Inlet). Additionally, for the database to be valid west of the old ENPAC03 model domain, a more accurate representation of the Aleutian Island chain and the connection to the Bering Sea would be necessary. It could also be

informative to use a mesh with coarser coastal resolution, such as ESTOFS-trim, to further explore the effects of boundary location on the accuracy of the tidal harmonics.

It is important to note that the simulation used to compute the ENPAC15 database does not include all physical processes which can affect the model response including (but not limited to) density driven flows, riverine discharge, sediment transport and resulting bed morphological changes, large-scale oceanic currents or wind and atmospheric pressure driven flows. To minimize the effects of these limitations, it is recommended that users of the ENPAC15 tidal database follow three basic guidelines: (1) choose your regional open ocean boundary location to be well outside of estuaries and bays; (2) make sure that your regional model bathymetry matches the database bathymetry at your boundary and (3) do not extract any data west of the old ENPAC03 model domain (near 160° W) as the Aleutian Island chain is treated as a mainland boundary and results are not accurate past this point. Additionally, while harmonic information is available for 37 constituents, use caution when applying larger suites as only eight have been validated. For the interested reader, further guidelines and limitations are provided in Appendix E. The ENPAC15 tidal database is available on the ADCIRC website [59].

Table 8. Summary of RMS errors (cm) for the 165 common validation stations: global means for the 8 primary constituents and regional means summed over all eight primary harmonic constituents.

Mean Global Constituent RMS Errors (cm)								
Run Designation	**O1**	**K1**	**P1**	**Q1**	**M2**	**S2**	**N2**	**K2**
ENPAC03	3.83	5.98	2.22	0.70	16.90	6.33	3.72	2.75
ENPAC03R	3.77	6.12	2.21	0.65	18.03	5.92	3.85	2.07
ESTOFS-trim1	2.83	4.70	1.53	0.47	11.09	3.77	2.47	1.47
ESTOFS-trim2	2.60	4.27	1.36	0.42	10.29	3.41	2.25	1.43
ESTOFS-trim6	2.99	4.52	1.47	0.59	11.16	3.73	2.50	1.54
ENPAC15-CF	2.26	3.56	1.16	0.41	8.42	2.94	1.89	1.36
ENPAC15-Vdat	1.94	2.87	1.09	0.45	7.80	2.86	1.95	1.24
ENPAC15-Mann	2.16	3.30	1.08	0.41	7.71	2.75	1.79	1.28

Mean Regional RMS Errors (cm)				
Run Designation	**Global**	**Alaska**	**Pacific Northwest**	**California and Mexico**
ENPAC03	5.36	5.39	9.03	2.21
ENPAC03R	5.39	4.97	9.47	2.36
ESTOFS-trim1	3.58	3.46	6.40	1.49
ESTOFS-trim2	3.29	3.34	5.48	1.52
ESTOFS-trim6	3.60	3.43	6.35	1.63
ENPAC15-CF	2.78	3.40	3.94	1.49
ENPAC15-Vdat	2.55	3.62	2.91	1.22
ENPAC15-Mann	2.59	3.45	3.21	1.34

Author Contributions: Conceptualization, R.K. and T.C.M.; Data Curation, C.S.; Formal Analysis, C.S.; Funding Acquisition, T.C.M.; Investigation, C.S.; Methodology, C.S.; Project Administration, R.K.; Resources, R.K. and T.C.M.; Software, C.S. and K.D.; Supervision, K.D. and T.C.M.; Validation, C.S.; Visualization, C.S.; Writing—Original Draft, C.S.; Writing—Review and Editing, C.S., K.D., R.K. and T.C.M.

Funding: This research was funded by the Institute of Water Resources and the Engineer Research and Development Center | U.S. Army Corps of Engineers BAA 12-5008 under contract W912HZ-13-P-0046. Additional resources were provided by the University of Oklahoma. Any opinions, conclusions, or findings are those of the authors and are not necessarily endorsed by the funding agencies.

Acknowledgments: The computing for this project was performed at the OU Supercomputing Center for Education and Research (OSCER) at the University of Oklahoma (OU). The authors would also like to acknowledge Mike Foreman at IOS-FOC for providing model domains and validation data for the areas covering British Columbia, as well as Pete Bacopoulos for creating the LTEA mesh for the Vancouver Island region. Finally, the authors acknowledge the assistance of Jiangtao Xu, Edward Myers and Jesse Feyen (among others) at NOAA for providing a summary of harmonic validation data for all stations currently covered by CO-OPS, VDatum models and input files for the US West Coast, the ESTOFS-Pacific operational mesh for the West Coast of the United States, and for assisting in extracting input data from the FES12 global database. Figures 1–6 were generated using a modified version of FigureGen [14]. The authors also thank the reviewers for providing constructive comments to improve the presentation of the paper.

Conflicts of Interest: The authors declare no conflict of interest. T.M. as a representative of the funding sponsor was involved in designing the study and reviewing the final product. The funders had no role in the collection, analyses, or interpretation of data; in the writing of the manuscript; or in the decision to publish the results.

Appendix A

The locations of the 258 validation stations are plotted with the model domain boundaries shown for the ENPAC03 (green) and ENPAC15 (gray) databases. Each figure in this Appendix zooms into a specific sub-region of the ENPAC domain in order to show the details of the coastline near the stations. Stations indicated with a black X designate those which scatter plots are provided for in Appendix C and the numbers correspond to the list of stations provided in Appendix B. The three data sources are indicated by color as follows: CO-OPS in blue, IOS-FOC in red and IHO in magenta. Furthermore, those stations that are dry in the ENPAC03 database, and will not be used for comparison with other models, are indicated with a cyan circle around the station point.

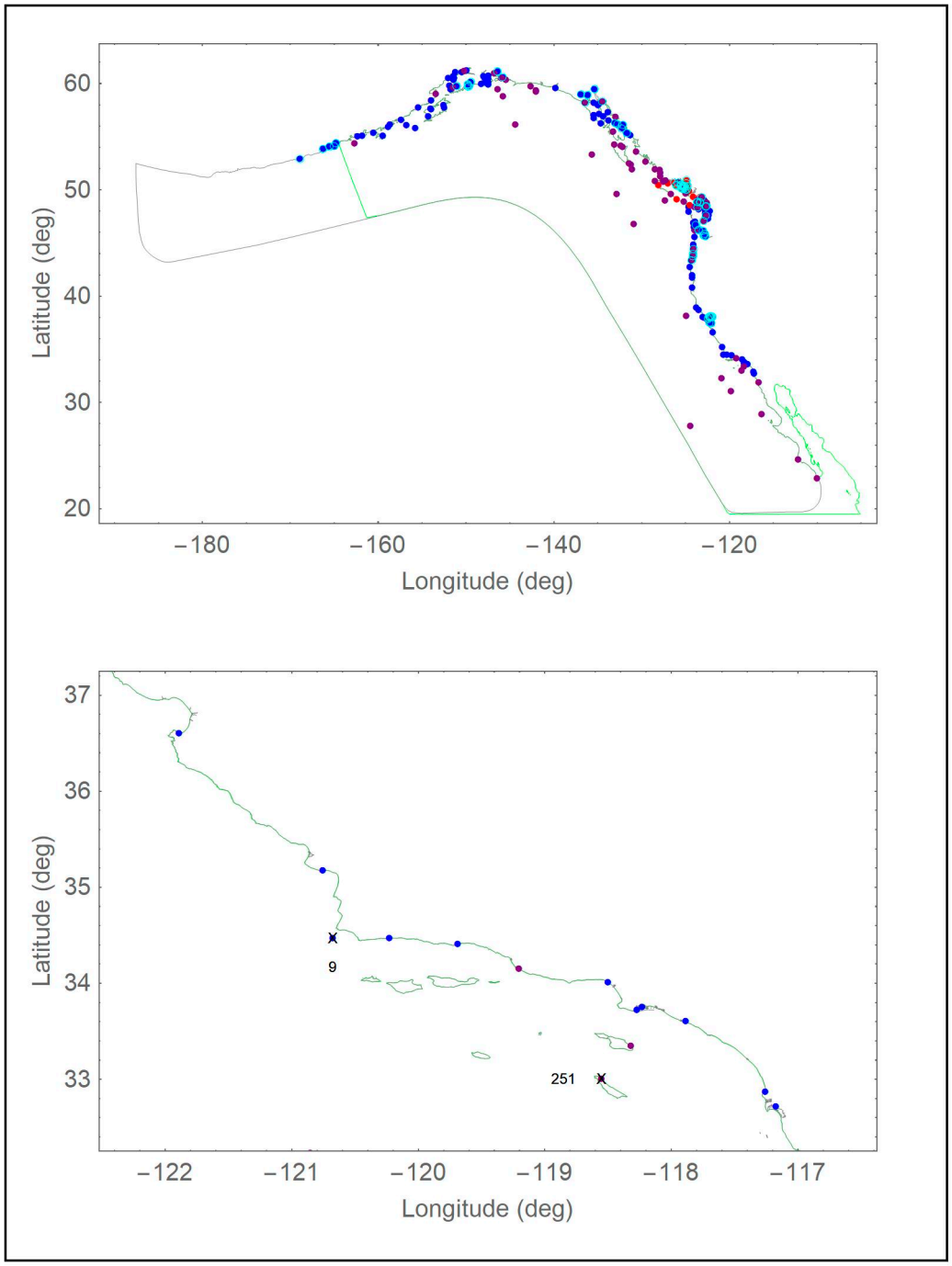

Figure A1. Location of validation stations: global and Southern California.

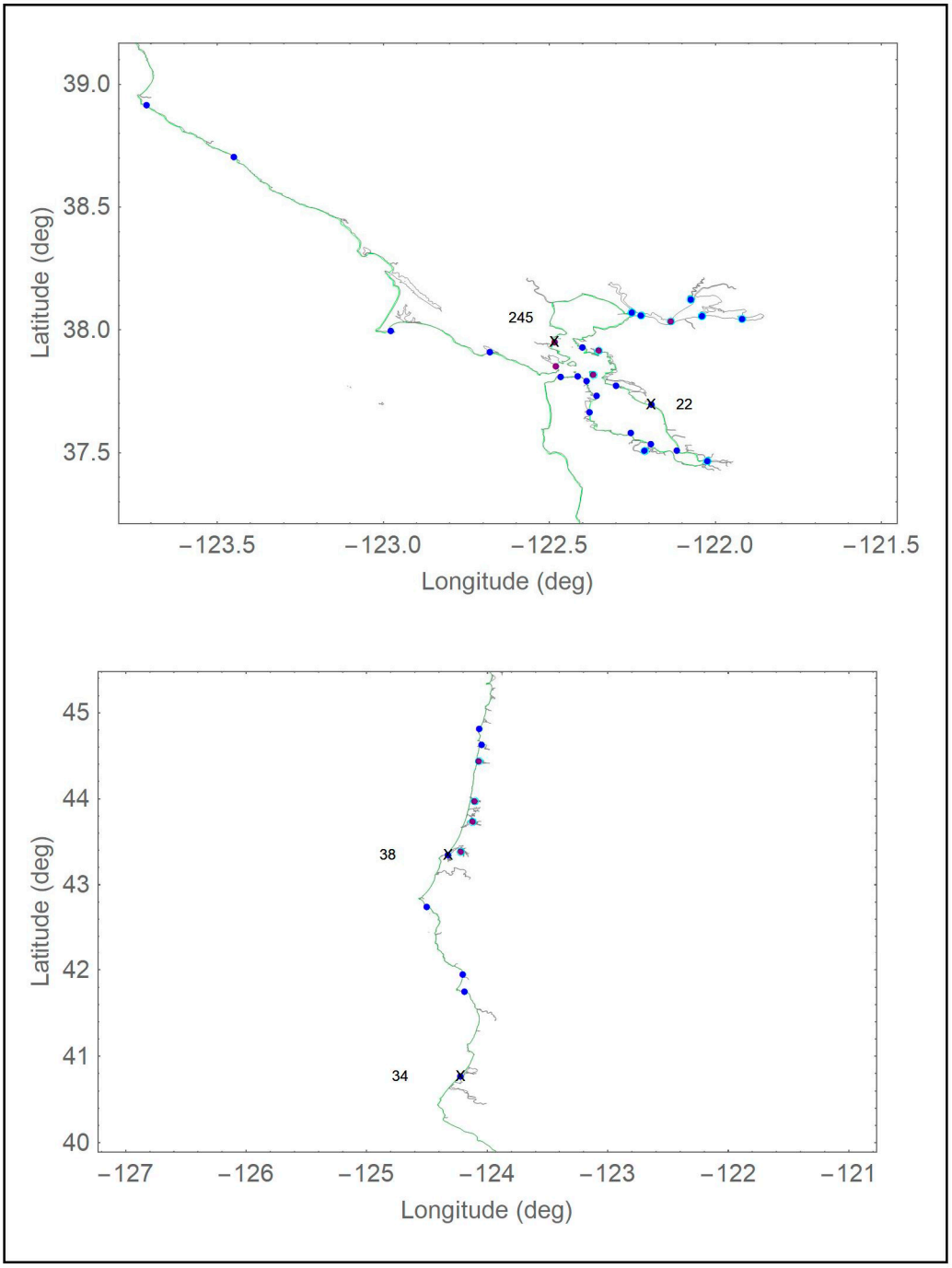

Figure A2. Location of validation stations: San Francisco Bay and Northern California.

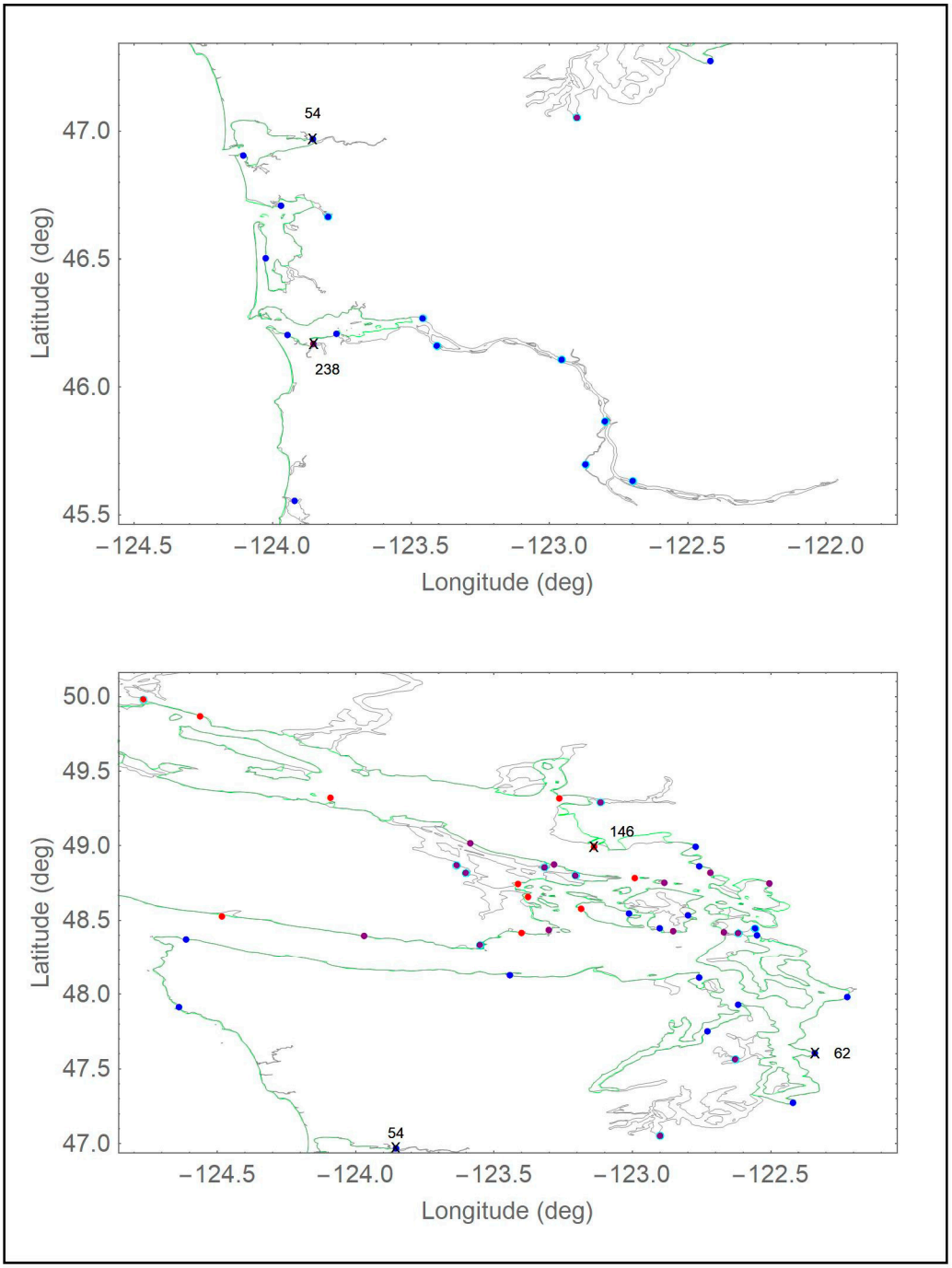

Figure A3. Location of validation stations: Columbia River and Puget Sound.

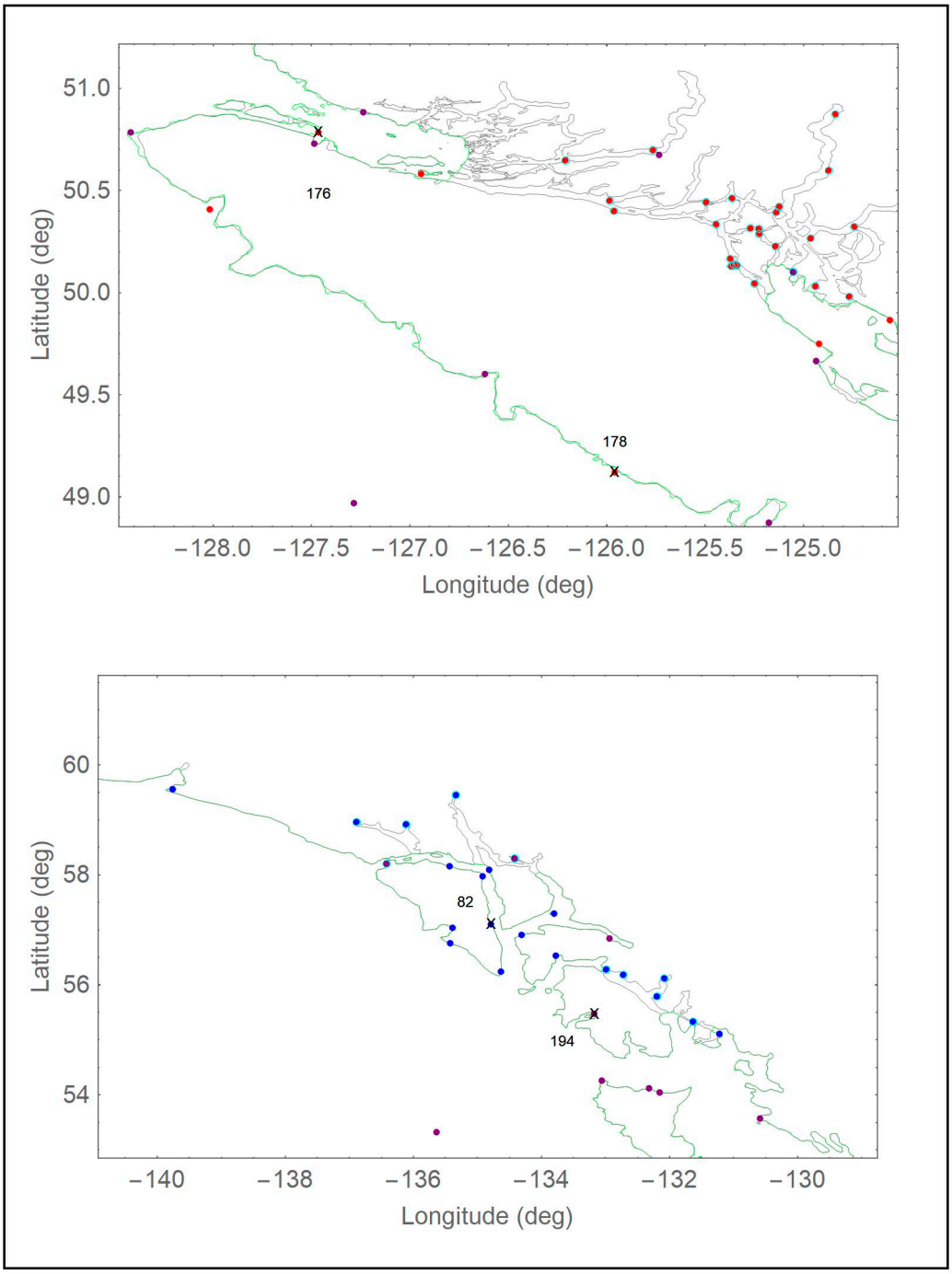

Figure A4. Location of validation stations: British Columbia and Southeast Alaska.

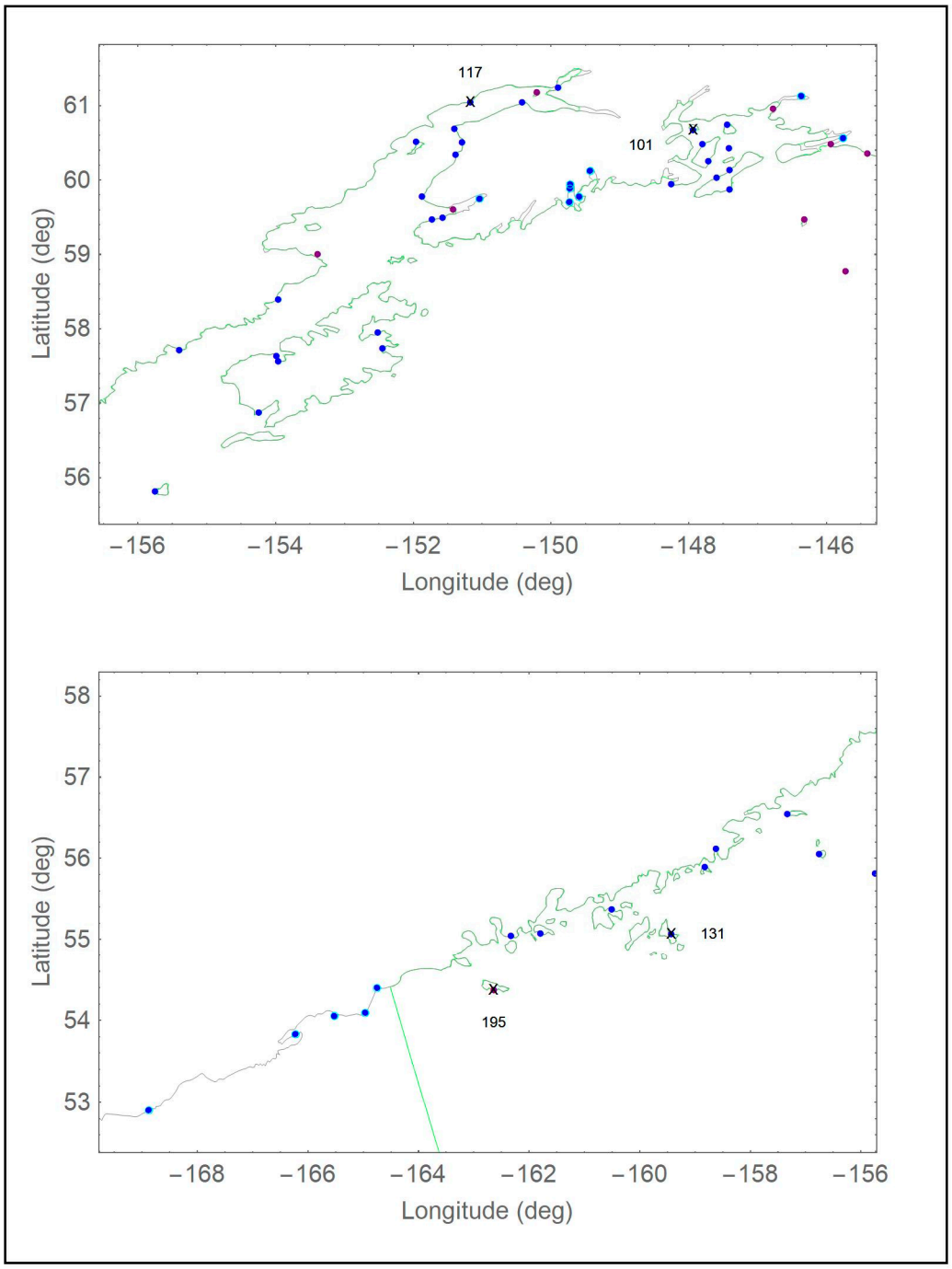

Figure A5. Location of validation stations: South Alaska.

Appendix B

The locations, names and regional classification of all 258 validation stations are given herein. For the first 139 stations, the official CO-OPS station number is provided in the source designation column, while IOS-FOC is used to designate those stations from the Institute of Ocean Sciences—Fisheries and Oceans Canada and IHO to designate the historical stations from the International Hydrographic Organization. Stations marked with a single asterisk are considered wet in the ENPAC03 model even though they are approximated by their nearest neighbor (actual longitude and latitude coordinates were not shifted when extracting from the ENPAC03 database, as the nearest element is most likely where the station would have been manually shifted anyway). Meanwhile, those marked with a double asterisk are not included in

scatter plots or statistical error metrics for the ENPAC03 database since they are well outside the domain of the boundary or are in channels and other features that are not represented in the ENPAC03 model domain. Abbreviations for the region designations are as follows: Alaska—AK, British Columbia—BC, Washington—WA, Oregon—OR, California—CA, Mexico—MX, and deep water—D. Note that for statistics, the British Columbia, Washington and Oregon stations were grouped into a single Pacific Northwest category; however, they are listed separately for interested readers. Similarly, the California and Mexico stations were grouped into a single category for statistical analysis.

Table A1. Location and source information for validation data. For the first 139 stations, the number in the Source column is the CO-OPS station identifier.

Station	Longitude	Latitude	Station Name	Region	Source
1 *	−117.17360	32.71400	San Diego, San Diego Bay	CA	9410170
2	−117.25800	32.86670	La Jolla, Pacific Ocean	CA	9410230
3 *	−117.88300	33.60330	Newport Beach, Newport Bay Ent	CA	9410580
4 *	−118.27200	33.72000	Los Angeles, Outer Harbor	CA	9410660
5 *	−118.22700	33.75170	Long Beach, Terminal Island	CA	9410680
6 *	−118.50000	34.00830	Santa Monica, Pacific Ocean	CA	9410840
7	−119.68501	34.40830	Santa Barbara, Pacific Ocean	CA	9411340
8 *	−120.22831	34.46939	Gaviota State Park, Pacific Ocean	CA	9411399
9	−120.67300	34.46830	Oil Platform Harvest (Topex)	CA	9411406
10 *	−120.76000	35.17670	Port San Luis, San Luis Obispo	CA	9412110
11 *	−121.88800	36.60500	Monterey, Monterey Harbor	CA	9413450
12 *	−122.46500	37.80669	San Francisco, San Francisco Bay	CA	9414290
13 *	−122.41300	37.81000	North Point [Pier 41] S.F.Bay	CA	9414305
14 *	−122.38698	37.79002	Pier 22 1/2, San Francisco Bay	CA	9414317
15	−122.35700	37.73000	Hunters Point, S.F. Bay	CA	9414358
16	−122.37700	37.66500	Oyster Point Marina, S.F. Bay	CA	9414392
17	−122.25300	37.58000	San Mateo Bridge, West Side	CA	9414458
18	−122.19300	37.53330	Redwood Creek, C.M. No. 8,S.F.B	CA	9414501
19	−122.11500	37.50670	Dumbarton Bridge, S. F. Bay	CA	9414509
20 **	−122.21200	37.50670	Redwood City, Wharf 5, S.F. Bay	CA	9414523
21 **	−122.02300	37.46500	Coyote Creek, Alviso Slough	CA	9414575
22 *	−122.19200	37.69500	San Leandro Marina, S.F.Bay	CA	9414688
23	−122.29833	37.77167	Alameda, San Francisco Bay	CA	9414750
24	−122.40000	37.92830	Richmond, Chevron Oil Pier	CA	9414863
25 **	−121.91800	38.04330	Mallard Island, Suisun Bay	CA	9415112
26 **	−122.22300	38.05830	Crockett, Carquinez Strait	CA	9415143
27 **	−122.03950	38.05600	Port Chicago, Suisun Bay	CA	9415144
28 **	−122.25000	38.07000	Mare Is.Naval Shipyard, Carquin	CA	9415218
29 **	−122.07300	38.12323	Suisun Slough Entrance	CA	9415265
30 *	−122.67854	37.90871	Bolinas, Bolinas Lagoon	CA	9414958
31 *	−122.97670	37.99610	Point Reyes, Drakes Bay	CA	9415020
32	−123.44940	38.70329	Green Cove, Pacific Ocean	CA	9416409
33 *	−123.71061	38.91330	Arena Cove, Pacific Ocean	CA	9416841
34 *	−124.21700	40.76670	North Spit, Humboldt Bay	CA	9418767
35	−124.18300	41.74500	Crescent City, Pacific Ocean	CA	9419750
36 *	−124.20092	41.94525	Pyramid Point, Smith River	CA	9419945
37	−124.49828	42.73897	Port Orford, Pacific Ocean	OR	9431647
38 *	−124.32200	43.34500	Charleston, Coos Bay	OR	9432780
39 *	−124.04300	44.62500	South Beach, Yaquina River	OR	9435380
40 *	−124.06300	44.81000	Depoe Bay	OR	9435827
41 *	−123.91894	45.55453	Garibaldi, Tillamook Bay	OR	9437540
42 *	−123.94500	46.20170	Hammond, Columbia River	OR	9439011
43 *	−123.76831	46.20731	Astoria, Tongue Point, Columbia	OR	9439040
44 **	−123.40500	46.16000	Wauna, Columbia River	OR	9439099
45 **	−122.86800	45.69670	Rocky Point, Multnomah Channel	OR	9439189
46 **	−122.79700	45.86500	St. Helens, Columbia River	OR	9439201

Table A1. *Cont.*

Station	Longitude	Latitude	Station Name	Region	Source
47 **	−122.69704	45.63158	Vancouver, Columbia River	WA	9440083
48 **	−122.95420	46.10559	Longview, Columbia River	WA	9440422
49 **	−123.45602	46.26707	Skamokawa, Columbia River	WA	9440569
50	−124.02300	46.50170	Nahcotta, Willapa Bay	WA	9440747
51 **	−123.79800	46.66404	South Bend	WA	9440875
52 *	−123.96692	46.70746	Toke Point, Willapa Bay	WA	9440910
53 *	−124.10508	46.90431	Westport, Grays Harbor	WA	9441102
54 *	−123.85300	46.96830	Aberdeen, Grays Harbor	WA	9441187
55 *	−124.63700	47.91330	La Push, Quillayute River	WA	9442396
56	−124.61170	48.37081	Neah Bay, Strait of Juan De Fuca	WA	9443090
57 *	−123.44000	48.12500	Port Angeles, Juan De Fuca	WA	9444090
58	−122.75800	48.11170	Port Townsend, Admiralty Inlet	WA	9444900
59	−122.61700	47.92670	Foulweather Bluff, Twin Spits	WA	9445016
60 *	−122.72700	47.74830	Bangor	WA	9445133
61 *	−122.41670	47.27120	Tacoma, Commencement Bay	WA	9446484
62 *	−122.33931	47.60264	Seattle, Puget Sound	WA	9447130
63 *	−122.22300	47.98000	Everett	WA	9447659
64	−122.54800	48.40000	Sneeoosh Point, Skagit Bay	WA	9448576
65 **	−122.55500	48.44500	Turner Bay, Similk Bay	WA	9448657
66	−122.75800	48.86330	Cherry Point, Strait of Georgia	WA	9449424
67 *	−122.76900	48.99227	Blaine, Drayton Harbor	WA	9449679
68 *	−123.00980	48.54580	Friday Harbor, San Juan Channel	WA	9449880
69 *	−122.79700	48.53500	Armitage Island	WA	9449932
70 *	−122.90000	48.44670	Richardson, Lopez Island	WA	9449982
71 *	−131.21900	55.10280	Custom House Cove, Mary Island	AK	9450296
72 **	−131.62619	55.33183	Ketchikan, Tongass Narrows	AK	9450460
73 **	−132.19088	55.78828	Magnetic Point, Union Bay	AK	9450753
74 **	−132.07650	56.11512	Thoms Point, Zimovia Strait	AK	9450970
75 **	−132.71750	56.17830	Point Harrington, Clarence Strait	AK	9451005
76 **	−132.98500	56.27670	Bushy Island, Snow Passage	AK	9451074
77	−133.76610	56.52760	Monte Carlo Island	AK	9451247
78	−134.62713	56.23934	Port Alexander, Baranof Island	AK	9451054
79	−135.41829	56.75322	Golf Island, Necker Islands	AK	9451421
80	−134.30400	56.90856	Saginaw Bay, Kuiu Island	AK	9451497
81	−135.38450	57.03000	Sitka, Baronof Island, Sitka Sound	AK	9451600
82	−134.77960	57.09860	Baranof, Warm Spring Bay	AK	9451625
83 *	−133.79700	57.29500	The Brothers, Stephens Passage	AK	9451785
84 **	−134.41200	58.29818	Juneau, Gastineau Channel	AK	9452210
85 *	−134.80600	58.08410	Hawk Inlet Entrance	AK	9452294
86	−134.91580	57.96780	False Bay, Chatham Strait	AK	9452328
87 **	−135.32880	59.44960	Skagway, Taiya Inlet	AK	9452400
88	−135.43190	58.15240	Hoonah	AK	9452438
89 **	−136.10800	58.91330	Muir Inlet, Glacier Bay	AK	9452584
90 **	−136.88110	58.95960	Tarr Inlet	AK	9452749
91 *	−139.74890	59.54850	Yakutat, Yakutat Bay	AK	9453220
92 **	−145.75300	60.55830	Cordova, Orca Inlet, Pr William Sd	AK	9454050
93 **	−146.36200	61.12360	Valdez, Prince William Sound	AK	9454240
94	−147.40050	60.13250	Perch Point, Montague Island	AK	9454561
95 *	−147.39840	59.87220	Wooded Island	AK	9454562
96	−147.41000	60.42500	Seal Island	AK	9454564
97 *	−147.43700	60.73670	Storey Island North Side	AK	9454571
98	−147.59300	60.02800	Montague Island, Ne Bazel Pt	AK	9454616
99 *	−147.70950	60.24760	Snug Harbor, Knight Island	AK	9454662
100 *	−147.79270	60.47560	Herring Point, Knight Island,	AK	9454691
101 *	−147.93200	60.66910	Perry Island (South Bay)	AK	9454721
102 *	−148.24540	59.94370	Point Erlington, Erlington Island	AK	9454814
103 **	−149.42667	60.12000	Seward, Resurrection Bay	AK	9455090
104 **	−149.58630	59.77430	Agnes Cove	AK	9455120

Table A1. *Cont.*

Station	Longitude	Latitude	Station Name	Region	Source
105 **	−149.71340	59.94060	Aialik Bay, North End	AK	9455145
106 **	−149.71800	59.88500	Aialik Sill, Aialik Bay	AK	9455146
107 **	−149.72500	59.70240	Camp Cove, Harris Penninsula	AK	9455151
108 *	−151.71990	59.46400	Seldovia, Cook Inlet	AK	9455500
109	−151.56500	59.49150	Kasitsna Bay, Kachemak Bay	AK	9455517
110 **	−151.03000	59.74400	Bear Cove, Kachemak Bay	AK	9455595
111	−151.86703	59.77197	Anchor Point	AK	9455606
112 *	−151.38240	60.33670	Cape Kasilof, Cook Inlet	AK	9455711
113 *	−151.95200	60.51170	Kaligan Island, Cook Inlet	AK	9455732
114	−151.28470	60.50330	Chinulna Point, Cook Inlet	AK	9455735
115 *	−151.39800	60.68330	Nikiski, Cook Inlet	AK	9455760
116	−150.41300	61.03670	Point Possession (T-39, Opr-469)	AK	9455866
117	−151.16300	61.04331	North Foreland	AK	9455869
118	−149.89180	61.24010	Anchorage, Knik Arm, Cook Inlet	AK	9455920
119 *	−153.95800	58.39170	Nukshak Island, Shelikof Strait	AK	9456717
120 *	−152.51090	57.94530	Ouzinkie	AK	9457287
121 *	−152.43930	57.73170	Kodiak Island, Womens Bay	AK	9457292
122	−153.95800	57.56340	Larsen Bay, Kodiak Island	AK	9457724
123 *	−153.98280	57.63500	Uyak (Cannery Dock), Uyak Bay	AK	9457728
124 *	−154.23530	56.87600	Alitak, Lazy Bay	AK	9457804
125	−155.39300	57.70670	Puale Bay	AK	9458209
126	−155.74000	55.80830	Chirikof Island, Sw Anchorage	AK	9458293
127 *	−156.74550	56.05170	Chowiet Island, Semidi Island	AK	9458519
128	−157.32760	56.54120	West End, Sutwik Island	AK	9458665
129	−158.61160	56.11330	Hump Island, Kuiukta Bay	AK	9458964
130 *	−158.82000	55.89030	Mitrofania Island	AK	9459016
131 *	−159.41870	55.06730	Herendeen Island, Shumagin	AK	9459163
132	−160.50200	55.36600	Sand Point, Popof Island	AK	9459450
133	−161.79200	55.07320	Dolgoi Harbor, Dolgoi Island	AK	9459758
134	−162.32700	55.03890	King Cove, Deer Passage, Pacific	AK	9459881
135 **	−164.74572	54.39364	Scotch Cap, Unimak Island	AK	9462808
136 **	−164.95370	54.09160	Tigalda Bay, Tigalda Island	AK	9462782
137 **	−165.51417	54.05222	Rootok Island, Rootok Strait	AK	9462723
138 **	−166.21625	53.82892	Biorka Village, Beaver Inlet	AK	9462645
139 **	−168.87130	52.90130	Nikolski	AK	9462450
140	−124.48200	48.52500	Port Renfrew	BC	IOS-FOC
141	−123.39900	48.41300	Victoria Harbour	BC	IOS-FOC
142	−123.18300	48.57700	Hanbury Point	BC	IOS-FOC
143	−123.37400	48.65600	Sidney	BC	IOS-FOC
144	−123.41100	48.74400	Fulford Harbour	BC	IOS-FOC
145	−122.98900	48.78200	Patos Island	BC	IOS-FOC
146	−123.13700	48.99100	Tsawwassen	BC	IOS-FOC
147	−123.26300	49.31700	Point Atkinson	BC	IOS-FOC
148	−124.08900	49.31900	Winchelsea Islands	BC	IOS-FOC
149	−124.55960	49.86450	Powell River	BC	IOS-FOC
150	−124.91820	49.74880	Little River	BC	IOS-FOC
151 **	−124.76550	49.97900	Lund	BC	IOS-FOC
152 **	−124.93720	50.02990	Twin Islands	BC	IOS-FOC
153 **	−124.73990	50.32120	Channel Islands	BC	IOS-FOC
154 **	−124.96110	50.26480	Redonda Bay	BC	IOS-FOC
155 **	−125.24650	50.04300	Campbell River	BC	IOS-FOC
156 **	−125.33670	50.13330	Maude Island East	BC	IOS-FOC
157 **	−125.36330	50.12830	Nymphe Cove	BC	IOS-FOC
158 **	−125.34790	50.13540	Seymour Narrows	BC	IOS-FOC
159 **	−125.36870	50.16460	Brown Bay	BC	IOS-FOC
160 **	−125.13930	50.22560	Welsford Island	BC	IOS-FOC
161 **	−125.22280	50.28750	Bodega Anchorage	BC	IOS-FOC
162 **	−125.22410	50.31140	Owen Bay	BC	IOS-FOC

Table A1. *Cont.*

Station	Longitude	Latitude	Station Name	Region	Source
163 **	−125.26810	50.31480	Okis Islands	BC	IOS-FOC
164 **	−125.13620	50.39250	Big Bay	BC	IOS-FOC
165 **	−125.12120	50.42020	Turnback Point	BC	IOS-FOC
166 **	−124.86940	50.59790	Orford Bay	BC	IOS-FOC
167 **	−124.83560	50.87270	Waddington Harbour	BC	IOS-FOC
168 **	−125.44160	50.33280	Chatham Point	BC	IOS-FOC
169 **	−125.36110	50.46090	Shoal Bay	BC	IOS-FOC
170 **	−125.49190	50.44240	Cordero Islands	BC	IOS-FOC
171 **	−125.96010	50.39870	Kelsey Bay	BC	IOS-FOC
172 **	−125.98330	50.45000	Yorke Island	BC	IOS-FOC
173 **	−125.76300	50.69800	Siwash Bay	BC	IOS-FOC
174 **	−126.20700	50.64700	Montagu Point	BC	IOS-FOC
175	−126.94100	50.58100	Alert Bay	BC	IOS-FOC
176	−127.46300	50.78400	Port Hardy	BC	IOS-FOC
177	−128.01400	50.40700	Winter Harbour	BC	IOS-FOC
178	−125.95700	49.11900	Tofino	BC	IOS-FOC
179	−150.20000	61.17500	Fire Island Cook Inlet	AK	IHO
180	−146.76666	60.95000	Rocky Point	AK	IHO
181	−145.93000	60.47600	Cape Whitshed	AK	IHO
182	−145.39999	60.35300	Pete Dahl Slough	AK	IHO
183	−142.56667	59.71667	Iapso #30_2.1.5	AK	IHO
184	−151.41667	59.60000	Homer	AK	IHO
185	−146.31667	59.46667	Middleton Island	AK	IHO
186	−141.98334	59.33333	Iapso #30_2.1.6	AK	IHO
187	−141.98334	59.25000	Iapso #30_2.1.4	AK	IHO
188	−153.38333	59.00000	Shaw Island Cook Inlet	AK	IHO
189	−145.71666	58.76667	Iapso #30_2.1.3	D	IHO
190	−134.41667	58.29900	Juneau	AK	IHO
191	−136.41450	58.20000	Granite Cove	AK	IHO
192	−132.93330	56.83470	Petersburg	AK	IHO
193	−144.36667	56.13334	Surveyor Seamount	D	IHO
194	−133.16700	55.47020	Craig	AK	IHO
195	−162.63333	54.37030	Peterson Bay Sanak Island	AK	IHO
196	−133.05000	54.25450	Langara Island	BC	IHO
197	−132.31667	54.11666	Wiah Point	BC	IHO
198	−132.14999	54.04210	Masset Harbour	BC	IHO
199	−130.57550	53.57020	Griffith Harbour	BC	IHO
200	−135.63333	53.31667	Bowie Seamount	D	IHO
201	−129.48334	52.65000	Mc Kenny Island	BC	IHO
202	−131.35330	52.46650	Section Cove	BC	IHO
203	−131.16667	52.35000	Copper Island	BC	IHO
204	−131.01666	51.93333	Cape St James	BC	IHO
205	−128.43333	51.90000	Gosling Island	BC	IHO
206	−127.89020	51.86666	Namu	BC	IHO
207	−127.82160	51.58850	Addenbroke Island	BC	IHO
208	−127.83334	51.25000	Egg Island	BC	IHO
209	−127.23334	50.88334	Raynor Group	BC	IHO
210	−128.41667	50.78333	Cape Scott	BC	IHO
211	−127.48334	50.72710	Port Hardy	BC	IHO
212	−125.73172	50.67270	Glendale Cove	BC	IHO
213	−125.05000	50.10000	Whaletown Bay	BC	IHO
214	−124.93266	49.66520	Comox	BC	IHO
215	−126.61667	49.60100	Nootka	BC	IHO
216	−132.78334	49.58333	Union Seamount	D	IHO
217	−123.11353	49.28978	Vancouver	BC	IHO
218	−123.58334	49.01667	Porlier Pass	BC	IHO
219	−127.28333	48.96667	Iapso #30_2.1.2	D	IHO
220	−123.28030	48.87370	Georgina Point	BC	IHO

Table A1. *Cont.*

Station	Longitude	Latitude	Station Name	Region	Source
221	−123.63333	48.86907	Crofton	BC	IHO
222	−123.31541	48.85398	Village Bay	BC	IHO
223	−125.17420	48.87250	Bamfield Inlet	BC	IHO
224	−123.60001	48.81667	Maple Bay	BC	IHO
225	−122.71667	48.81667	Ferndale	WA	IHO
226	−123.20420	48.80000	Samuel Islands (S. Shore)	BC	IHO
227	−122.88333	48.75000	Echo Bay	WA	IHO
228	−122.50250	48.74680	Bellingham	WA	IHO
229	−123.30000	48.43333	Oak Bay	BC	IHO
230	−122.85001	48.42765	Aleck Bay	WA	IHO
231	−122.66666	48.41667	Reservation Bay	WA	IHO
232	−122.61540	48.41420	Yokeko Point	WA	IHO
233	−123.96790	48.39380	Point No Point	BC	IHO
234	−123.54885	48.33427	Pedder Bay	BC	IHO
235	−122.62604	47.56237	Bremerton	WA	IHO
236	−122.89850	47.05180	Olympia	WA	IHO
237	−130.81667	46.76667	Iapso #30-2.1.1	D	IHO
238	−123.85001	46.16667	Astoria Youngs Bay	OR	IHO
239	−124.06667	44.43333	Waldport_Alsea Bay	OR	IHO
240	−124.10001	43.96667	Florence	OR	IHO
241	−124.11667	43.73333	Gardiner_Umpqua River	OR	IHO
242	−124.21667	43.38334	Marshfield_Coos Bay	OR	IHO
243	−124.89999	38.15000	Iapso #30-2.1.14	D	IHO
244	−122.13333	38.03333	Benicia	CA	IHO
245	−122.48334	37.95000	Point San Quentin	CA	IHO
246	−122.35001	37.91490	Richmond	CA	IHO
247	−122.47970	37.85000	Sausalito	CA	IHO
248	−122.36667	37.81667	Yerba Buena Island	CA	IHO
249	−119.20200	34.14865	Port Hueneme	CA	IHO
250	−118.31667	33.35000	Avalon_Catalina Island	CA	IHO
251	−118.54814	33.00115	Wilson Cove San Clemente Island	CA	IHO
252	−120.85001	32.23333	Iapso #30-2.1.12	D	IHO
253	−116.63351	31.84948	Ensenada	MX	IHO
254	−119.80000	31.03333	Iapso #30-2.1.11	D	IHO
255	−116.28333	28.86667	Isla Guadalupe	D	IHO
256	−124.43333	27.75000	Iapso #30-2.1.13	D	IHO
257	−112.15340	24.63060	Magdalena Bay	MX	IHO
258	−109.97200	22.84400	Cabo San Lucas	MX	IHO

* All stations denoted by a single asterisk are outside the model domain of the ENPAC03 database but are extracted using the nearest wet neighbor as they are suitably near the coastline. ** All stations denoted by a double asterisk are not extracted from ENPAC03 for data analysis or plotting as they are either well outside the model domain or located in small channels or other features that are not resolved in the ENPAC03 model domain.

Appendix C

Scatter plots for the eighteen stations denoted with a black X in Appendix A are provided herein. Both the ENPAC15 Manning's n and VDatum friction variations are compared to the ENPAC03 model. Note that the different friction formulations generally create more of a difference in the amplitude response than they do in the phase response. Plots are grouped according to region, starting at the southern extent of the domain.

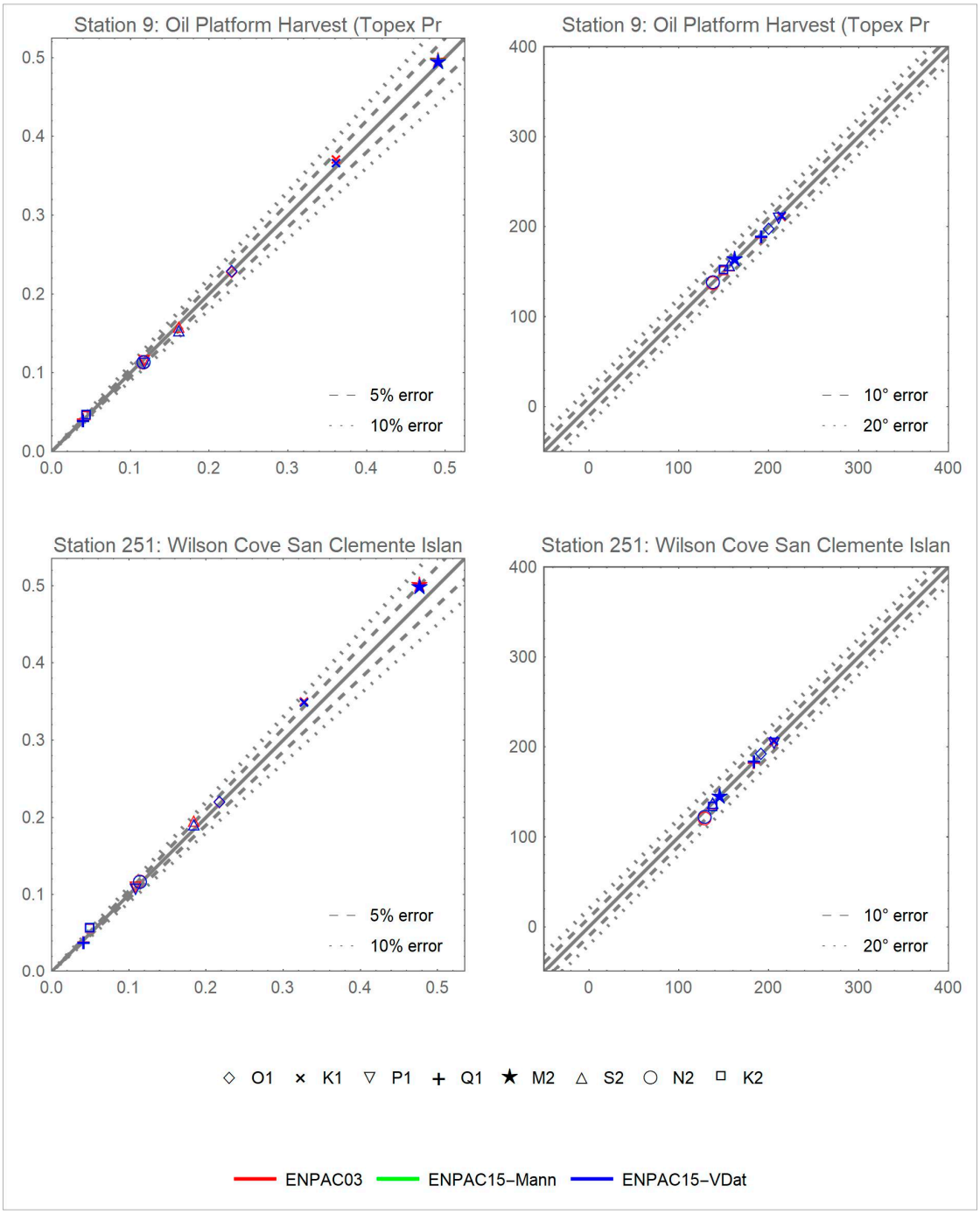

Figure A6. Scatterplots of errors for two Southern California stations, locations shown in Figure A1.

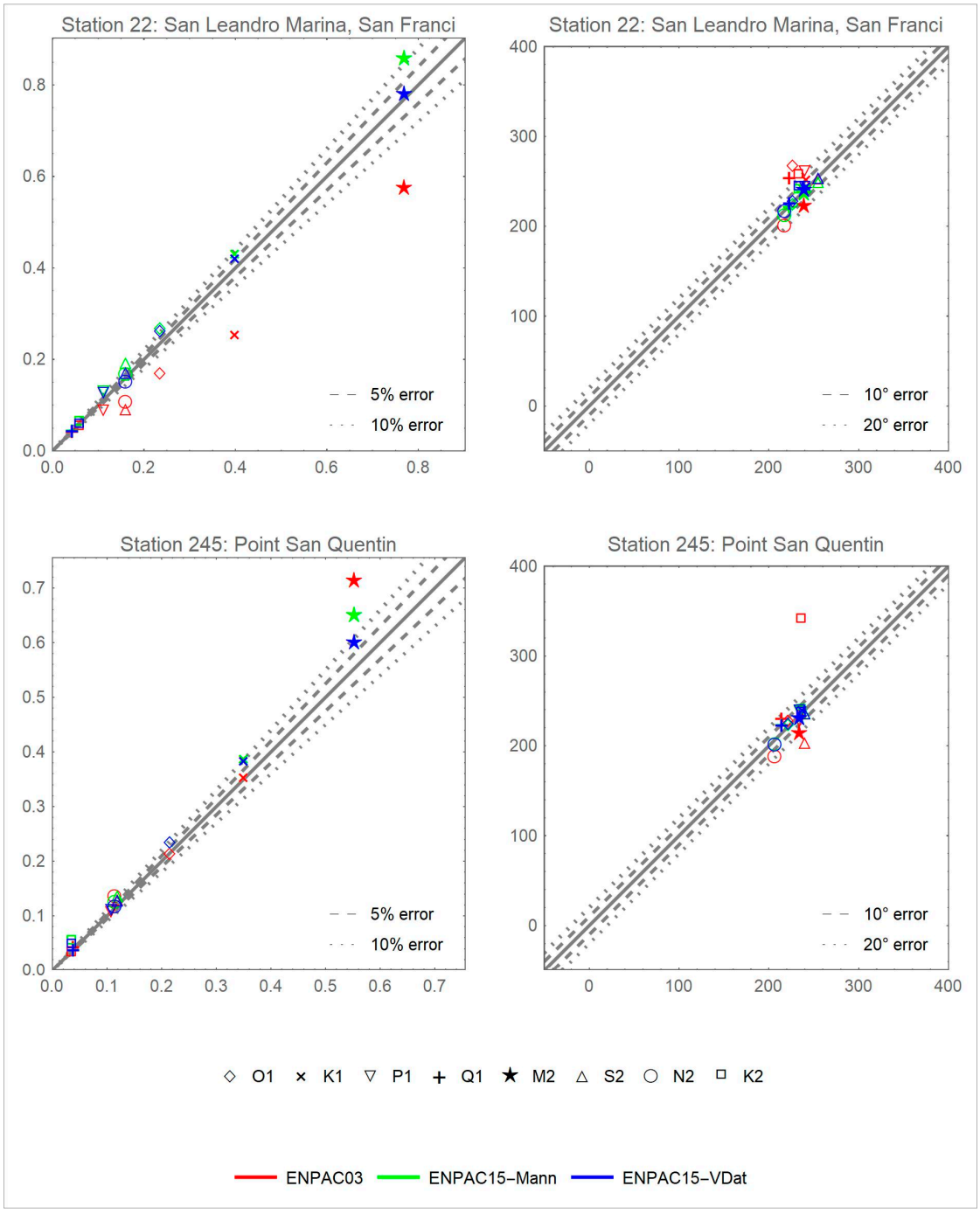

Figure A7. Scatterplots of errors for two San Francisco Bay stations, locations shown in Figure A2.

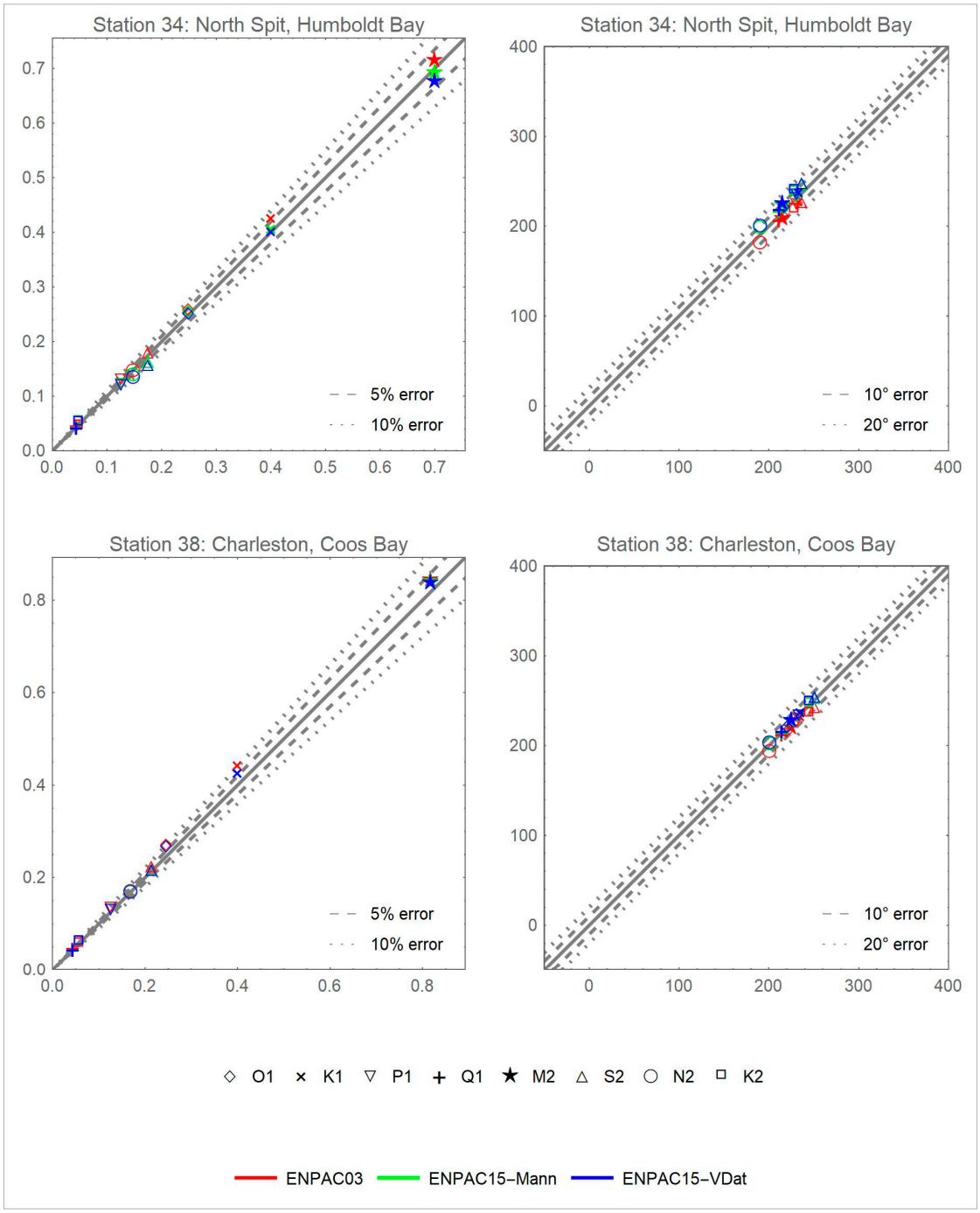

Figure A8. Scatterplots of errors for two Northern California stations, locations shown in Figure A2.

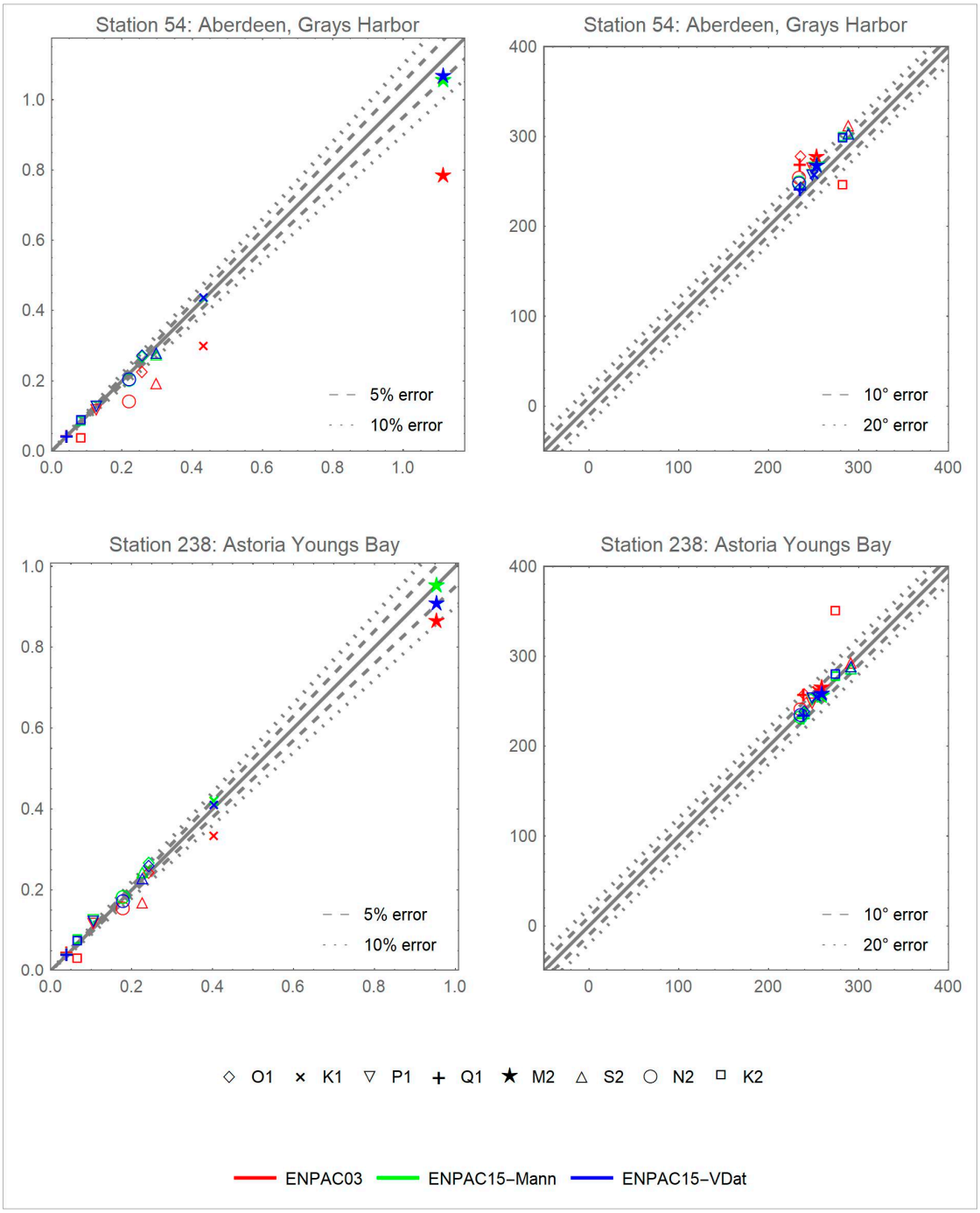

Figure A9. Scatterplots of errors for two Oregon/Washington stations, locations shown in Figure A3.

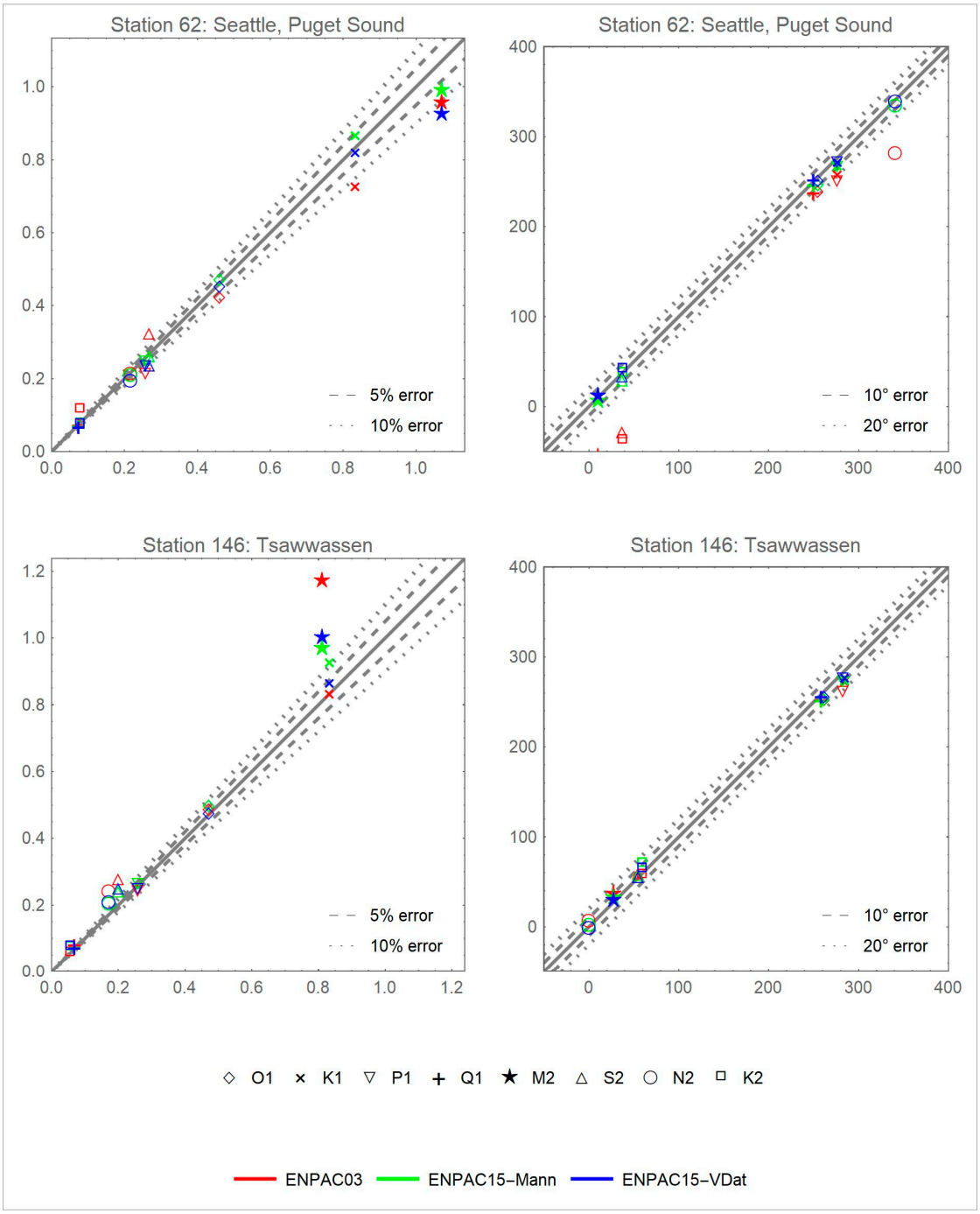

Figure A10. Scatterplots of errors for two Puget Sound stations, locations shown in Figure A3.

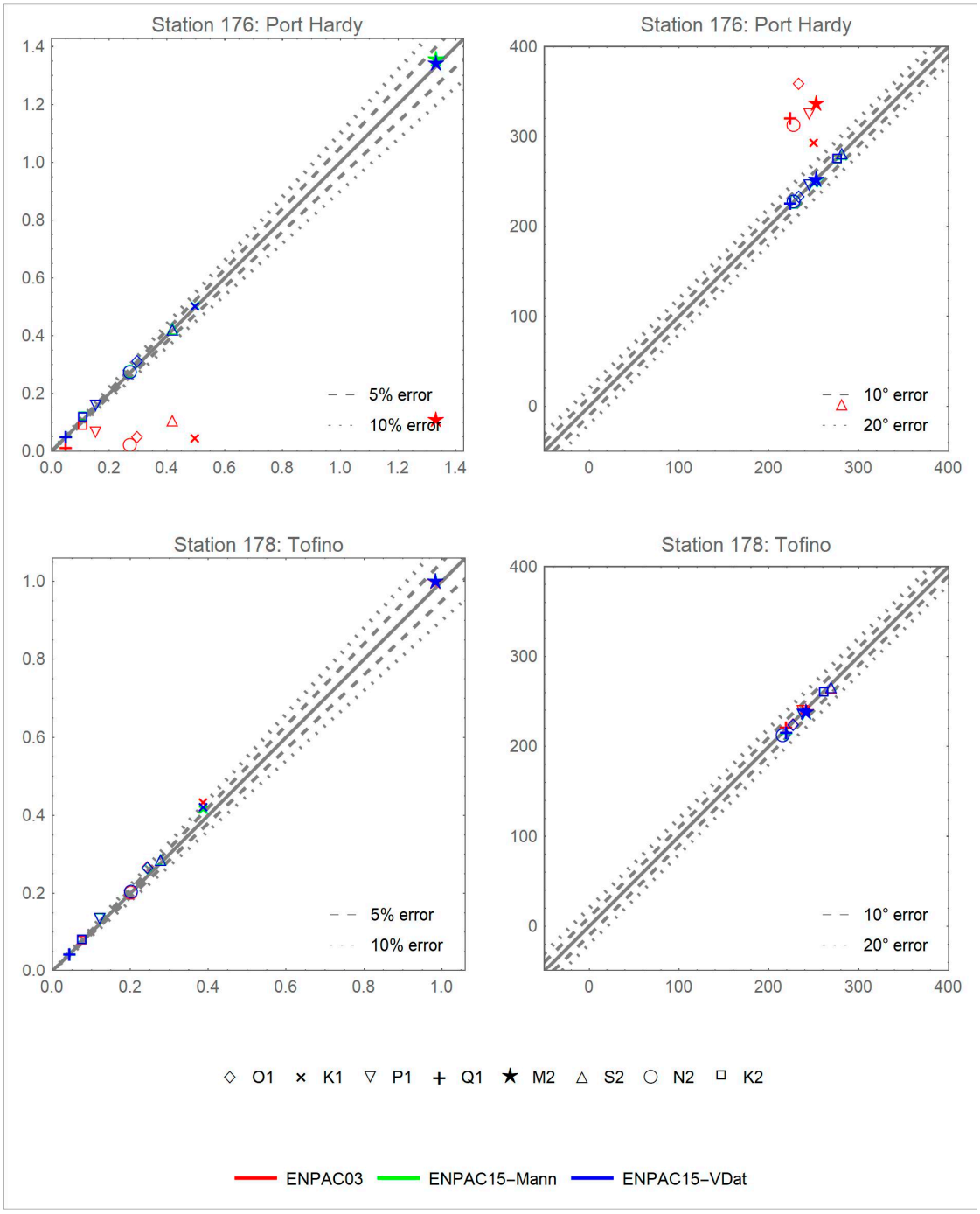

Figure A11. Scatterplots of errors for two British Columbia stations, locations shown in Figure A4.

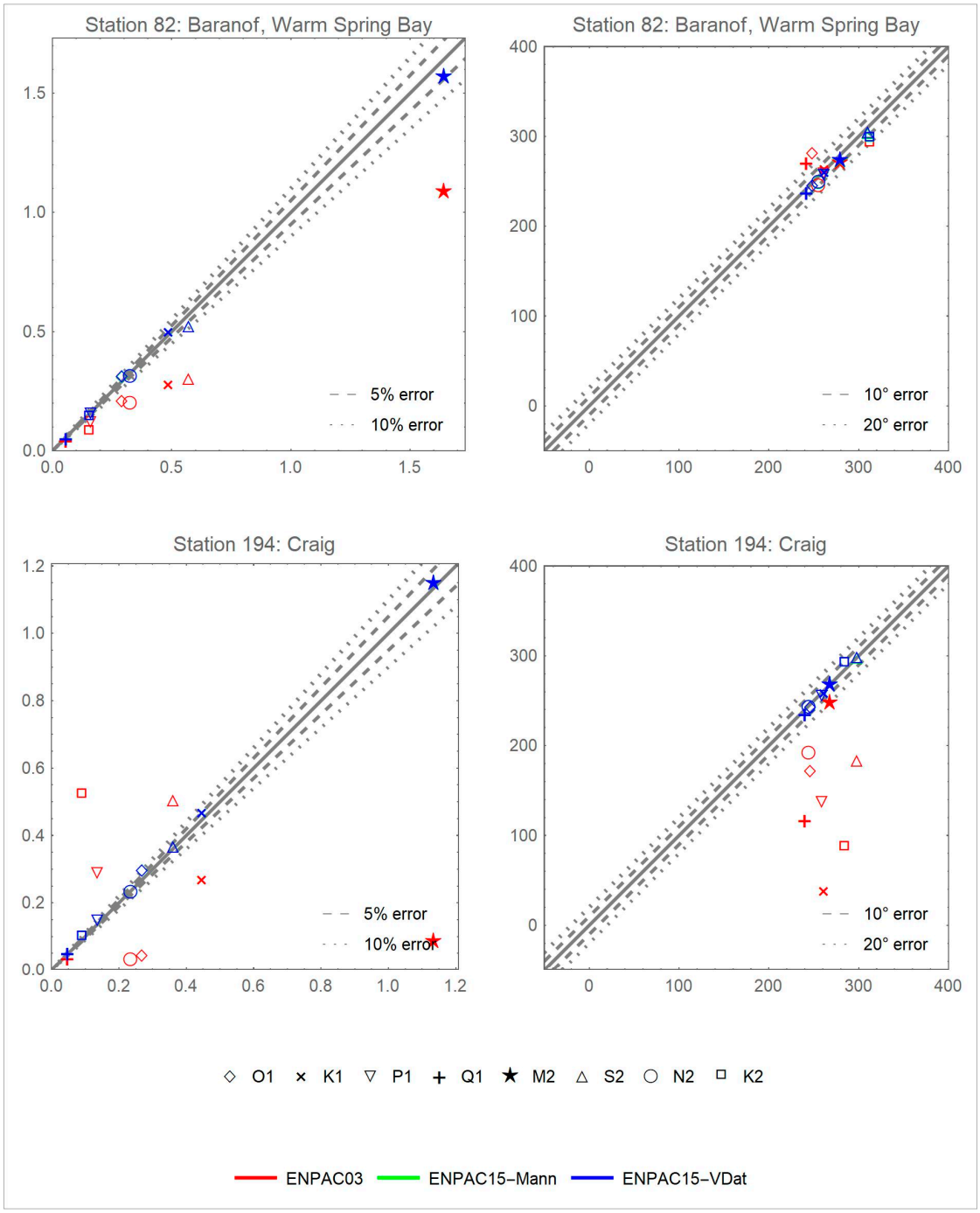

Figure A12. Scatterplots of errors for two Southeast Alaska stations, locations shown in Figure A4.

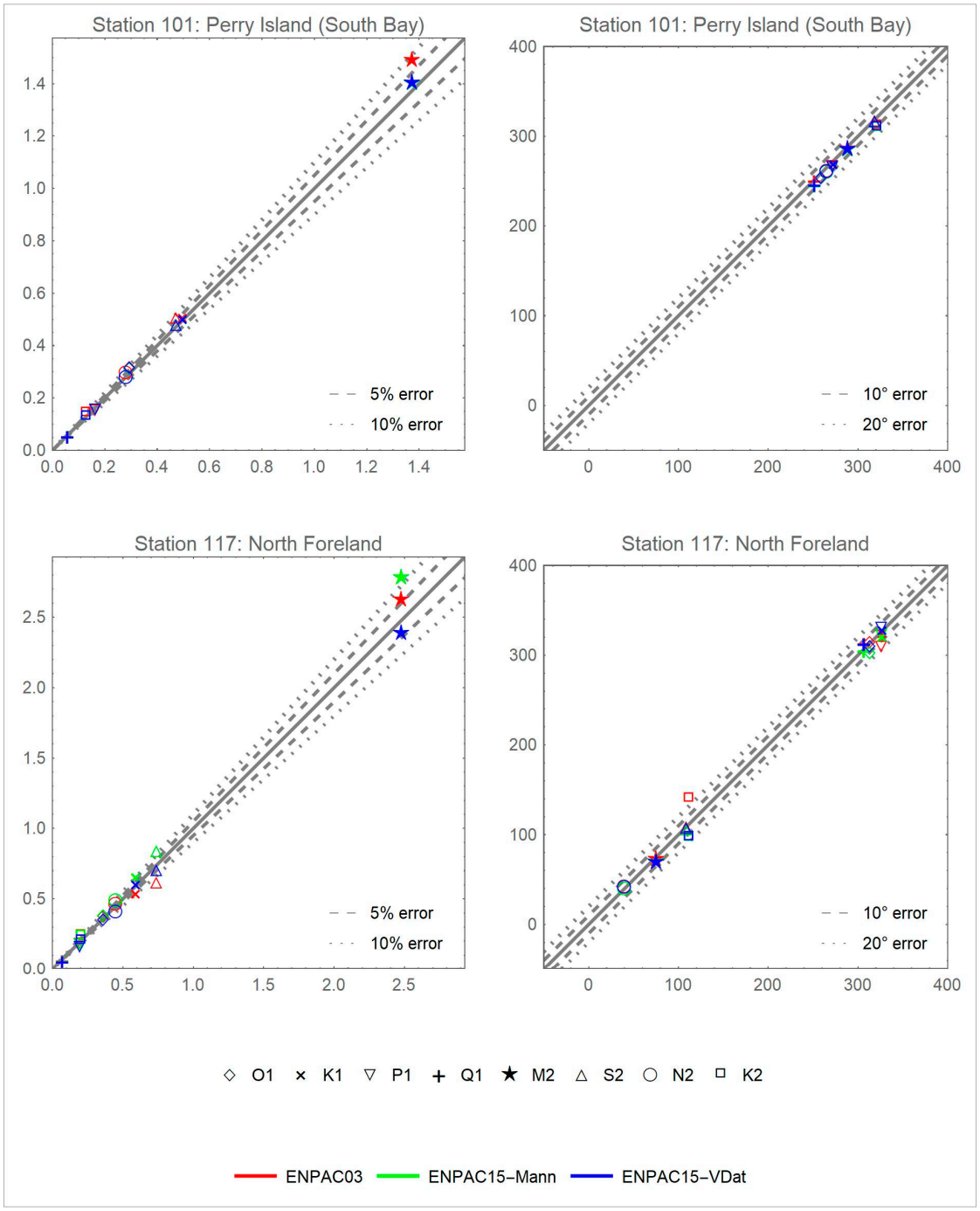

Figure A13. Scatterplots of errors for two Southern Alaska coast stations, locations shown in Figure A5.

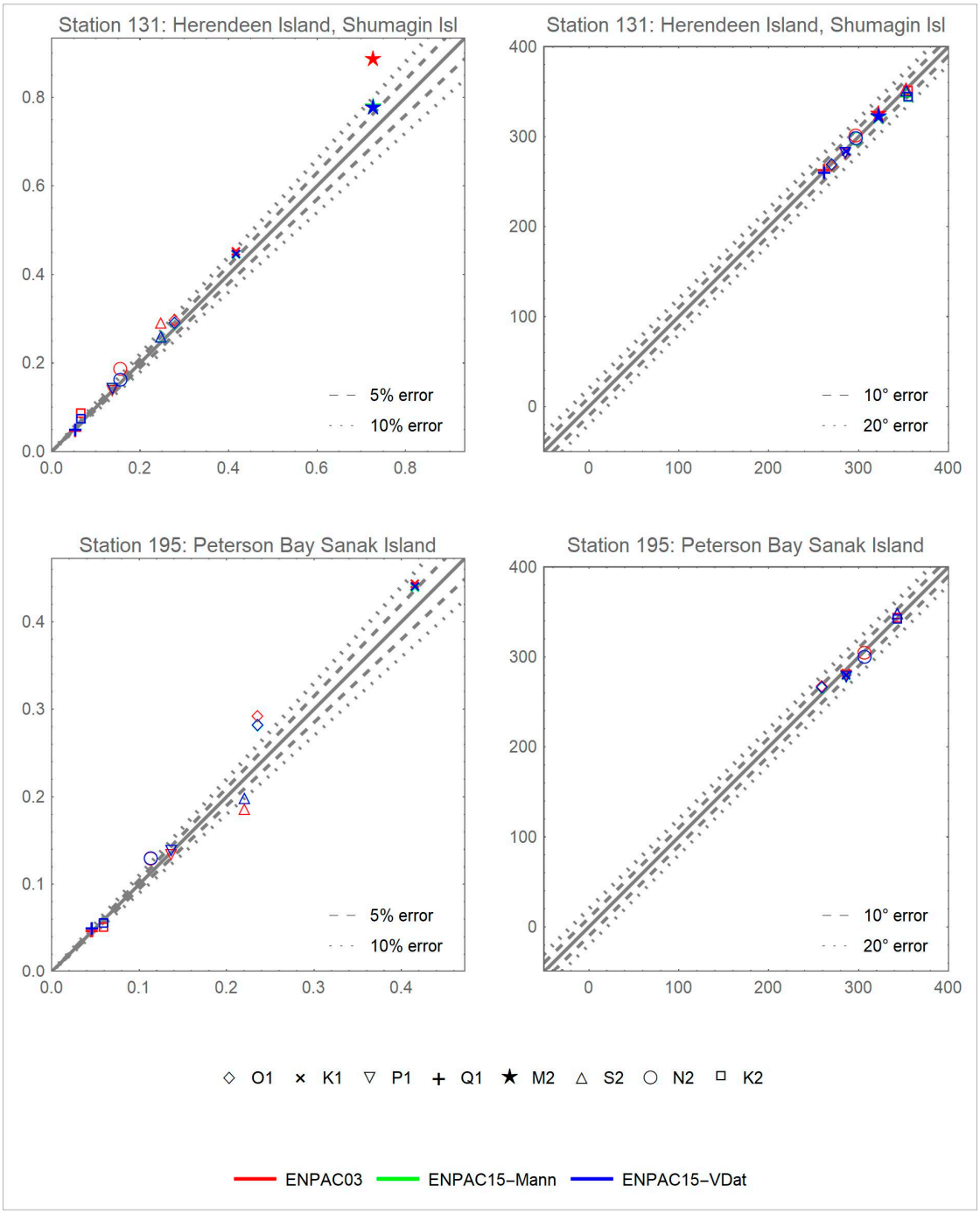

Figure A14. Scatterplots of errors for two Southern Alaska coast stations, locations shown in Figure A5.

Appendix D

The actual geographic distribution of errors for the M_2 and K_1 constituents in the ENPAC15 tidal database are provided at all 258 validation stations in the following seven figures. The dominant M_2 constituent is plotted for all of the same regional views shown in Figures A1–A5; however, the K_1 constituent is only shown for the Vancouver Island area shown in Figure A4. Symbol shapes denote the magnitude of the errors while the colors represent whether the ENPAC15 model is over (red) or underestimating (blue) the amplitudes. Similarly, blue symbols denote locations where the model exhibits a phase lag while red symbols denote a phase lead.

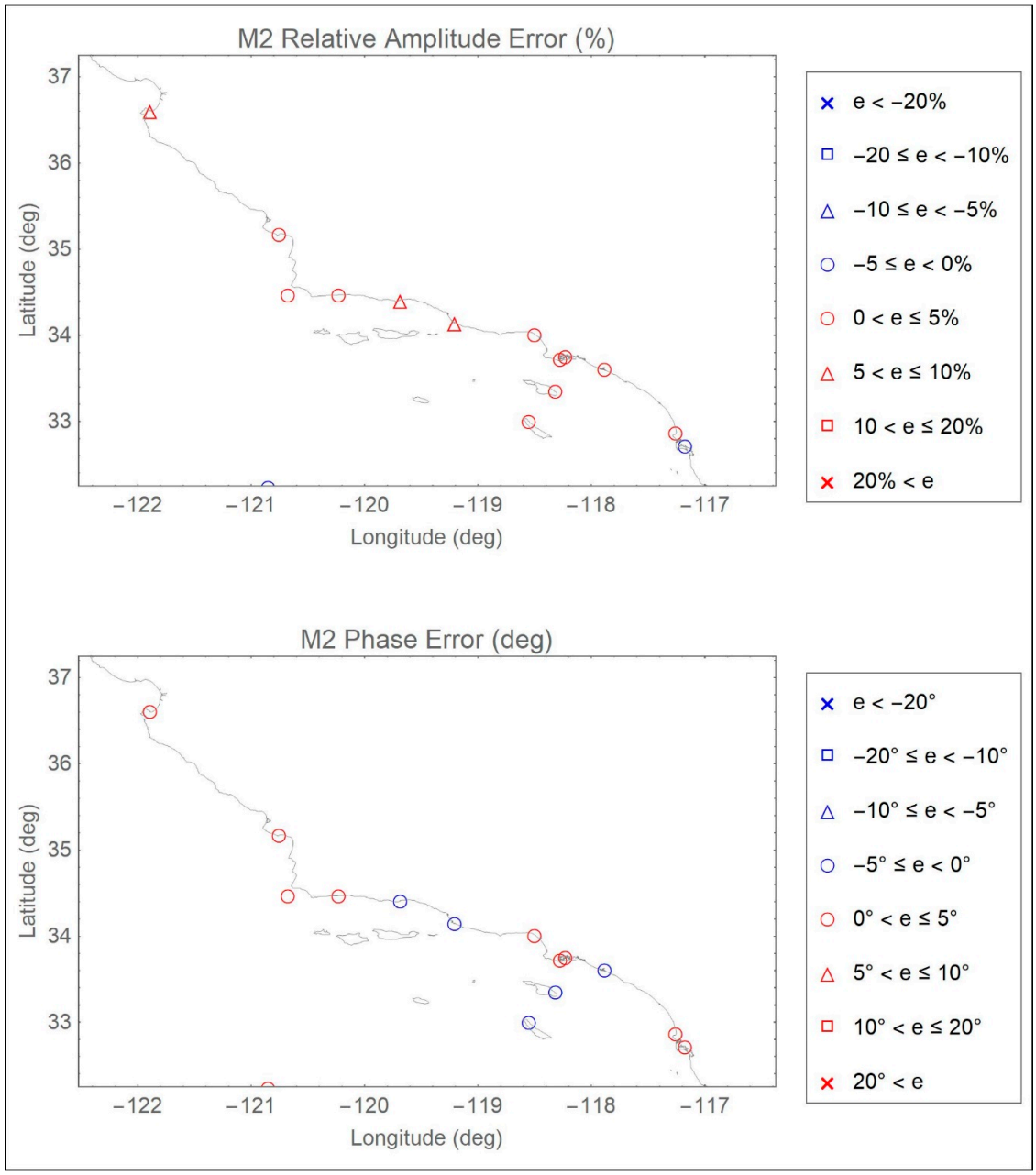

Figure A15. Distribution of ENPAC15 relative amplitude (%) and absolute phase (deg) errors for the M_2 constituent: Southern California coast view.

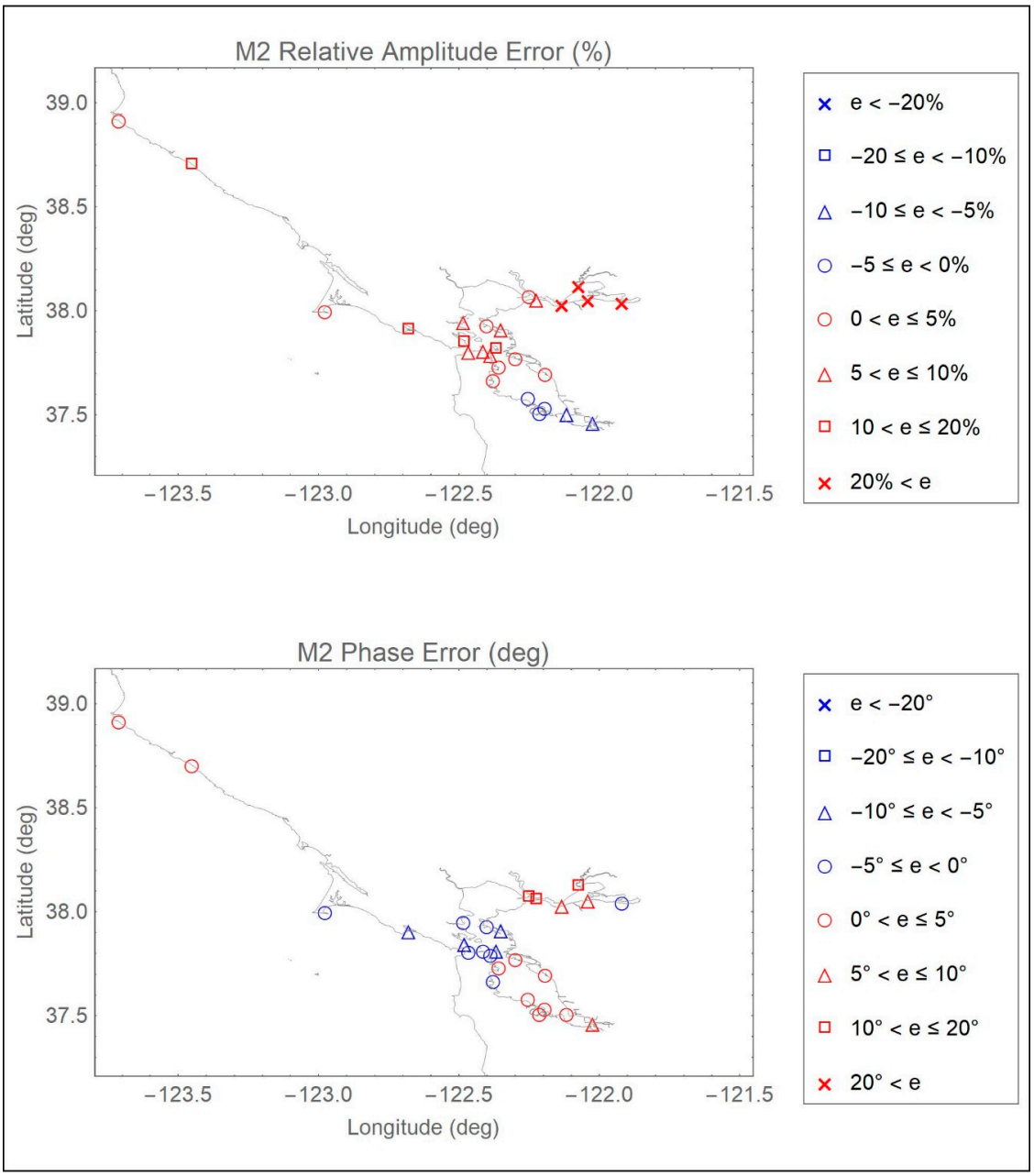

Figure A16. Distribution of ENPAC15 relative amplitude (%) and absolute phase (deg) errors for the M_2 constituent: San Francisco Bay view.

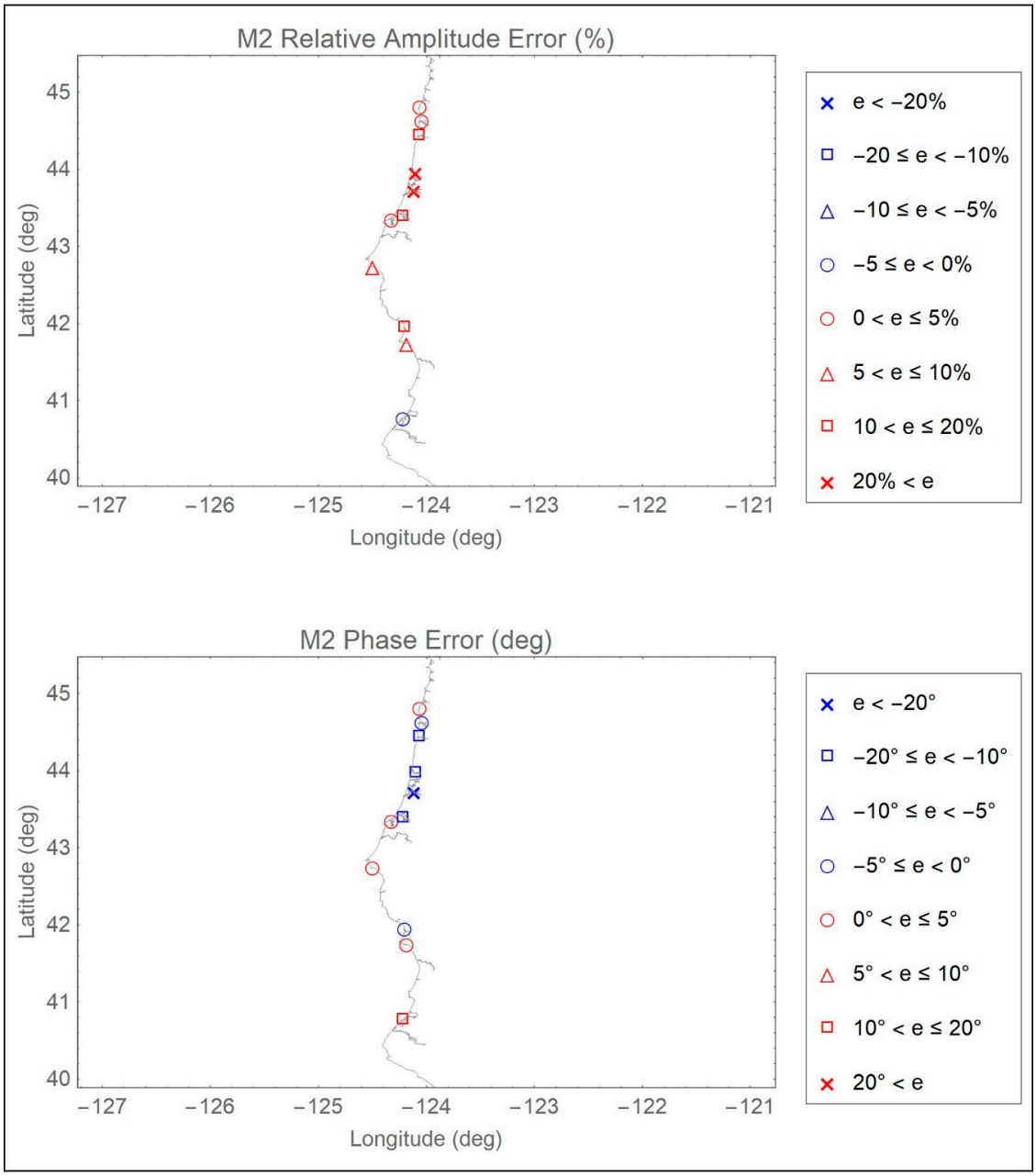

Figure A17. Distribution of ENPAC15 relative amplitude (%) and absolute phase (deg) errors for the M_2 constituent: Northern California coast view.

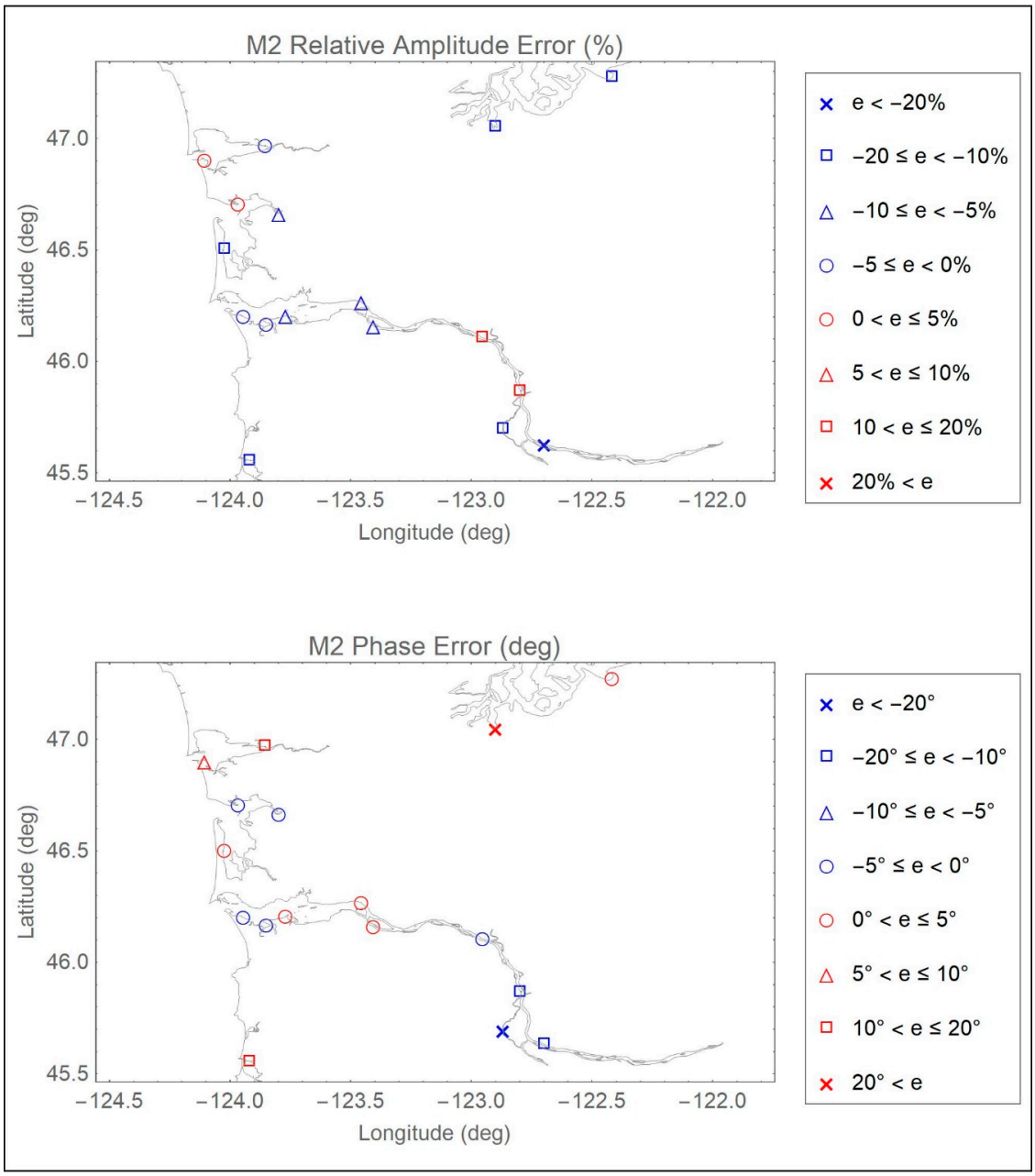

Figure A18. Distribution of ENPAC15 relative amplitude (%) and absolute phase (deg) errors for the M_2 constituent: Oregon and Washington coast view.

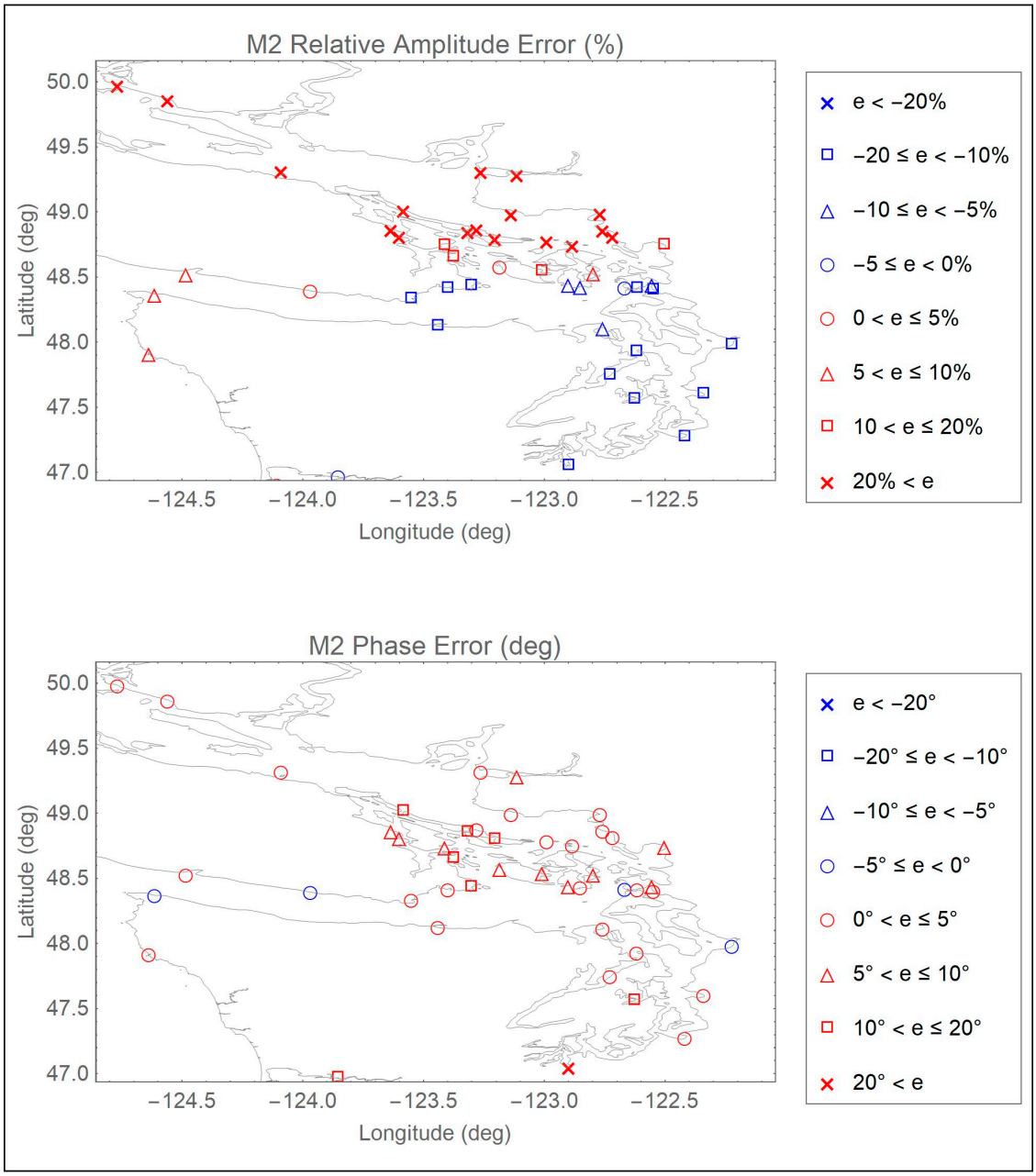

Figure A19. Distribution of ENPAC15 relative amplitude (%) and absolute phase (deg) errors for the M_2 constituent: Puget Sound view.

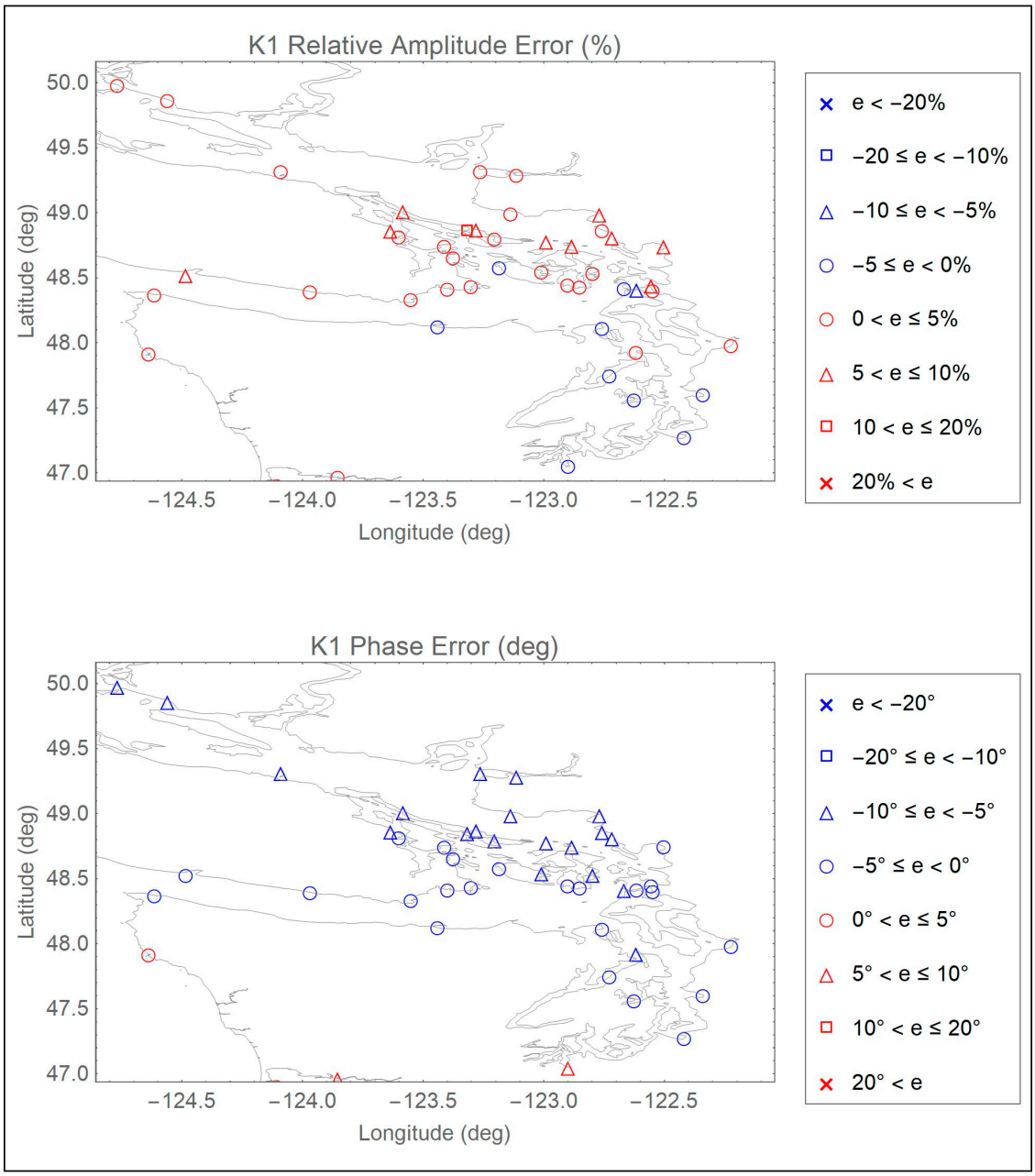

Figure A20. Distribution of ENPAC15 relative amplitude (%) and absolute phase (deg) errors for the K_1 constituent: Puget Sound view.

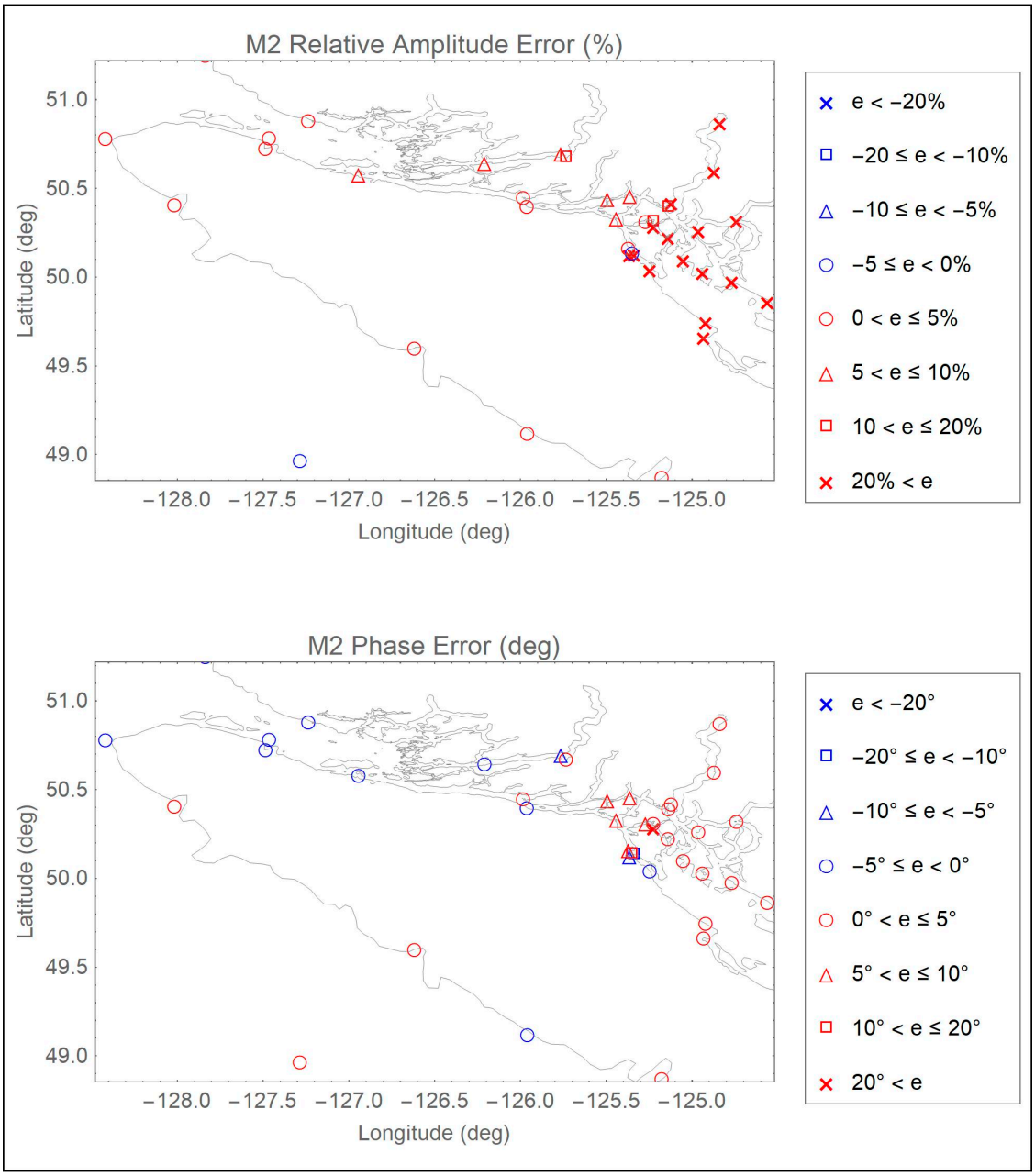

Figure A21. Distribution of ENPAC15 relative amplitude (%) and absolute phase (deg) errors for the M_2 constituent: British Columbia coast view.

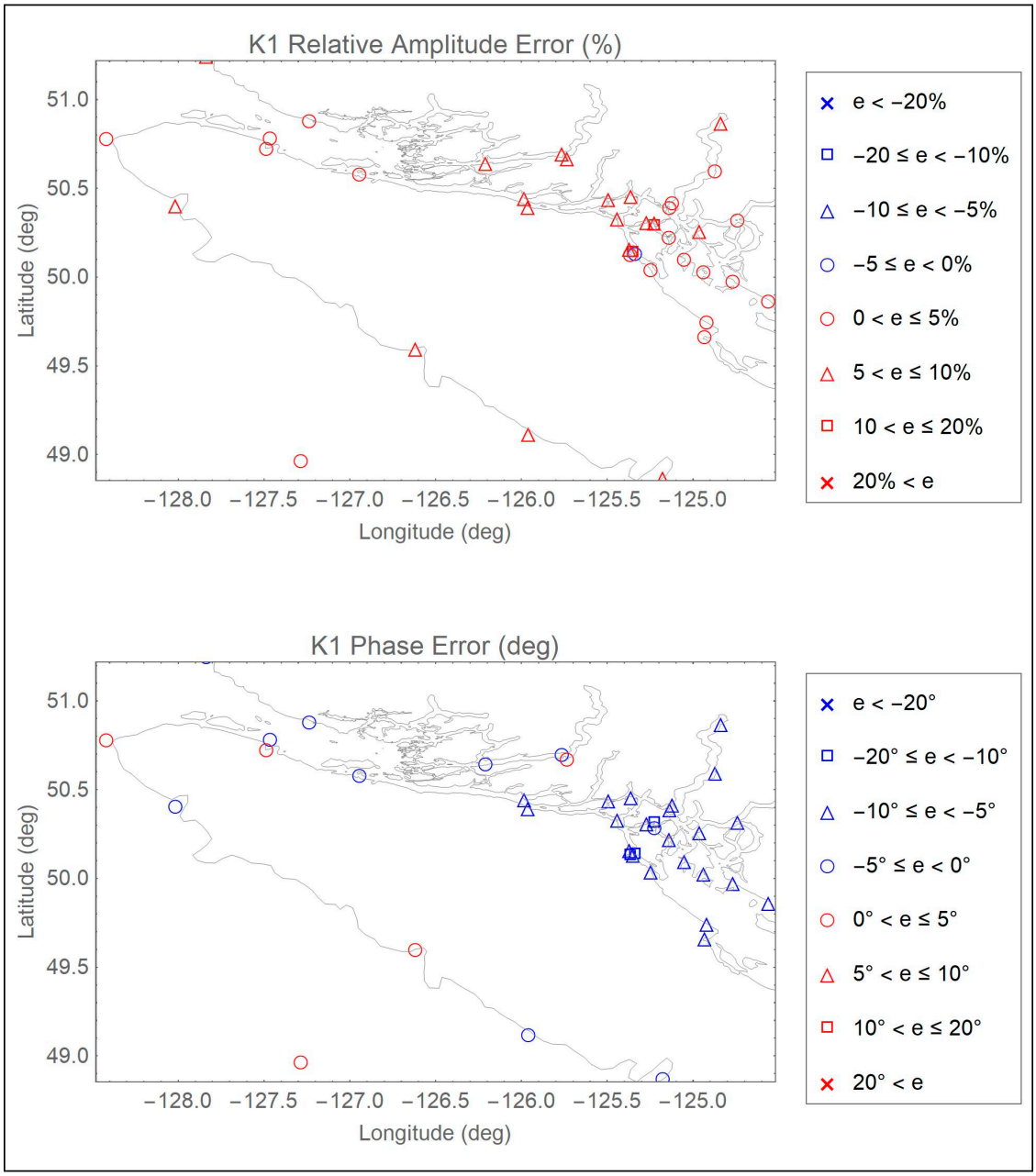

Figure A22. Distribution of ENPAC15 relative amplitude (%) and absolute phase (deg) errors for the K_1 constituent: British Columbia coast view.

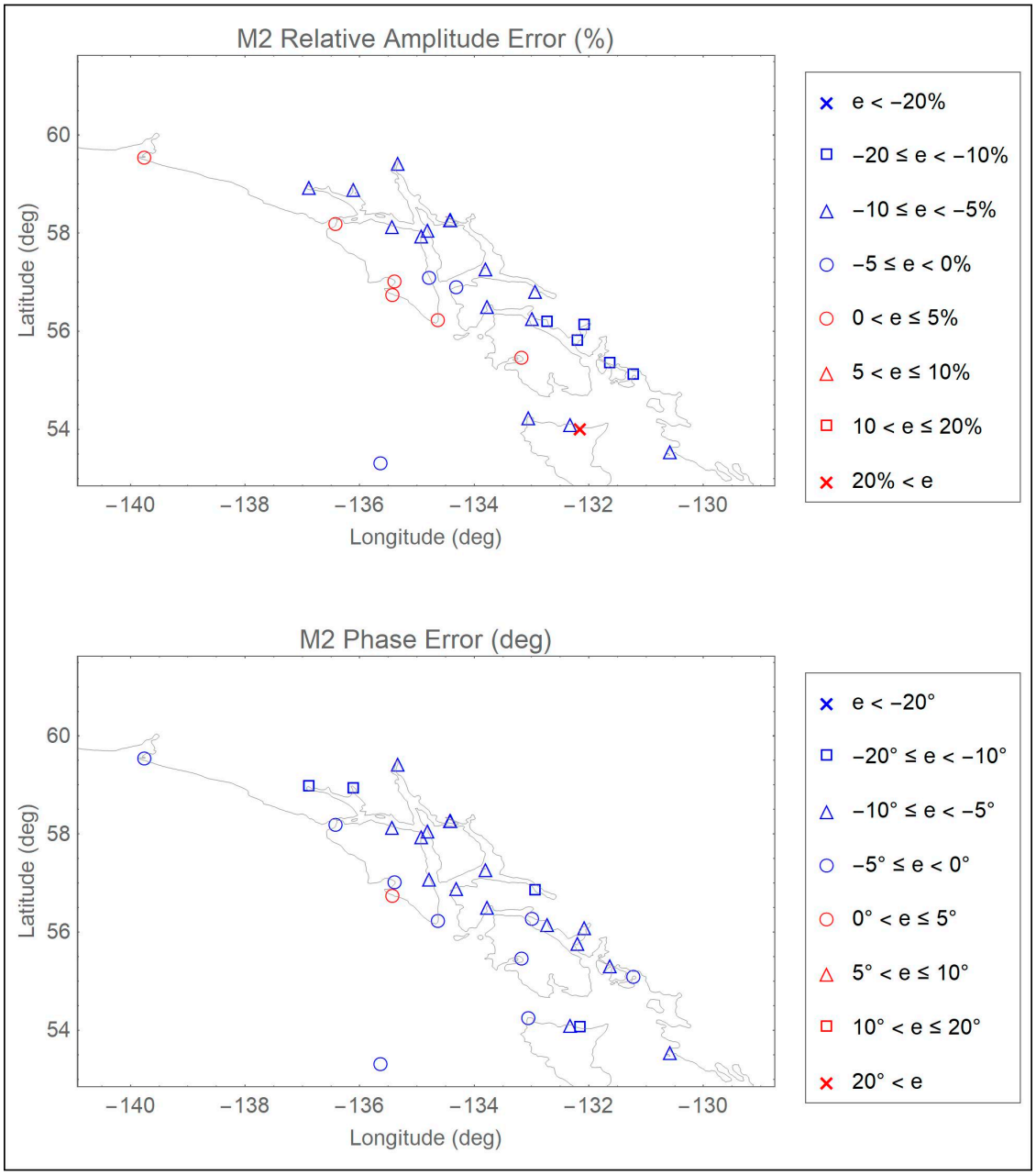

Figure A23. Distribution of ENPAC15 relative amplitude (%) and absolute phase (deg) errors for the M_2 constituent: Southeast Alaska view.

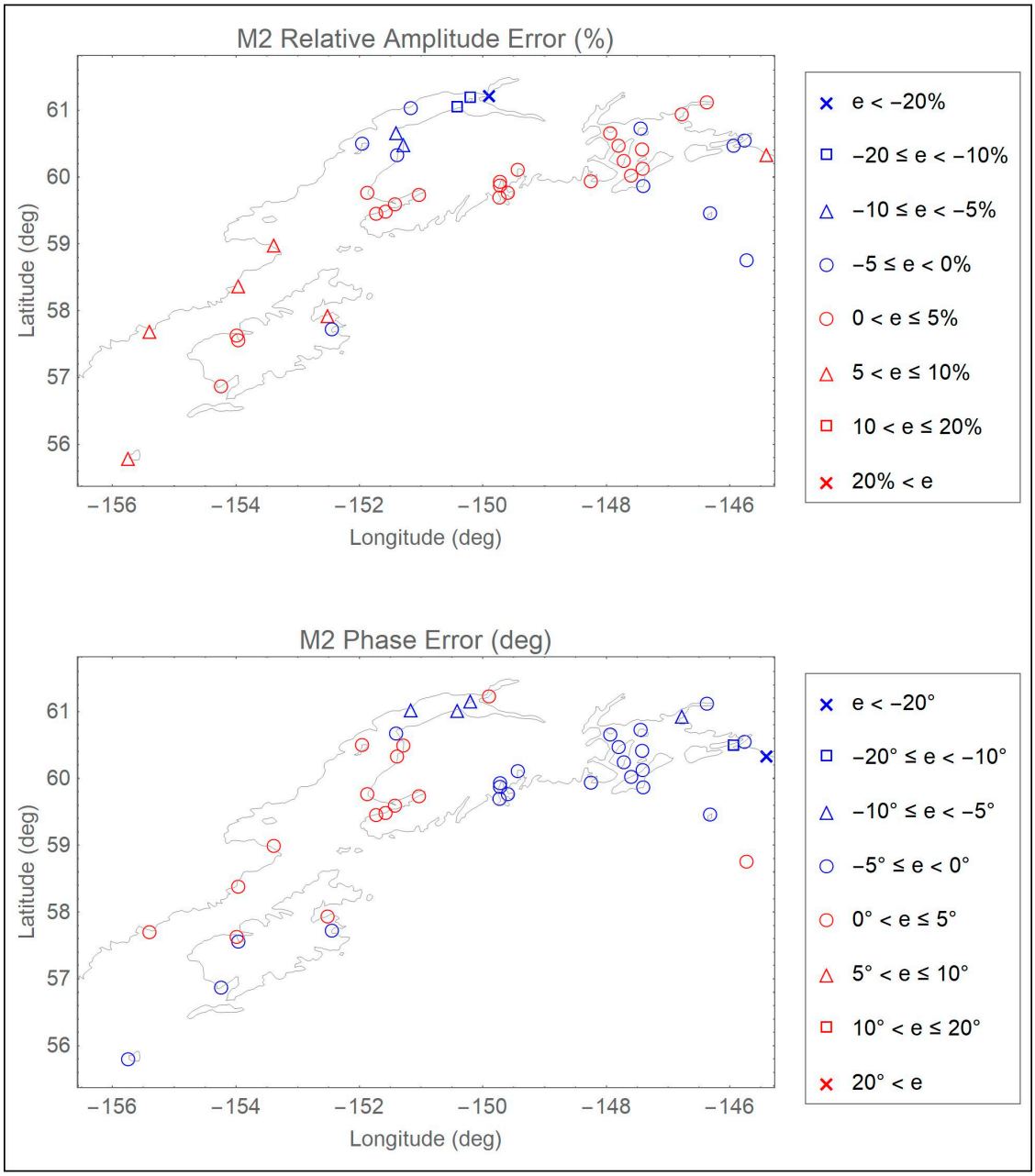

Figure A24. Distribution of ENPAC15 relative amplitude (%) and absolute phase (deg) errors for the M_2 constituent: Southern Alaska coast view one.

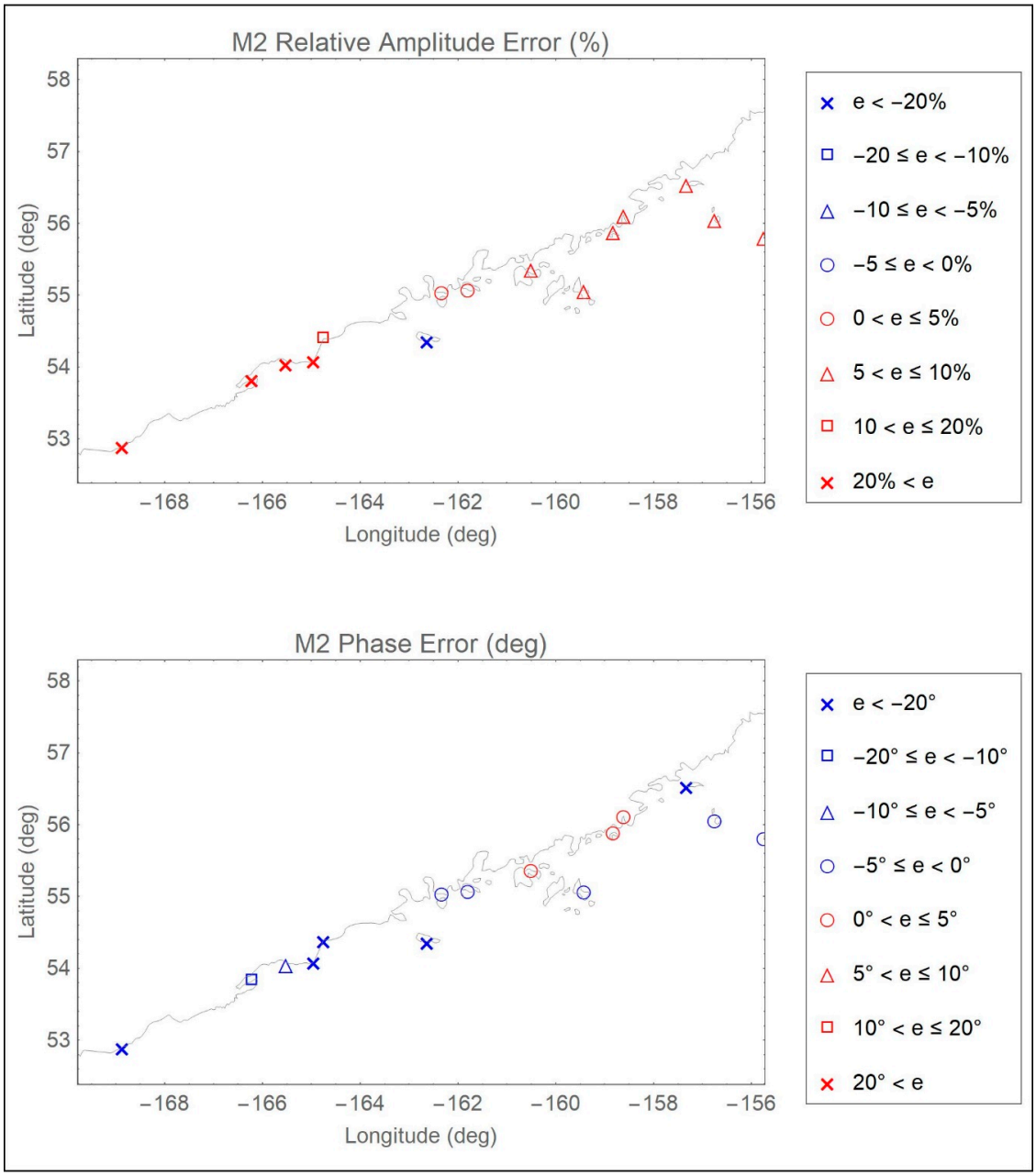

Figure A25. Distribution of ENPAC15 relative amplitude (%) and absolute phase (deg) errors for the M_2 constituent: Southern Alaska coast view two.

Appendix E

Herein, we provide general applicability and usage guidelines for the ENPAC15 tidal database. It is recommended that users read through these sections to understand the limitations of the database before they apply it to their own regions of interest.

Appendix E.1. Applicability Guidelines for the ENPAC15 Tidal Database

The ENPAC15 tidal database provides elevation amplitudes and phases throughout the ENPAC domain for all 37 constituents frequently used by NOS. Although data for all 37 constituents are included in the database, care should be taken when deciding how many of these constituents are important for the user's intended application. Often, accurate results can be obtained when using only the primary astronomic tides, particularly if the boundary of interest is in deeper water, far removed

from the coastline. Furthermore, only the eight primary astronomic constituents (M_2, S_2, N_2, K_2, O_1, K_1, P_1 and Q_1) were validated in this study.

It is important to note that the ENPAC15 database does not include all physical processes which can affect the model response including (but not limited to) density driven flows, riverine discharge, sediment transport and resulting bed morphological changes, large-scale oceanic currents or wind and atmospheric pressure driven flows. Depending upon the magnitude, each of these physical processes can have significant impacts on the accuracy of a given model. The user is cautioned that the database includes only barotropic computations of tidal circulation and does not consider any other physical processes.

Furthermore, how accurately the ENPAC15 grid geometry and bathymetry describe the region of specific interest influences the accuracy and appropriateness of applying database values. Therefore, further caution is recommended when applying the database along the Alaskan coast, as the coastline has not been significantly updated since the 2003 release. Recall that the Aleutian Island chain is approximated as a mainland boundary west of Unimak Island, Alaska, neglecting interaction with the Bering Sea. Therefore, the tidal response of the model west of this point, and, in the immediate area, is not accurate and the database should not be used to extract values in those areas.

Finally, the prevailing hydrodynamics in a specific region will determine how accurately the currents will be predicted. If the surface elevation response and currents are dominated by astronomical tides, then the database will provide an excellent prediction of the response. A good estimate of the accuracy of the ENPAC15 tides can be obtained by examining the regional error estimates given in Tables 7 and 8, or by examining the error plots provided for the dominant constituents in Appendix D; although plots are only provided for the M_2 and K_1 constituents, in general, all four of the semi-diurnal constituents follow the same regional trends, as do the diurnal constituents.

Appendix E.2. Usage Guidelines for the ENPAC15 Tidal Database

The ENPAC15 tidal constituent database can be applied anywhere *east* of Unimak Island, Alaska (160° W) within the defined ENPAC domain—refer to Figure 1. For locations that are tidally dominated and for which the ENPAC15 grid accurately describes both local geometry and bathymetry, the database can be directly applied to extract tidal elevations and currents. Because the thirty-seven constituents are computed at every node and are defined within the framework of a finite element grid, values at any point within the domain can be readily interpolated from the nodal values within which the point lies.

The location of the boundary where values are to be extracted should be placed away from the region of immediate interest and should never be placed within embayments, estuaries, or other small water bodies. In general, it is best to locate the regional boundary in deeper water somewhat removed from the coast whenever possible. Finally, it is recommended that the regional model be developed in such a way that the bathymetry at the regional boundary matches the bathymetry of the database model domain.

The ENPAC15 tidal database is available on the ADCIRC website as two separate compressed files: ENPAC15_elev-only_tidaldatabase.tar, which contains all of the extraction programs, grids, input files and sample notes but only has the fort.53 elevation harmonics; and ENPAC15_tidaldatabase.tar, which has everything given in the previous file with the addition of the fort.54 velocity harmonics [58]. Users will only need to download one of the files depending upon whether they wish to have access to the velocity data as well.

An extraction program, ADCIRC_db_extract_2015.F90, together with the ENPAC15 finite element grid file, wc2015_v1a_chk.grd, and input control files accompany the tidal database. The user must supply an input file that provides the number of extraction points desired followed by the list of coordinates for those points. The extraction program will prompt the user for this input files as well as the name of the grid used to create the database. The program will also prompt the user whether they would like to produce the harmonic constituent output for elevations, velocities or both and then will produce the harmonic extraction output for amplitude and phase at the specified location(s) according to the user's request. Elevation output is stored in elev_hc.out while velocity output is stored in vel_hc.out. Additionally, diagnostic output is written to tides.dia and provides the location

of each extraction point in the global mesh as well as the interpolation weights used to calculate the harmonic constituents. The KDTREE2 search algorithms have been incorporated into the new extraction program to facilitate a speedier search response. Finally, the program takes advantage of dynamic allocation in order to avoid the old hardcoded array limitations found in previous extraction routines. The ADCIRC_db_extract_2015.F90 program will work with any old ADCIRC databases that utilized the individual fort.53 and fort.54 file formats.

In addition to the extraction program, the database files also include another utility for "cutting" a portion of the global database out for visualization. The HarmonicResultScope.f90 program works much the same way as ResultScope.f90, for those who are familiar with that ADCIRC utility program. Additional notes about the usage of each of these programs, as well as sample input and output files for each, are included in the TidalExtract/ directory within the database tar file.

For the interested reader, a time-history of response can be readily Fourier synthesized using the outputs in the elev_hc.out and vel_hc.out files. For example, a time-history of water-surface elevation can be computed as

$$\zeta(x,y,t) = \sum A_i(x,y) f_i(t_0) \cos[\sigma_i(t-t_0) + V_i(t_0) - h_i(x,y)], \quad \text{(A1)}$$

where $A_i(x,y)$ and $h_i(x,y)$ are the amplitude and phase, respectively, at the location (x,y) of interest for constituent i, which are provided by the ENPAC15 tidal database, and the frequency $\sigma_i = 2\pi/T_i$. The frequencies σ_i in rad/sec and periods T_i in hours for each of the 37 constituents included in the database are presented in Table A2. It is important to specify frequencies precisely, at least to eight significant figures. The nodal factor $f_i(t_0)$ and the equilibrium argument, $V_i(t_0)$, relative to reference time t_0 can be computed using program tide_fac.f, which is available as a utility program on the ADCIRC website [60].

Table A2. Frequencies and periods for ENPAC15 harmonic constituents.

Constituent	Frequency (rad/s)	Period (h)
M(2)	0.0001405189	12.42
N(2)	0.0001378797	12.66
S(2)	0.0001454441	12.00
O(1)	0.0000675977	25.82
K(1)	0.0000729212	23.93
K(2)	0.0001458423	11.97
L(2)	0.0001431581	12.19
2N(2)	0.0001352405	12.91
R(2)	0.0001456432	11.98
T(2)	0.0001452450	12.02
Lambda(2)	0.0001428049	12.22
Mu(2)	0.0001355937	12.87
Nu(2)	0.0001382329	12.63
J(1)	0.0000755604	23.10
M(1)	0.0000702820	24.83
OO(1)	0.0000782446	22.31
P(1)	0.0000725229	24.07
Q(1)	0.0000649585	26.87
2Q(1)	0.0000623193	28.01
Rho(1)	0.0000653117	26.72
M(4)	0.0002810378	6.21
M(6)	0.0004215567	4.14
M(8)	0.0005620756	3.11
S(4)	0.0002908882	6.00
S(6)	0.0004363323	4.00
M(3)	0.0002107784	8.28
S(1)	0.0000727221	24.00

Table A2. *Cont.*

Constituent	Frequency (rad/s)	Period (h)
MK(3)	0.0002134401	8.18
2MK(3)	0.0002081166	8.39
MN(4)	0.0002783986	6.27
MS(4)	0.0002859630	6.10
2SM(2)	0.0001503693	11.61
Mf	0.0000053234	327.86
Msf	0.0000049252	354.37
Mm	0.0000026392	661.31
Sa	0.0000001991	8765.82
Ssa	0.0000003982	4382.91

References

1. Dietsche, D.; Hagen, S.C.; Bacopoulos, P. Storm surge simulations for hurricane hugo (1989): On the significance of inundation areas. *J. Waterw. Port Coast. Ocean Eng.* **2007**, *133*, 183–191. [CrossRef]
2. Irish, J.L.; Resio, D.T.; Ratcliff, J.J. The influence of storm size on hurricane surge. *J. Phys. Oceanogr.* **2008**, *38*, 2003–2013. [CrossRef]
3. Kerr, P.C.; Donahue, A.S.; Westerink, J.J.; Luettich, R.A.; Zheng, L.Y.; Weisberg, R.H.; Huang, Y.; Wang, H.V.; Teng, Y.; Forrest, D.R.; et al. U.S. IOOS coastal and ocean modeling testbed: Inter-model evaluation of tides, waves, and hurricane surge in the Gulf of Mexico. *J. Geophys. Res. Ocean* **2013**, *118*, 5129–5172. [CrossRef]
4. Pandoe, W.W.; Edge, B.L. Case study for a cohesive sediment transport model for Matagorda Bay, Texas, with Coupled ADCIRC 2D-Transport and SWAN wave models. *J. Hydraul. Eng.* **2008**, *134*, 303–314. [CrossRef]
5. Grzegorzewski, A.S.; Johnson, B.D.; Wamsley, T.V.; Rosati, J.D. Sediment transport and morphology modeling of Ship Island, Mississippi, USA, during storm events. In Proceedings of the Coastal Dynamics 2013, Arcachon Convention Centre, Arcachon, France, 24–28 June 2013; pp. 1505–1516.
6. Miles, T.; Seroka, G.; Kohut, J.; Schofield, O.; Glenn, S. Glider observations and modeling of sediment transport in Hurricane Sandy. *J. Geophys. Res. Ocean* **2015**, *120*, 1771–1791. [CrossRef]
7. Feyen, J.; Hess, K.; Spargo, E.; Wong, A.; White, S.; Sellars, J.; Gill, S. Development of a continuous bathymetric/topographic unstructured coastal flooding model to study sea level rise in North Carolina. In Proceedings of the Ninth International Conference on Estuarine and Coastal Modeling, Charleston, SC, USA, 3 October 2005; pp. 338–356.
8. Atkinson, J.; McKee Smith, J.; Bender, C. Sea-level rise effects on storm surge and nearshore waves on the Texas coast: Influence of landscape and storm characteristics. *J. Waterw. Port Coast. Ocean Eng.* **2013**, *139*, 98–117. [CrossRef]
9. Bilskie, M.V.; Hagen, S.C.; Medeiros, S.C.; Passeri, D.L. Dynamics of sea level rise and coastal flooding on a changing landscape. *Geophys. Res. Lett.* **2014**, *41*, 927–934. [CrossRef]
10. Cheng, T.K.; Hill, D.F.; Beamer, J.; García-Medina, G. Climate change impacts on wave and surge processes in a Pacific Northwest (USA) estuary. *J. Geophys. Res. Ocean* **2015**, *120*, 182–200. [CrossRef]
11. Mattocks, C.; Forbes, C. A real-time, event-triggered storm surge forecasting system for the state of North Carolina. *Ocean Model.* **2008**, *25*, 95–119. [CrossRef]
12. Fleming, J.G.; Fulcher, C.W.; Luettich, R.A.; Estrade, B.D.; Allen, G.D.; Winer, H.S. A real time storm surge forecasting system using ADCIRC. In Proceedings of the 10th International Conference on Estuarine and Coastal Modeling, Newport, RI, USA, 5–7 November 2008; pp. 893–912.
13. Dresback, K.M.; Fleming, J.G.; Blanton, B.O.; Kaiser, C.; Gourley, J.J.; Tromble, E.M.; Luettich, R.A.; Kolar, R.L.; Hong, Y.; Van Cooten, S.; et al. Skill assessment of a real-time forecast system utilizing a coupled hydrologic and coastal hydrodynamic model during Hurricane Irene (2011). *Cont. Shelf Res.* **2013**, *71*, 78–94. [CrossRef]
14. Dietrich, J.; Dawson, C.; Proft, J.; Howard, M.; Wells, G.; Fleming, J.; Luettich, R.; Westerink, J.; Cobell, Z.; Vitse, M.; et al. Real-time forecasting and visualization of hurricane waves and storm surge using SWAN + ADCIRC and FigureGen. In *Computational Challenges in the Geosciences*; Dawson, C., Gerritsen, M., Eds.; Springer: New York, NY, USA, 2013; Volume 156, pp. 49–70.

15. Dietrich, J.C.; Trahan, C.J.; Howard, M.T.; Fleming, J.G.; Weaver, R.J.; Tanaka, S.; Yu, L.; Luettich, R.A.; Dawson, C.N.; Westerink, J.J.; et al. Surface trajectories of oil transport along the Northern Coastline of the Gulf of Mexico. *Cont. Shelf Res.* **2012**, *41*, 17–47. [CrossRef]
16. Carr, S.; Hench, J.; Luettich, R.; Forward, R.; Tankersley, R. Spatial patterns in the ovigerous Callinectes sapidus spawning migration: Results from a coupled behavioral-physical model. *Mar. Ecol.* **2005**, *294*, 213–226. [CrossRef]
17. Oliveira, A.; Fortunato, A.B.; Pinto, L. Modelling the hydrodynamics and the fate of passive and active organisms in the Guadiana estuary. *Estuar. Coast. Shelf Sci.* **2006**, *70*, 76–84. [CrossRef]
18. Reyns, N.B.; Eggleston, D.B.; Luettich, R.J.A. Secondary dispersal of early juvenile blue crabs within a wind-driven estuary. *Limnol. Oceanogr.* **2006**, *51*, 1982–1995. [CrossRef]
19. Alizad, K.; Hagen, S.C.; Morris, J.T.; Bacopoulos, P.; Bilskie, M.V.; Weishampel, J.F.; Medeiros, S.C. A coupled, two-dimensional hydrodynamic-marsh model with biological feedback. *Ecol. Model.* **2016**, *327*, 29–43. [CrossRef]
20. Tromble, E.; Kolar, R.; Dresback, K.; Luettich, R. River flux boundary considerations in a coupled hydrologic-hydrodynamic modeling system. In Proceedings of the 12th International Conference on Estuarine and Coastal Modeling 2011, St. Augustine, FL, USA, 7–9 November 2011; pp. 510–527.
21. Lyard, F.; Lefevre, F.; Letellier, T.; Francis, O. Modelling the global ocean tides: modern insights from FES2004. *Ocean Dyn.* **2006**, *56*, 394–415. [CrossRef]
22. OTIS Regional Tidal Solutions. Available online: http://volkov.oce.orst.edu/tides/region.html (accessed on 19 September 2018).
23. Parrish, D.M.; Hagen, S.C. A tidal constituent database for the east coast of Florida. In Proceedings of the Fourth International Symposium on Ocean Wave Measurement and Analysis, San Francisco, CA, USA, 2–6 September 2002; pp. 1605–1614.
24. Westerink, J.J.; Luettich, R.A.; Muccino, J.C. Modelling tides in the western North Atlantic using unstructured graded grids. *Tellus* **1994**, *46*, 178–199. [CrossRef]
25. Mukai, A.Y.; Westerink, J.J.; Luettich, R.A.; Mark, D. *Eastcoast 2001: A Tidal Constituent Database for the Western North Atlantic, Gulf of Mexico and Caribbean Sea*; Technical Report for ERDC/CHL TR-02-24; U.S. Army Engineer Research and Development Center, Coastal and Hydraulics Laboratory: Vicksburg, MS, USA, 2002; p. 201. Available online: http://www.unc.edu/ims/adcirc/publications/2002/2002_Mukai01.pdf (accessed on 27 June 2016).
26. Szpilka, C.; Dresback, K.; Kolar, R.; Feyen, J.; Wang, J. Improvements for the western north Atlantic, Caribbean and Gulf of Mexico ADCIRC tidal database (EC2015). *J. Mar. Sci. Eng.* **2016**, *4*, 72. [CrossRef]
27. Spargo, E.; Westerink, J.; Luettich, R., Jr.; Mark, D. *ENPAC 2003: A Tidal Constituent Database for Eastern North Pacific Ocean*; Technical Report ERDC/CHL TR-04-12; U.S. Army Engineer Research and Development Center, Coastal and Hydraulics Laboratory: Vicksburg, MS, USA, 2004; Available online: http://www.unc.edu/ims/ccats/tides/ENPAC_2003_report.pdf (accessed on 18 September 2018).
28. Guillou, N.; Neill, S.P.; Robins, P.E. Characterising the tidal stream power resource around France using a high-resolution harmonic database. *Renew. Energy* **2018**, *123*, 706–718. [CrossRef]
29. Kelleher, G.; Bleakley, C.; Wells, S. *A Global Representative System of Marine Protected Areas IV*; The World Bank: Washington, DC, USA, 1995.
30. *ETOPO-5 Bathymetry/Topography Data*; Data Announcement 88-MGG-02, National Geophysical Data Center; National Oceanic and Atmospheric Administration, U.S. Department of Commerce: Boulder, CO, USA, 1988.
31. *GEODAS CD-ROM Hydrographic Survey Data*; Data Announcement 98-MGG-03, National Geophysical Data Center; National Oceanic and Atmospheric Administration, U.S. Department of Commerce: Boulder, CO, USA, 1998.
32. Schureman, P. *Manual of Harmonic Analysis and Prediction of Tides*; Special Publication 98, Coast and Geodetic Survey; U.S. Dept. of Commerce: Washington, DC, USA, 1958; p. 317.
33. Kinnmark, I. *The Shallow Water Wave Equations: Formulation, Analysis and Application*; Lecture Notes in Engineering; Springer: Berlin/Heidelberg, Germany, 1986; Volume 15, ISBN 9783540160311.
34. Luettich, R.A.; Westerink, J.J.; Scheffner, N.W. *ADCIRC: An Advanced Three-Dimensional Circulation Model for Shelves, Coasts, and Estuaries; Report 1: Theory and Methodology of ADCIRC-2DDI and ADCIRC-3DL*; Technical Report CERC-TR-DRP-92-6; U.S. Army Corps of Engineers, U.S. Department of the Army: Washington, DC, USA, 1992.

35. Kolar, R.L.; Gray, W.G.; Westerink, J.J.; Luettich, R.A. Shallow water modeling in spherical coordinates: equation formulation, numerical implementation, and application. *J. Hydraul. Res.* **1994**, *32*, 3–24. [CrossRef]
36. Bunya, S.; Dietrich, J.C.; Westerink, J.J.; Ebersole, B.A.; Smith, J.M.; Atkinson, J.H.; Jensen, R.; Resio, D.T.; Luettich, R.A.; Dawson, C.; et al. A high-resolution coupled riverine flow, tide, wind, wind wave, and storm surge model for Southern Louisiana and Mississippi. Part I: Model Development and Validation. *Mon. Weather Rev.* **2010**, *138*, 345–377. [CrossRef]
37. OSU Tidal Data Inversion. Available online: http://volkov.oce.orst.edu/tides/tpxo8_atlas.html (accessed on 21 July 2018).
38. Xu, J.; Feyen, J. *The Extratropical Surge and Tide Operational Forecast System for the Eastern North Pacific Ocean (ESTOFS-Pacific): Development and Skill Assessment*; NOAA Technical Memorandum NOS CS 36; U.S. Department of Commerce: Silver Spring, MD, USA, 2016. Available online: https://repository.library.noaa.gov/view/noaa/8441 (accessed on 20 September 2018).
39. NOAA/NOS's VDatum 3.6: Vertical Datums Transformation. Available online: http://vdatum.noaa.gov/welcome.html (accessed on 21 July 2016).
40. Myers, E.; Woolard, J.; Yang, Z.; Aikman, F. Development of a vertical datum transformation tool and a bathymetric/topographic digital elevation model for southern California. In Proceedings of the Coastal Society 2008, Redondo Beach, CA, USA, 29 June–2 July 2008.
41. Xu, J.; Myers, E.; White, S. *VDatum for the Coastal Waters of North/Central California, Oregon and Western Washington: Tidal Datums and Sea Surface Topography*; NOAA Technical Memorandum NOS CS 22; U.S. Department of Commerce: Silver Spring, MD, USA, 2010. Available online: https://vdatum.noaa.gov/download/publications/CS_22_FY09_33_Jiangtao_PNW_VDatum_techMemor.pdf (accessed on 19 September 2018).
42. VDatum Manual for Development and Support of NOAA's Vertical Datum Transformation Tool, VDatum. Version 1.01. 2012. Available online: http://www.nauticalcharts.noaa.gov/csdl/publications/Manual_2012.06.26.doc (accessed on 27 June 2016).
43. Foreman, M.G.G.; Sutherland, G.; Cummins, P.F. M2 tidal dissipation around Vancouver Island: an inverse approach. *Cont. Shelf Res.* **2004**, *24*, 2167–2185. [CrossRef]
44. Foreman, M.G.G.; Stucchi, D.J.; Garver, K.A.; Tuele, D.; Isaac, J.; Grime, T.; Guo, M.; Morrison, J. A circulation model for the discovery islands, British Columbia. *Atmosphere-Ocean* **2012**, *50*, 301–316. [CrossRef]
45. Bacopoulos, P.; (University of North Florida, Jacksonville, FL, USA). Personal communication, 2015.
46. Parrish, D.M.; Hagen, S.C. 2D unstructured mesh generation for oceanic and coastal tidal models from a localized truncation error analysis with complex derivatives. *Int. J. Comput. Fluid Dyn.* **2007**, *21*, 277–296. [CrossRef]
47. NOS Hydrographic Survey Data and Products. Available online: https://www.ngdc.noaa.gov/mgg/bathymetry/hydro.html (accessed on 20 September 2018).
48. Smith, W.H.F.; Sandwell, D.T. Global sea floor topography from satellite altimetry and ship depth soundings. *Science* **1997**, *277*, 1956–1962. [CrossRef]
49. Carrère, L.; Lyard, F.; Cancet, M.; Roblou, L.; Guillot, A. FES2012: A new global tidal model taking advantage of nearly 20 years of altimetry measurements. In Proceedings of the Meeting "20 Years of Progress in Radar Altimetry Symposium", Venice, Italy, 24–29 September 2012.
50. Global Tide—FES: Aviso+. Available online: http://www.aviso.altimetry.fr/en/data/products/auxiliary-products/global-tide-fes.html (accessed on 27 June 2016).
51. Egbert, G.D.; Bennett, A.F.; Foreman, M.G.G. TOPEX/POSEIDON tides estimated using a global inverse model. *J. Geophys. Res.* **1994**, *99*, 24821. [CrossRef]
52. Egbert, G.D.; Erofeeva, S.Y. Efficient inverse modeling of Barotropic Ocean tides. *J. Atmos. Ocean. Technol.* **2002**, *19*, 183–204. [CrossRef]
53. USGS Coastal and Marine Geology—usSEABED. Available online: http://walrus.wr.usgs.gov/usseabed/ (accessed on 29 June 2016).
54. Kolar, R.L.; Westerink, J.J.; Cantekin, M.E.; Blain, C.A. Aspects of nonlinear simulations using shallow-water models based on the wave continuity equation. *Comput. Fluids* **1994**, *23*, 523–538. [CrossRef]
55. NOAA Tides and Currents. Available online: http://tidesandcurrents.noaa.gov/ (accessed on 21 July 2018).
56. Foreman, M.G.G.; (Institute of Ocean Sciences—Fisheries and Oceans Canada, Sidney, BC, Canada). Personal communication, 2015.

57. *IHO Tidal Constituent Bank: Station Catalogue*; Department of Fisheries and Oceans: Ottawa, ON, Canada, 1979.
58. Foreman, M.G.G.; Walters, R.A.; Henry, R.F.; Keller, C.P.; Dolling, A.G. A tidal model for eastern Juan de Fuca Strait and the southern Strait of Georgia. *J. Geophys. Res.* **1995**, *100*, 721. [CrossRef]
59. ADCIRC Tidal Database—ADCIRC. Available online: http://adcirc.org/products/adcirc-tidal-databases/ (accessed on 23 September 2018).
60. ADCIRC Utility Programs—ADCIRC. Available online: http://adcirc.org/home/related-software/adcirc-utility-programs/ (accessed on 23 September 2018).